Influences of behavioral state and developmental vocal learning on neural coding in the songbird auditory system

Joseph William Schumacher

Submitted in partial fulfillment of the
requirements for the degree of
Doctor of Philosophy
under the Executive Committee
of the Graduate School of Arts and Sciences

COLUMBIA UNIVERSITY

2014

ABSTRACT

Influences of behavioral state and developmental vocal learning on neural coding in the songbird auditory system

Joseph W. Schumacher

Vocal communicators such as humans and songbirds rely on their auditory systems to learn, recognize, and encode acoustic features of communication vocalizations. Yet it remains unclear how varying behavioral, experimental, and developmental contexts impact neural coding in the songbird auditory system. In this dissertation I demonstrate that experimental and behavioral contexts relating to arousal are sufficient to alter neural excitability in a way that has implications for neural coding in the songbird auditory system. First I show that urethane, a common anesthetic used in neurophysiological studies of songbird and mammalian auditory neurons, suppresses neural excitability but does not alter spectrotemporal tuning or neural discrimination in single auditory midbrain neurons. Next, I demonstrate that neurons in the songbird primary auditory cortical region Field L are sensitive to local concentrations of norepinephrine, a neurotransmitter involved mediating changes in arousal and behavioral state. Lastly, I report the results of a developmental study that demonstrates experience-dependent changes in temporal and spectral tuning in songbird auditory cortical neurons during vocal learning. These developmental effects were found to have region and cell-type specificity, and highlight potential functional roles for dorsal and ventral auditory cortical neurons in the songbird auditory cortex. The findings reported here have important implications for future studies into the neurophysiology of vocal learning.

Table of Contents

List of abbreviations: ..... **xi**

ACKNOWLEDGEMENTS ..... **xii**

Part 1: Probing the behavioral state-dependence of sound coding in the songbird auditory cortex **1**

Chapter 1: Introduction **2**

1.1 The songbird as a model for the neurobiology of vocal communication **2**

1.2 The neuroethology of song learning **3**

1.3 The neural substrate for auditory coding in the songbird **5**

1.3.1 Subcortical auditory processing: from cochlea to thalamus 5

1.3.2 Primary Auditory Cortex: Field L 10

1.3.3 Secondary Auditory Cortical Areas 12

1.3.4 Beyond the classical auditory hierarchy 14

1.4 Discussion **17**

Chapter 2: Anesthetic state modulates intrinsic excitability but not spectral tuning or neural discrimination in the songbird midbrain **19**

2.1 Abstract **19**

2.2 Introduction **19**

2.3 Materials and Methods **22**

2.4 Results **33**

2.5 Discussion **48**

Chapter 3: Noradrenergic modulation of auditory coding in the songbird auditory forebrain **54**

3.1 Abstract **54**

3.2 Introduction **54**

3.3 Materials and Methods **56**

3.4 Results **61**

3.5 Discussion **68**

Part 2: Assessing developmental properties of the songbird auditory cortex **72**

Chapter 4: Dynamic structure and function in the developing auditory system **73**

4.1 The role of experience in the developing brain **73**

4.1.1 Development of perceptual skills 74

4.1.2 Development of functional auditory circuits 75

4.2 Discussion: limitations and future directions in experimental frameworks for probing functional auditory development **80**

Chapter 5: Vocal learning drives experience dependent changes in the coding properties of auditory cortical neurons in a region and cell-type specific manner **84**

5.1 Abstract **84**

5.2 Introduction **84**

5.3 Methods **87**

5.4 Results **92**

5.5 Discussion **110**

Chapter 6: Concluding remarks **113**

Bibliography **116**

Appendix: Protocol for construction and implantation of chronic single channel Microdrive **137**

List of Figures and Tables:

Figure 2.1: Major ascending auditory pathway and vocal motor pathway depicting subcortical regions in grey, primary cortical regions in yellow and orange, and secondary cortical regions in red. Vocal motor output is depicted in blue.

Page 6

Figure 2.1: Neural responses to conspecific song vary across cells and are depressed in anesthetized neurons. A. Stimulus waveforms (top), song spectrograms (middle) and raster plots representing 10 cells' responses to 10 presentations of 2 conspecific songs. Unanesthetized (blue) and anesthetized (red) units each produce robust spiking responses, and show variable levels of spontaneous and song-evoked firing. B. Distributions and box plots of spontaneous firing rates (top), song-evoked firing rates (middle), and response strength (bottom) plotted as overlapping histograms. Blue histograms indicate unanesthetized units, red histograms indicate anesthetized units, and purple areas show distribution overlaps. Blue and red diamonds indicate median values for unanesthetized and anesthetized groups, respectively. Anesthetized units (n = 124) had significantly lower spontaneous firing rates, song-evoked firing rates, and response strength than unanesthetized units (n = 85). * $P < 0.05$; ** $P < 0.0001$

Page 24

Figure 2.2: STRF tuning properties. A. STRF tuning measures are plotted along the axes of representative STRFs estimated from unanesthetized (left) and anesthetized (right) responses to conspecific song. Color denotes excitatory (red) and inhibitory (blue) regions of the STRFs, normalized to the peak value of each STRF. Dashed black lines demarcate the bandwidths calculated from spectral (BW) and temporal (tBW) axes. Red dashed lines illustrate BF and LAT relative to the spectral and temporal axes, respectively. B-E. Tuning parameters are displayed as overlapping histograms (unanesthetized = blue; anesthetized = red; overlap = purple). Blue and red diamonds indicate median values for unanesthetized and anesthetized groups, respectively. B. BF. C. BW. D. tBW. E. LAT was shorter in unanesthetized neurons than in anesthetized neurons, indicating longer response latencies under urethane anesthesia. ** $P < 0.0001$

Page 27

Figure 2.3: Neural discriminability performance is not affected by urethane anesthesia. Distributions of performance from discriminability metrics are plotted as overlapping

histograms. Blue and red diamonds indicate median values for unanesthetized and anesthetized groups, respectively. A. K-means % correct did not differ between unanesthetized and anesthetized recordings. B. d' values for single neuron discriminability did not differ between unanesthetized and anesthetized recordings. C. The relationship between d' performance and driven firing rate is highly linear in both unanesthetized ($P < 0.0001$; r-square = 0.63) and anesthetized ($P < 0.0001$; r-square = 0.77) recordings, but the two groups share different slopes with respect to this relationship. D. Rate normalized d', d'spike, was higher for anesthetized MLd neurons, indicating that discriminability is more efficient under urethane anesthesia. ** $P < 0.0001$

Page 36

Figure 2.4 Population responses are time-lagged but show conserved temporal structure under anesthesia. A. A sample song spectrogram (top; color denotes relative power) is aligned with unanesthetized and anesthetized neurograms and their corresponding pPSTHs (blue and red, respectively). Each row of each neurogram represents the log of the instantaneous firing rate of an individual neuron (n = 73 per neurogram), arranged in order of their STRF BFs. Spontaneous and driven responses are distributed across the frequency range in both unanesthetized and anesthetized units. The unanesthetized neurogram is characterized by strong driven firing on top of considerable noise. B. Unanesthetized (blue) and anesthetized (red) pPSTHs for the same song shown in A are aligned by subtracting mean spontaneous firing rate. The red trace follows the blue trace with an apparent time lag. C. The region delimited by black dashed lines in B is expanded. D. The distribution of t values corresponding to the lags in the cross correlation of pPSTHs for the 20 song stimuli is entirely below zero, and has a median t of -4 ms ($p < 0.0001$, Wilcoxon signed rank test for zero median). E. The distribution of lag-corrected correlation coefficients, with a mean of 0.9346 (±0.02 s.d.), indicates that the temporal patterns of the average neural responses to songs are highly similar in unanesthetized and anesthetized populations. F. Median d' values for the unanesthetized population were significantly lower than in the anesthetized population, indicating that stimulus representations are more easily distinguishable in anesthetized neurons. ** $P < 0.0001$

Page 38

Figure 2.5: Frequency-response area tuning and temporal response profiles in single neurons. A. Representative FRA plots for a single unanesthetized (left) and a single anesthetized unit (right). Neurons were presented with 220 ms pure tone stimuli at 128 frequency (0.5 to 8 kHz) and intensity (20 to 90 dB SPL) combinations. B. FRAs were computed as color maps of response strength and were upsampled 3x in the frequency and intensity dimensions. Black contour lines mark boundaries of significant response strengths (at least 20% of the maximum evoked spike rate, above baseline). Color map FRAs from A are displayed with their measured tuning properties. CF and intensity threshold are plotted as dashed black lines along their respective axes. Spectral bandwidth at 20 dB above threshold is the distance between the two dashed red lines in the FRA. The normalized sum of the FRA along the intensity axis is above the FRA. A dashed red line at the peak along the frequency axis indicates BF. C. Characteristic temporal

response patterns of the two neurons were calculated as the average PSTH at BF. The unanesthetized cell has a primary-like type response, and the anesthetized cell has an onset type response.

Page 42

Figure 2.6. Pure tone tuning properties of BF-matched samples of anesthetized (n = 91) and unanesthetized (n = 63) MLd neurons. Tuning property distributions are displayed as overlapping histograms and box plots; red histograms indicate anesthetized units, blue histograms indicate unanesthetized units, and the purple area indicates overlap in the distributions. Blue and red diamonds indicate median values for unanesthetized and anesthetized groups, respectively. A. BF. B. CF. C. BW at 20 dB above threshold. D. BW at 70 dB. E. BW at 90 dB. Tuning properties in A – E did not differ between unanesthetized and anesthetized units in the BF-matched samples. F. The average stimulus intensity threshold was lower for unanesthetized units than anesthetized units indicating that unanesthetized cells can respond to weaker inputs than anesthetized cells. * $P < 0.01$

Page 43

Figure 2.7. Unanesthetized MLd neurons show fewer onset type responses than anesthetized neurons. A. Representative examples of three temporal response types. MLd neurons that had a characteristic temporal response across intensities at BF were assigned to one of three response type groups: onset, primary-like, or sustained. Onset neurons (top) showed a strong onset response to pure tones, followed by little or no response. Primary-like neurons (middle) showed an onset response, followed by a lower firing rate sustained response. Sustained neurons (bottom) show a constant firing rate throughout the stimulus presentation. B. Onset index (the difference divided by the sum of the first and second halves of the characteristic temporal response pattern) distributions of BF-matched samples of anesthetized and unanesthetized neurons are displayed as overlapping histograms. Blue and red diamonds indicate median values for unanesthetized and anesthetized groups, respectively. The onset index was typically smaller in unanesthetized neurons than anesthetized neurons indicating that anesthetized units have slightly more transient temporal response patterns. * $P < 0.05$

Page 45

Figure 2.8. Anesthesia increases spike latencies to pure tone stimuli. Average spike latencies for BF matched samples of unanesthetized and anesthetized MLd neurons. Spike latencies were calculated for pure tone stimuli that generated response strengths that were at least 20% of the maximum song-driven firing rate. Distributions of spike latencies are depicted as overlapping histograms and box plots. Blue and red diamonds indicate median values for unanesthetized and anesthetized groups, respectively. Unanesthetized units had significantly lower spike latencies than anesthetized units. * $P < 0.01$

Page 47

Figure 3.1. NE application depresses firing rates in a dose-dependent manner. a.) An example neuron demonstrates the effect of a prolonged 200 mM NE injection. A single unfamiliar bird's song (top) was repeated 50 times while recording responses (bottom). Trials 1 through 10 (baseline) and 36 through 50 (wash) were recorded during vehicle injection. Trials 11 through 35 were recorded during NE injection. b.) Spontaneous and driven firing rates of the same neuron are depicted across trials, demonstrating the NE-dependent suppression of excitability. c.) Across our population of recordings, high doses of NE (100 or 200 mM) significantly suppressed spontaneous firing rates, while low doses (5 mM) did not systematically alter excitability. ***$p < 0.0001$

Page 62

Figure 3.2: NE-mediated changes in neural excitability are correlated with changes in phase locking performance. a.) Robust responses to click-train stimuli with varied in ICIs in a single representative Field L neuron are sensitive to local a NE injection. During vehicle injection (left) the neuron exhibits a high spontaneous firing rate, which is suppressed during injection of 100 mM NE (right). b.) Phase locking as measured by vector strength in the example neuron from a. (Figure 4.2, cont.) is enhanced for specific ICIs during NE injection (red) compared to baseline and washout vehicle injections (black). c.) Modulation of vector strength is strongly correlated with SMI for 17 phase-locking Field L neurons.

Page 64

Figure 4.3 Spike timing reliability, but not precision, is altered by NE injections. a.) 1st spike jitter, as measured by the standard deviation of first spike times following a click, was not significantly different between vehicle or NE injections. b.) The timescale of neural precision, as measured by the width of the click-aligned PSTH autocorrelogram, was not different for vehicle or NE injections. c.) Spiking event reliability was significantly reduced during NE injections compared to vehicle injections in 17 phase locking neurons. * $P < 0.01$.

Page 66

Figure 4.4: Neural discriminability of birdsong stimuli is diminished during NE injections. a.) This schematic illulstrates how spike train distance metrics measure the discriminability of individual sounds. First, a pair of spike trains is convolved with an exponential decay, and then subtracted to determine their inter-spike train distance (left). Neighboring clusters of spike trains in a high dimensional "spike train space" can be homogeneously comprised of spike trains from an individual song, or heterogeneously comprised of spike trains from different songs. The cartoon example on the left illustrates a good discriminator, while the example on the right illustrates a poor discriminator. b.) K-means discrimination performance did not differ between vehicle or NE injection, while c.) d' discrimination was significantly reduced during NE injection. d.) Decreased d' discrimination was likely due to decreases in intercluster distance, which would inhibit discrimination performance. e.) Spike train cluster size, as measured by

average spike train distance within clusters, also decreased, but was not sufficient to overcome reductions in intercluster distance seen in d.).

Page 67

Figure 5.1: Testing the sensitivity of auditory cortical coding to the onset of sensory learning. **(a.)** We developed an experimental paradigm that allows us to control for the onset of vocal learning in juvenile songbirds while recording longitudinally throughout the AC. **(b.)** A schematic of the songbird auditory forebrain shows the basic connectivity of the songbird AC. **(c.)** Representative reconstructions of electrode paths show electrolytic lesions, indicating an electrode track through multiple auditory subregions. Nissl stained sections (top left) and fresh wet tissue (top right) reveal relevant lamina and anatomical features for delineating subregions. Composite anatomy of recording subjects (bottom) shows individual electrode tracks and lesion locations (blue lines).

Page 94

Figure 5.2: Experimental pupils form accurate copies of their tutor's song. a.) Sample song spectrograms from subjects in various rearing categories, including one of the subject tutors (top). Colony-reared and experimental pupil spectrograms visually resemble their tutors. Isolate-reared pupils and a single failed experimental pupil demonstrate abnormal song learning. b.) Song copy similarity scores for individual subjects in four rearing categories. Box plots denote ranges of similarity scores between pairs of song motifs from each tutor and pupil. Colony-reared and experimental pupils show comparable levels of song copying, while isolate-reared and a single failed pupil demonstrate no motif copying. ANOVA reveals a significant main effect for rearing condition ($p<0.0001$), and post-hoc analysis indicates that colony-reared and experimental pupils show enhanced learning compared to isolates and the single failed learner ($*p<0.01$).

Page 95

Figure 5.3: Fast-spiking (FS) neurons in L2 show enhanced onset responses following the onset of song learning. (a.) Two distinct cell types, delineated by their action potential shapes, are found in all regions of songbird AC. FS neurons are characterized by narrow action potentials and high firing rates. Regular spiking (RS) neurons are characterized by sparse firing and broad action potential shapes. (b.) Example FRA for an onset neuron tuned to 4 kHz. PSTH plots for each frequency/intensity combination, overlaying an interpolated heat map of neural response strengths at each frequency intensity combination. (c.) We quantified the temporal structure of each neuron's tone step response (top) using an onset index (OI). Raster plot of tone-evoked activity (middle) and the PSTH (bottom) of the fast spiking cell from (b.) shows strong onset responses (orange) and a deminished sustained response (aqua) with an OI of 0.95. (d.) FS neurons in L2 have higher OI following the onset relative to early in the pretutoring phase, late in

the pretutoring phase, and compared to age matched Ctrl. birds (red bars). This is not the case in RS cells. Bars indicate mean values +/- S.E.M. *p<0.01

Page 97

Figure 5.4: Spike timing precision to tutor song playback increases following tutor onset. a.) Raster plots from 5 different L2 FS neurons recorded across multiple post-tutoring days (red) to 20 repetitions of the same tutor song (top spectrogram). As post-tutor days progress, spike timing precision in L2 FS cells appears more refined. b.) The PSTH autocorrelogram function (red) for the top raster from a. (day T2) is fit with a Gaussian curve (blue). The Gaussian curve is used to measure the half width at half height (HWHH, red dotted line) and sigma (blue dotted line). c.) 20 L2 FS neurons recorded in the days post-tutor onset show an exponential decay in both HWHH and sigma, indicating that spike timing precision rapidly increases following the onset of tutoring.

Page 99

Figure 5.5. Tuning coherence increases following tutoring onset in L3 RS cells, and in CSt cells. a.) FRA tuning coherence is measured using Geary's contiguity (C) ratio. Black and white binary matrices illustrate potential Geary's C values for dispersed values (top left, C = -1), randomly scattered values (middle left, C = 0), and clustered values (bottom left, C = 1). Representative FRAs are depicted in the right column with their corresponding C values and range from randomly arranged (top) to coherently arranged (bottom). FRAs are plotted in a 3X upsampled form, but actual C values are computed on raw FRAs. b.) Geary's C values for all auditory neurons across all subregions in naïve, untutored birds are shown split in to FS (n =) and RS (n =) cells. FS cells had significantly higher C values across all regions. c.) L3 RS cells (left, black bars) display experience-dependent increases in tuning coherence. Neurons recorded following tutor onset (Tut.) were higher than those recorded 10 to 6 days prior to tutoring (Pre-T1), 5 to 1 day prior to tutoring (Pre-T2), and in age-matched control birds following the day 50 onset of tutor exposure (Ctrl.). No differences were observed for different rearing conditions in L3 FS cells. d.) CSt neurons had an experience-dependent increase in coherence following the onset of tutoring compared to Pre-T and Ctrl. neurons. Bars in c.) and d.) indicate mean values +/- S.E.M. *P<0.01, ***P<0.0001

Page 101

Figure 5.6: a.) CM RS neurons (left), but not FS neurons (right) undergo experience-dependent decreases in tuning coherence compared to Pre-T and Ctrl. neurons. b.) Plotting mean coherence measures (+/- S.E.M.) across days reveals an approximately week long gradual decrease in Geary's C values. * P < 0.01

Page 103

Figure 5.7: Tutoring experience shapes frequency representation in CM RS cells, but not Field L neurons. a.) Tutor song spectrograms (left) and power spectra (right) for the two experimental tutors reveal similar spectral characteristic. Peak power in the frequency distributions is centered from 3 – 5 kHz in both birds, with similar frequency roll-offs to neighboring frequencies. b.) Best frequency distributions for Pre-T, Tut., and Ctrl. conditions reveal that frequency tuning increases in CM RS cells (top) but not FS cells following the onset of tutoring. This increase in BFs shifts the frequency representation of CM RS cells into the range of peak power for the tutors' songs. c.) Neither RS cells (top) nor FS cells (bottom) across subregions of Field L have BF differences across rearing conditions. $*P < 0.01$

Page 105

Figure 5.8: Dorsal output regions of the songbird auditory cortex are highly sensitive auditory behavioral context compared to ventral neurons. a.) An example CM neuron displays robust bursts of action potentials aligned to individual syllables of live singing motifs, but fails to respond reliably to playback of the same sounds. The average spectrogram (top) of the juvenile's live singing is aligned by the amplitude envelopes of individual live motifs (second row). Raster plots and PSTHs show profound differences in the firing pattern of vocal auditory feedback and song playback in this example neuron. b.) Groups of neurons recorded at either the dorsal extent of the auditory forebrain (CM and L1, red) or ventral extent (L3 and CSt) display different sensitivity to live singing vs. playback. As a population, dorsal neurons were highly sensitive to live singing, while ventral neurons responded more linearly between contexts.

Page 109

Table 5.1: Summary of the number of each type of cell recorded during each rearing condition. Pre-T1 corresponds to days 10 to 6 prior to tutor onset at P50. Pre-T2 corresponds to days 5 to 1 prior to tutor onset. Tut. corresponds to all recording days following the onset of tutoring. Ctrl. corresponds to days P50+ in age-matched control birds that were never tutored. In each region, other than CSt, we divide our cells into RS and FS subpopulations, with corresponding n's reported. Neurons in the "other" region were recorded in hippocampus, or anterior to the auditory forebrain.

Page 98

Figure A.1: Wiring schematic for the omnetics connector.

Page 138

Figure A.2: Glue 14-pin omnetics connector to the body of the microdrive.

Page 141

Figure A.3: Encase the motor and gearbox with 4mm polymide tubing.
Page 141

Figure A.4: Glue motor in place at the top of the body. Use the tip to gauge how far the motor axis rests within the shuttle guide slot.
Page 142

Figure A.5: Solder motor wires to pins 1, 8, and 9. Glue the wires into place along the junction of the body and omnetics connector. Insert a fixation bar (black pin) through the tip.
Page 143

Figure A.6: Connect the electrode wire to the shuttle, glue it to the top of the shuttle, solder it to pin 14, and attach elastic string to the fixation bar and wire to add tension.
Page 144

Figure A.7: Solder the reference wire to pin 11and glue in place.
Page 144

Figure A.8: Attach the ground wire to pin 4, wrap it around the fixation bar, and glue it in place.
Page 145

Figure A.9: Cut electrode to desired length, insert into polymide guide tube, solder to shuttle, and fix guidetube to tip with dab of epoxy. Finally, attach a clear plastic cover to prevent the bird from breaking the electrode.
Page 146

List of abbreviations:

AM: amplitude modulation
BF: best frequency
BOS: bird's own song
BW: spectral bandwidth
CF: characteristic frequency
DBH: dopamine-beta-hydroxylase
FM: frequency modulation
FRA: frequency response area
FS: fast-spiking, putative inhibitory interneurons
GLM: generalized linear model
ICI: inter-click interval
IEG: immediate early gene
ILD: interaural level difference
ITD: interaural time difference
LAT: latency
ML: modulation limited noise
NE: norepinephrine
OI: onset index
PSTH: peristimulus time histogram
pPSTH: population PSTH
RS: regular or broad spiking, putative glutamatergic neurons
SMI: spontaneous activity modulation index
STRF: spectrotemporal receptive field
tBW: temporal bandwidth
VMI: vector strength modulation index
VS: vector strength

A1: primary auditory cortex
AFP: anterior forebrain pathway
CLM: caudolateral mesopalium
CM: caudal mesopalium
CMM: caudomedial mesopalium
CN: cochlear nuclei
CNIC: central nucleus of the inferior colliculus
CSt: caudal striatum
DIC: dorsal nucleus of the inferior colliculus
DLM: dorsolateral thalamus
DNLL: dorsal nucleus of the lateral lemniscus
EIC: external nucleus of the inferior colliculus
IC: inferior colliculus
ICo: intracollicular complex
LL: lateral lemniscus
LocC: locus coeruleus
LSO: lateral superior olive
Ov: nucleus ovoidalis
MLd: Mesencephalicus Lateralis pars dorsalis
MNTB: medial nucleus of the trapezoid body
MSO: medial superior olive
NA: nucleus angularis
NCM: caudomedial nidopalium
NIf: interfacial nucleus of the nidopallium
NL: nucleus laminaris
NM: nucleus magnocellularis
RA: robust nucleus of the arcopalium
SCv: subcoeruleus
SO: superior olive
Uva: nucleus uvaeformis
VP: ventral palidum
VTA: ventral tegmental area

ACKNOWLEDGEMENTS

First and foremost, I owe a huge debt of gratitude to my advisor Sarah Woolley. Thank you, Sarah, for years of mentorship and for giving me a home in your lab. With seemingly endless patience, you've supported me, encouraged me, and helped me to develop my skills as a scientist. I will miss being a part of the Woolley lab, but will look back on these past few years with great fondness thanks to you.

I would like to thank my thesis committee for their thoughtful contributions to my research over the years. Thank you to Darcy Kelley for encouraging me to pursue difficult experimental goals, to Liam Paninski for fostering collaborations between his lab and Sarah's from which I could learn, to Nate Sawtell for helping me to ask better experimental questions, and to Dan Sanes for acting as my external committee member. I've benefited greatly from each of you and value your participation in my dissertation defense immensely. I would also like to thank Richard Hahnloser, Georg Keller, and Andreas Kotowicz for sharing their protocol for chronic electrophysiology in songbirds. This technique was pivotal for my research.

I'm grateful for the many friends, colleagues, and collaborators that I've made during my time at Columbia. Thanks to my dear friends and lab mates David Schneider, Ana Calabrese, Jordan Moore, Rahia Mashoodh, and all of the members of the Woolley lab for teaching me so much and for making it a joy to show up to work every day. Thanks to my bandmates Alex Ramirez and Annegret Falkner, and to my former roommates Burcin Ikiz and Mattia Rigotti for lots of great times. Special thanks to my former mentors John Long, Pietro Mazzoni, and John Krakauer for fostering my early interest in perception and behavior. Finally, I owe endless thanks to my wife Sarah. Your love and support quietly made all of this hard work possible.

Part 1: Probing the behavioral state-dependence of sound coding in the songbird auditory cortex.

Chapter 1: Introduction

1.1 The songbird as a model for the neurobiology of vocal communication

The transmission of social information between senders and receivers is the goal of communication and is shared across animal taxa. Most sensory modalities are used to receive and perceive communication signals. These include vision (e.g. gestures, facial expressions) and olfaction (e.g. pheromone detection, predator identification). Vocal communication signal encoding by the auditory system stands out as one of the more sophisticated strategies for transmitting diverse and informative signals for identifying and locating conspecifics, territorial defense, alerting others to danger, advertising status, and courtship. Humans and other vocal communicators rely on the coordination of auditory coding processes to transduce sound into meaningful information, and for controlling vocal-motor behaviors that convey information. The neural substrates for encoding vocal communication signals must be precise and robust enough to cope with variations in sound source locations, background noise, and other features of the acoustic environment that impact the fidelity of signal transmission in the natural world.

The animal models used to study auditory processing include bats (Pollak and Bodenhamer, 1981; Fuzessery and Pollak, 1985; Yan and Suga, 1998; Andoni et al., 2007), rodents (Aitkin et al., 1986; Froemke and Dan, 2002; Wehr and Zador, 2003), cats (Schreiner and Urbas, 1986; 1988), owls (Knudsen and Konishi, 1979; Pena and Konishi, 2001; Winkowski and Knudsen, 2006), songbirds (Gentner, 2004; Theunissen et al., 2008; Woolley et al., 2009), frogs (Kelley, 1980; Paton et al., 1982, Elliot et al., 2011), ferrets (Fritz et al., 2003; 2010), and primates (Aitkin et al., 1986). Each model system has unique advantages that make it well suited for asking specific questions about neural mechanisms of auditory perception, ranging from

spatial localization (Knudsen and Konishi, 1979; Pena and Konishi, 2001) and tonotopy (Aitkin et al., 1986), to active sensing and attentional modulation of neural responses (Fritz et al., 2003; Winkowski and Knudsen, 2006). Studies using these models have provided profound insights for understanding the processes underlying auditory perception and behavior.

In humans, speech production and perception are acquired early in life, during known critical periods of development. The speech sounds that we encounter as infants influence our perceptual skills and behavioral responses to sounds as adults. The most important animal model for the study of vocal learning through hearing is the songbird. Most animals rely on the ability to process auditory signals in order to classify the signal, but songbirds (like humans) also rely on auditory processing to learn their species-typical vocalizations. Among potential model animals for investigating the neurobiology of vocal learning and communication, the songbird's ability to listen, memorize, and copy vocal behaviors from others is special to the songbird.

1.2 The neuroethology of song learning

Most birds vocalize, but only birds in 3 of the 23 major orders learn to produce vocal content *de novo* through experience. These include parrots (*Psittaciformes*), hummingbirds (*Trochiliformes*), and songbirds (suboscine *Passeriformes*). These vocal learners differ from other classes in that they have specialized brain regions that enable the production and perception of complex sounds. The remaining birds rely on basal brain regions to vocalize and use vocal signals that are not learned (Jarvis, 2004; Ondracek and Hahnloser, 2014).

The longstanding hypothesis for how songbirds learn to sing is described as the auditory template theory. Under this model, juvenile birds are born with basic physiological constraints that define species-specific features of their songs. Early in life near the onset of hearing,

juvenile males enter into a sensory learning phase, during which they observe and memorize songs of their tutors and use these heard sounds to construct an auditory template the tutor song(s) (Konishi, 1985). Juvenile birds then enter a sensory-motor phase of song learning, in which they gradually produce more "song-like" vocalizations and use auditory feedback to match their own songs to the tutor song memory.

Juvenile songbirds first produce immature "subsong" vocalizations that are akin to human infant babbling (Doupe and Kuhl, 1999). Gradually, as a young bird continues to shape its vocalizations to match the template, syllable structure develops and the bird transitions into producing "plastic song". Plastic song gradually develops rhythm and a stereotyped syllable order. At sexual maturity (~90 days of age), a bird stabilized its song behavior, producing a "crystalized song" that is highly stereotyped, with consistent syllable structures and syllable sequences over time. The song of the young adult is acoustically well-matched to the tutor's song.

The song learning process of sensory experience, memorization, vocal practice and refinement depends on auditory feedback instructing motor output. Illustrating the importance of early experience in the formation of song, cross-fostering studies demonstrate that male zebra finch chicks can accurately copy Bengalese finch songs (Immelmann, 1969; Clayton, 1987; 1989; Woolley et al., 2010). Also, young birds raised in social isolation produce abnormal songs, referred to as isolate songs (Marler, 1970). Furthermore, auditory feedback during vocal practice is critical to forming accurate copies of the tutor's song. Birds that are deafened after exposure to a song model, but before the onset of the sensory-motor phase develop highly abnormal songs that show no signs of learning (Konishi, 1965).

1.3 The neural substrate for auditory coding in the songbird

The songbird auditory system shares a strong homology with that of the mammal, particularly with regards to subcortical auditory regions. Here I review many of the anatomical and functional principles that are observed in the songbird from the cochlea to the cortex. I will then outline some of the important limitations of previous work in the songbird auditory system, as well as open questions regarding functional properties of auditory neurons. For reference, a schematic of the major ascending auditory pathway and vocal motor pathway is provided in Figure 1.1.

1.3.1 Subcortical auditory processing: from cochlea to thalamus

The mechanical transduction of sound occurs at the ear. The avian middle ear has a similar function to that of its mammalian counterpart, namely the transfer of sound energy from vibrations of the tympanic membrane to the oval window of the cochlea. This is achieved by the leverage of a single ossicle, the columella, which is homologous to the mammalian stapes. The middle ear of birds acts as a strong low pass filter. Some avian species with specialized hearing, such as the barn owl, hear up to 11 kHz, while songbirds, such as the zebra finch, hear up to 8 kHz (Gleich and Manley, 2000).

The inner ear of birds consists of a cochlear duct, so named despite not having a spiraled, snail-like like appearance. This cochlear duct consists of fluid a filled scala tympani and scala vestibuli, which are separated by the basilar membrane, scala media, and basilar papilla (homologous to mammalian organ of corti). Hair cells of the basilar papilla belong to two populations: tall hair cells located mainly on the neural side of the basilar papilla and the short

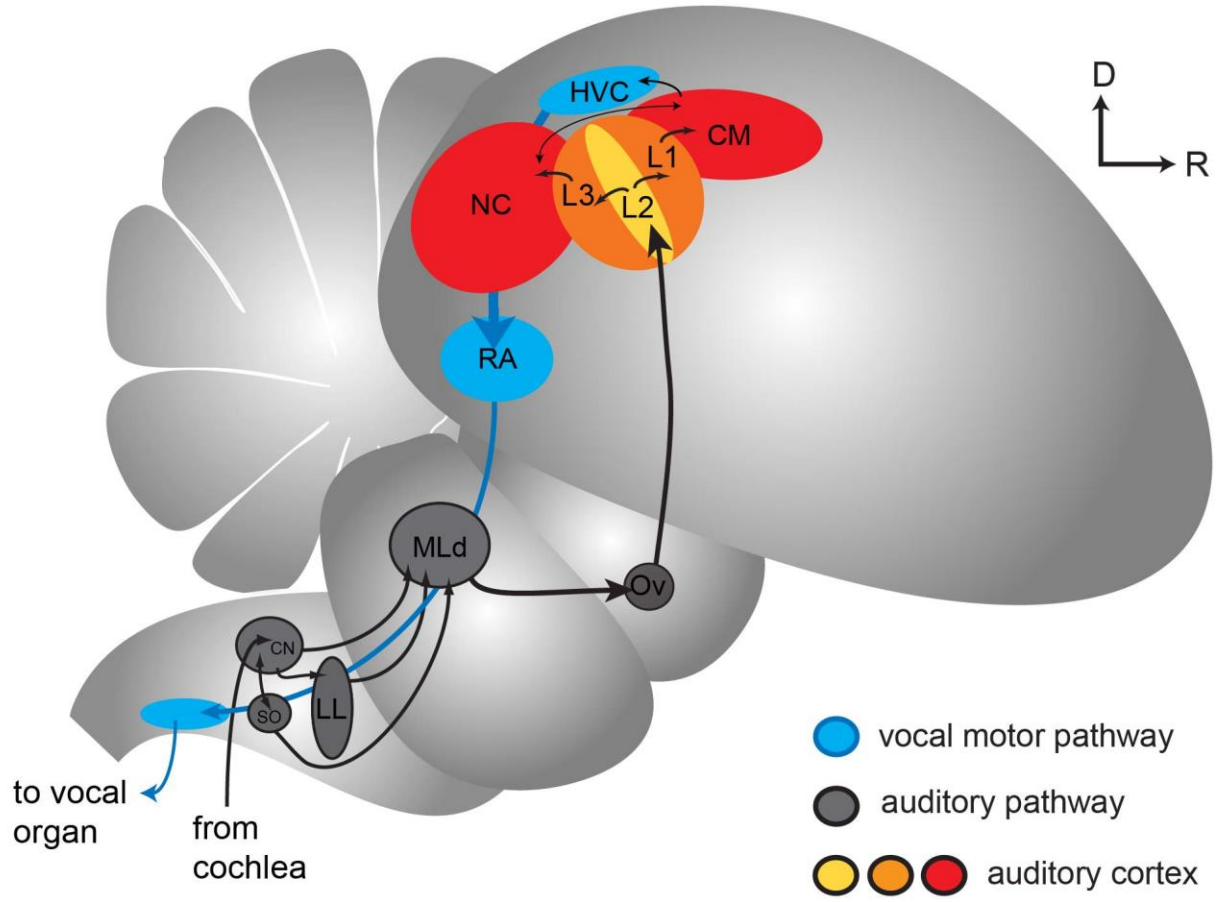

Figure 1.1: Anatomical distribution of the major ascending auditory pathways (grey), auditory cortex (yellow, red, orange) and vocal motor pathway (blue). Dorsal (D) and rostral (R) orientations are noted.

hair cells. Tall hair cells provide the afferent projections of the auditory nerve, while short hair cells receive efferent input (Fischer, 1994). Short hair cell motility may allow a selective amplification of low-intensity sounds and dampening of high-intensity sounds (Yates et al., 2000).

The songbird cochlear nerve consists of roughly 6000 to 9000 afferent fibers whose cell bodies reside in an acoustic-vestibular ganglion. When probed with different frequencies and intensities, fibers of the cochlear nerve elicit maximal spiking responses at a characteristic frequency (CF). As in mammals, fibers with synaptic terminals at the apical end of the basilar

papilla have low CFs, and fibers originating at the basal end have high CFs. Auditory nerve fibers will phase lock at CF up to 1 kHz (Gleich and Manley, 2000).

The auditory nerve projects to the ipsilateral brainstem, terminating on nucleus magnocellularis (NM) and nucleus angularis (NA). NM and NA neurons are arranged tonotopically, with NA neurons showing a wider band of CFs than NM neurons (Konishi, 1970) and project to the ipsi- and contralateral nucleus laminaris (NL) (Krützfeldt et al., 2010). NL neurons are sensitive to interaural time differences (ITD) that are important for sound source localization. NA and NL project to the ipsi- and contralateral superior olive (SO) and lateral lemniscal nuclei (LL) (Krützfeldt et al., 2010; Wild et al., 2010). LL neurons display sensitivity to interaural level differences (ILD) in the barn owl (Takahashi and Keller, 1992). SO and LL provide feedback projections to the lower four brainstem nuclei, as well as their contralateral counterparts (Wild et al., 2010). LL receives forebrain feedback from song motor nucleus RA Cup (Wild, 1993), and features some of the earliest connections to the forebrain, projecting bilaterally to the auditory thalamic nucleus ovoidalis (Ov) and thalamic nucleus uvaeformis (Uva) (Wild et al., 2010), which has been shown to gate auditory input to the premotor nucleus HVC (Coleman et al., 2007).

The auditory midbrain nucleus Mesencephalicus Lateralus pars dorsalis (MLd) is an evolutionarily conserved bottleneck for ascending and converging auditory brainstem nuclei, including the SO, LL, NA, and NL (Krützfeldt et al., 2010; Wild et al., 2010). As a central midbrain auditory processing stage, MLd is homologous to the inferior colliculus in mammals, and the torus semicircularus in amphibians(Woolley and Casseday, 2004). MLd is located anatomically in the intracollicular complex (ICo), and can be histologically divided into distinct inner and outer subregions (Logerot et al., 2011).

Electrophysiological studies in MLd have demonstrated important functional characteristics for these midbrain neurons. As in the mammalian inferior colliculus (IC), neurons in MLd fall along a noisy tonotopic gradient, with dorsal neurons responding to lower frequencies than ventral neurons (Woolley and Casseday, 2004; Woolley and Portfors, 2013). Most cells in MLd have classical v-shaped frequency tuning curves, indicating that these neurons encode simple subsets of the frequency spectrum (Woolley and Casseday, 2004). However, even at this early processing stage, MLd neurons display context specific tuning capabilities. Spectrotemporal receptive fields STRFs estimated from responses to conspecific song have wider frequency bandwidths than those estimated from responses to modulation limited (ML) noise stimuli (Woolley et al., 2006). This has been shown to be mediated by extraclassical receptive field properties that are engaged by the wider frequency "roll-off" around best frequency of song, but not noise (Schneider and Woolley, 2011).

STRFs estimated from MLd neuronal responses to songs reveal additional spectrotemporal functional properties. A majority of MLd neurons have been shown to be excited by wide frequency bands within narrow temporal windows, indicating the most neurons have strong onset responses to wide frequency bandwidths (Woolley et al., 2009), indicating that MLd neurons are likely to be important for coding the temporal pattern of acoustic features. Indeed, neurons in MLd have been shown to accurately discriminate between complex acoustic stimuli on the basis of distinct patterns of neural spiking(Schneider and Woolley, 2010), in both anesthetized and unanesthetized preparations (Schumacher et al., 2011).

Thalamic region Ov is the avian analogue to the mammalian medial geniculate body of the thalamus. It consists of a small, dense region of neural clustering that is histologically distinct from surrounding tissue, and like MLd, is divided into a shell and core region. The core

receives afferent input from MLd, while the shell receives feedback projections from the area surrounding the robust nucleaus of the arcopalium (RA cup), as well as medial portions of MLd (Zeng et al., 2004). Neurons in Ov core comprise the principal thalamocortical (Vates et al., 1996), while neurons in Ov shell project more diffusely throughout the auditory forebrain (Vates et al., 1996; Zeng et al., 2004).

Similarly to MLd neurons, Ov neurons display robust responses to a wide range or stimuli including noise, pure tones, and frequency- and amplitude-modulated sounds. Unlike MLd neurons, a majority of Ov neurons in starlings respond tonically throughout the duration of a stimulus, rather than favoring the onset portion of the response (Bigalke-Kunz et al., 1987). A subsequent study by showed however that a majority of STRFs had narrowband temporal windows, indicating strong onset responses in these cells(Amin et al., 2010). This study also found that while neurons in Ov seemed to inherit receptive field properties common in MLd neurons, new feature selectivity seemed to emerge in Ov, such as selectivity for frequency modulated (FM) sweeps. FM sweeps are common in birdsong, and the emergence of FM sweep selectivity indicates a degree of specialization within Ov for processing features of birdsong (Amin et al., 2010).

Another study found that Ov plays an important role in maintaining the structure of song in juvenile songbirds (Lei and Mooney, 2010). White noise perturbations blocking out a portion of a live song motif lead to gradual decrystalization of that element, and significantly drive multiunit activity in Ov. Stimulation of Ov during singing was shown to have a similar effect. Together, these results indicate that Ov is integral to online maintenance of song during practice (Lei and Mooney, 2010).

1.3.2 Primary Auditory Cortex: Field L

One century ago, Maximilian Rose (1914) used Nissl staining to first characterize Field L based on its distinct cellular organization. Its functional role was clarified much later when Karten (1968) oblated Ov in pigeons, and traced anterograde argyrophyllic degeneration to Rose's Field L. This region is now considered to be a part of a complex network of subregions that together form an analogue to mammalian auditory cortex (Jarvis et al., 2005). Field L is located anatomically in the central telencephalic nidopallium, and can be divided into several subregions based on histological assessment of cell body density and axonal projection patterns. These include L1, L2a, L2b, and L3 (Bonke et al., 1979; Fortune and Margoliash, 1992). A fifth subdivision, confusingly referred to as L, is used to describe an area where the original definitions of Rose (1914) and Karten (1968) do not overlap (Fortune and Margoliash, 1992).

L2a receives afferent projections from Ov core (Vates et al., 1996), while L2b receives projections from Ov shell. Together, L2 comprises the primary thalamorecipient input area of the avian auditory cortex, and shares reciprocal connections with the other subregions of Field L (Vates et al., 1996). L1 and L3 are reciprocally connected to L2a and each other, and receive projections from Ov shell. Input from Ov to Field L is subsequently distributed to a number of secondary auditory subregions including the caudal mesopalium (CM), the caudomedial nidopalium (NCM), the caudal striatum (CSt), and HVC shelf (Kelley and Nottebohm, 1979).

Field L is tonotopically organized, with caudal neurons responding preferentially to lower frequencies and rostral neurons responding to higher frequencies (Zaretsky and Konishi, 1976; Müller and Leppelsack, 1985). Neurons in Field L display responses to a wide variety of stimuli, but respond preferentially to complex sounds with temporal modulations, due in part to intrinsic

temporal dynamics of excitation and inhibition at the single cell level. Leppelsack (1974) recorded responses to modulated noise and tones, and found that most Field L neurons responded with strong onset responses, followed by sustained but weaker tonic firing (so-called "primary-like" responses), while other neurons featured phasic suppression, tonic suppression, or tonic activation throughout a stimulus, often with increases or decreases in firing rate at the offset of a stimulus. Compared to MLd neurons which predominantly encode onsets, and Ov neurons that predominantly respond tonically through the duration of a stimulus, Field L neurons display features that allow them to encode both onsets and offsets. The presence of high-density local GABAergic neurons in Field L suggest that inhibitory modulation may play a role in these temporal dynamics (Pinaud and Mello, 2007).

The auditory processing of behaviorally relevant sounds, such as a bird's own song (BOS), tutor's song, conspecific or heterospecific song, and acoustic manipulations of these natural stimuli, is a main focus in songbird neuroethology. Field L neurons in anesthetized white-crown sparrows do not demonstrate a firing rate preference for BOS or tutor songs compared to conspecific songs (Margoliash, 1986). Additionally, neurons in Field L of anesthetized zebra finches are less sensitive to perturbations of BOS than neurons in HVC, and respond equally well to BOS and reversed BOS (Lewicki and Arthur, 1996). These cells do, however, have selectivity for conspecific songs compared to artificial stimuli that match the acoustic properties of song (Theunissen et al., 2004), and are predominantly downstream from the input region L2 (Grace et al., 2003).

STRFs estimated from Field L responses illustrate diverse functional response properties in these neurons beyond firing rate selectivity. Broadly these neurons can be grouped as broadband onset cells, narrowband cells, and detectors of more complex features like harmonic

stacks, offsets, and frequency sweeps (Sen et al., 2001; Nagel and Doupe, 2008; Woolley et al., 2009; Amin et al., 2010). STRFs estimated from L2 neurons have shorter latencies to excitation and integrate inputs much faster than neurons in L1 and L3 (Sen et al., 2001; Nagel and Doupe, 2008) Furthermore, standard reverse correlation STRF models have greater predictive power in L2, suggesting that L2 neurons are more linear than neurons in L1 and L3 (Sen et al., 2001).

1.3.3 Secondary Auditory Cortical Areas

Caudal to L3, NCM is a large anatomical structure receiving input from L2a, L3, and Ov shell. This region shares reciprocal connections with the caudal mesopalium (CM) (Vates et al., 1996), and receives feedback from paraHVC (Foster and Bottjer, 1998).

NCM is thought to be involved in the formation of auditory memories, especially with respect to a tutor's song (Hahnloser and Kotowicz, 2010). Mello et al. (1992) found increased expression of the immediate early gene ZENK in response to conspecific song, but much less in response to heterospecific song, and none to tones. Repeated presentations of conspecific song cause this ZENK response to habituate to baseline levels over several minutes, but single presentations of unfamiliar songs reestablish high levels of ZENK expression (Mello et al., 1995; Gentner, 2004). Blocking ZENK expression in primary and secondary auditory areas prior to tutoring suppresses tutor song copying in zebra finches, indicating that ZENK related activity is important for auditory memory formation (London and Clayton, 2008). The habituation of ZENK expression is reflected in neuronal spiking responses. Multiunit response rates rapidly habituate to repeated presentations of the same conspecific song, but rebound following the presentation of a novel song (Chew et al., 1995; Stripling et al., 1997). Thompson and Gentner

(2010) did not find habituation to conspecific song following simple exposure, but only when coupled with go/no-go operant-conditioning. Ventral NCM neurons showed reductions in response rates to trained songs, while dorsal neurons showed no habituation. Adding to the evidence that NCM encodes a memory of tutor song, male zebra finches show a behavioral preference for hearing tutor song compared to unfamiliar conspecific song, but this preference is reduced following lesions of NCM (Gobes and Bolhuis, 2007).

Recent studies have focused on highly sparse and selective responses to familiar songs in NCM as evidence of an efficient coding strategy (Blättler and Hahnloser, 2011; Moore et al., 2013; Schneider and Woolley, 2013). Interestingly, sparse coding neurons in NCM have been shown to be background invariant, and may serve as a neural substrate for extracting behaviorally relevant stimuli from noisy environments (Schneider and Woolley, 2013).

CM is dorsal to Field L, and is delineated by the lamina hyperstriatica. It is subdivided into medial (CMM) and lateral (CLM) portions which are reciprocally connected. CLM is reciprocally connected to the subregions of Field L, and projects to NIf, HVC shelf and RA Cup, while CMM is reciprocally connected to NCM (Vates et al., 1996). Bauer et al. (2008) found evidence that CM has direct projections to HVC. CM has also been shown to receive input from Uva and Ov shell (Wild, 1993; Fortune and Margoliash, 1995; Vates et al., 1996).

Response latencies in CM are longer than in Field L, and STRF estimates are less predictive than most Field L neurons, possibly due to lower firing rates or less linear response properties (Sen et al., 2001). Neurons in CM show selectivity for BOS over conspecific song, BOS over reversed BOS, and conspecific song over artificial stimuli (Grace et al., 2003; Theunissen et al., 2004). In starlings, neurons in CM are selective for complex acoustic features (Meliza et al., 2010), and this feature selectivity can be entrained with operant conditioning.

Neurons in CM, especially in CMM, show higher mutual information between firing rates and sounds associated with food rewards than sounds that were not associated with rewards (Jeanne et al., 2011).

Recent studies (Meliza and Margoliash, 2012) have begun to classify CLM as the most superficial layer of primary auditory cortex, as axons from Field L appear to form radial columns that extend well into CLM. It is possible that medial regions of the auditory forebrain (NCM and CMM) form a network of secondary association areas, while more lateral regions in Field L and CLM form a sort of column analogous to primary auditory cortex.

1.3.4 Beyond the classical auditory hierarchy

A number of thalamic, basal ganglia, higher-order cortical regions involved in the learning and production of birdsong present interesting auditory phenomena. The integration of sensory and motor information is of particular interest in the songbird, and here I will outline some of the major observations of auditory processing beyond the classical auditory hierarchy.

The interfacial nucleus of the nidopallium (NIf) is a small cluster of neurons located between L1 and L2a (Fortune and Margoliash, 1995). NIf receives input from CLM (Vates et al., 1996; Bauer et al., 2008) and Uva (Nottebohm et al., 1982). NIf neurons display premotor activity related to singing (McCasland, 1987), and lesions to NIf in juveniles, but not adult birds, can significantly reduce sound quality (Hosino and Okanoya, 2000; Cardin et al., 2005; Naie and Hahnloser, 2011). Auditory responses in NIf are relayed from CLM (Bauer et al., 2008), and are dependent on behavioral state (Cardin and Schmidt, 2004a). NIf auditory neurons are more BOS

selective than CM neurons, indicating that this selectivity emerges gradually (Janata and Margoliash, 1999; Coleman and Mooney, 2004).

HVC is one of the most widely studied nuclei in the songbird brain, due to its specialized role in the production of song. It is located in the caudal nidopallium and receives input from Uva, NIf, CM, and the medial magnocellular nucleus of the anterior nidopallium (MMAN) (Nottebohm et al., 1982; Fortune and Margoliash, 1995; Vates et al., 1997). HVC is sexually dimorphic, appearing 10 times larger in males than females (Nottebohm and Arnold, 1976). The size of HVC is positively correlated with the size of song repertoire across species (Devoogd et al., 1993). Bilateral lesions of HVC will abolish crystalized song, but preserve calls and subsong (Aronov et al., 2008). Cooling HVC, but not downstream nucleaus RA, slows the tempo of song (Long and Fee, 2008). HVC is comprised of three principal cell types: RA projecting- (HVC_{RA}), Area X projecting- (HVC_X), and interneurons (HVC_{int}). HVC_{RA} and HVC_X cells fire sparse reliable bursts of spikes while singing, HVC_{int} neurons fire throughout the duration of song (Hahnloser et al., 2002; Kozhevnikov and Fee, 2007). Auditory responses in HVC are gated by the behavioral state of the bird. In zebra finches, HVC neurons respond to auditory playback under anesthesia and during sleep, but not while aroused or singing (Schmidt and Konishi, 1998; Cardin and Schmidt, 2003; 2004b). This gating is controlled primarily by norepinephrine sensitive neurons in NIf (Cardin and Schmidt, 2004a; 2004b). Deactivation of CM eliminates HVC auditory responses (Coleman and Mooney, 2004). Under conditions that allow for auditory responses in HVC, all three principal cell types are highly selective for BOS playback. Prather et al. (2008) found precise mirroring of spiking responses to auditory playback and singing in HVC_X neurons, indicating that these neurons may be specialized to serve as a predictive model for auditory feedback.

Uva is a multisensory thalamic nucleus that receives bilateral auditory input from LL (Wild, 1994; Wild et al., 2010), and projects to NIf and HVC. Neurons in Uva are sensitive to behavioral state, and are capable of gating auditory responses in HVC (Coleman et al., 2007; Hahnloser et al., 2008). Neurons in UVA show unselective auditory responses under anesthesia (Coleman et al., 2007).

RA receives input from HVC both directly and indirectly through the anterior forebrain pathway (AFP) (Nottebohm and Arnold, 1976; Bottjer et al., 1989). It projects ipsilaterally to the hypoglossal nucleus, which innervates the muscles of the syrinx, and projects ipsilaterally to brainstem nuclei controlling respiration. RA is required for song production, and neurons in RA show auditory selectivity for BOS that is gated by behavioral state (Doupe and Konishi, 1991; Dave et al., 1998).

The AFP is a cortico-basal ganglia-thalamic loop involved in the learning and maintenance of song. HVC projects to Area X, which projects to the medial nucleus of the dorsolateral thalamus (DLM). DLM projects to the lateral magnocellular nucleus of the anterior nidopallium (LMAN), which projects back to Area X, as well as RA (Vates and Nottebohm, 1995). Area X is a basal ganglia structure that also projects to the ventral tegmental area (VTA) via the ventral pallidum (VP). Dopaminergic neurons in VTA ipsilatterally project back to the striatal part of Area X (Gale et al., 2008). This AFP circuit is not needed for song production in adults, but drives song development in juveniles (Scharff and Nottebohm, 1991; Aronov et al., 2008), and the output of LMAN induces variability in song that may be important for song maintenance (Brainard and Doupe, 2000; Kao et al., 2005). Area X and LMAN respond selectively to BOS playback in adult birds, but this selectivity is diminished in juvenile birds singing plastic song (Doupe and Konishi, 1991). Neurons in the MMAN project to HVC and

paraHVC (Vates et al., 1997). Although the source of auditory input to MMAN is unknown, MMAN neurons display auditory selectivity to BOS that resemble sparse responses in HVC (Williams et al., 2012). Other AFP regions such as the VTA and VP contain neurons that display BOS-selective auditory responses (Gale and Perkel, 2010).

HVC shelf and RA cup border their respective premotor nuclei, and receive input from L1, L3, CM. RA cup receives projections from HVC shelf, and projects back to Ov shell, MLd, and LL (Martin Wild et al., 1993; Mello et al., 1998). It remains unclear if these regions provide input to their premotor nuclei (Fortune and Margoliash, 1995; Vates et al., 1996; Shaevitz and Theunissen, 2007). The functional role of this auditory feedback loop running in parallel to the premotor nuclei remains unclear.

Finally, non-specific projections from Field L have been observed terminating in the caudal striatum (Kelley and Nottebohm, 1979; Fortune and Margoliash, 1995), a region known to exhibit auditory responses (Smith et al., 2006). The precise connectivity of CSt with other auditory regions is unknown.

1.4 Discussion

The songbird is a longstanding model system for understanding the neural basis of vocal communication. Because of the songbird's well characterized behavioral specialization as a vocal learner, auditory and vocal motor neural circuits have provided many insights into the mechanisms involved in acquiring vocalizations. The auditory system of the songbird shares many similarities with its mammalian counterpart from the cochlea to the cortex, and consists of multiple pathways ascending in parallel and converging to endow distinct anatomical nuclei with the functional coding properties required to represent information about the external

environment. One important principle illustrated by the complex functional and anatomical connectivity patterns of the auditory system is that auditory processing in the songbird is intimately intertwined with vocal motor and basal ganglia circuits, which has important implications for the nature of auditory processing in vocal learning.

In both songbirds and mammals, a majority of neurophysiological studies in the auditory system have used anesthetized animals. Modern techniques, allow a greater number of experiments to be conducted in awake and behaving animals, where neural processes involved in attention and behavior can be examined. Because current experiments and conclusions are informed by the results of previous studies and because future studies will likely be conducted using a variety of anesthetic and behavioral states, it is important to determine whether and to what extent neural response properties are state-dependent. In chapter 2, I will present a study investigating the role of anesthesia in modulating the response properties of songbird auditory midbrain neurons. In chapter 3, I explore the role of the neurotransmitter norepinephrine in modulating songbird auditory forebrain neurons. These studies will inform our understanding of the degree to which behavioral state matters for varying experimental contexts, and provide basic insights into the role of neural excitability in neural coding.

Part II of this dissertation concerns the role of experience in shaping the neural coding properties of the developing songbird auditory cortex. Birdsong is a developmentally acquired skill, but few studies have examined the coding properties of auditory neurons in juvenile birds that are learning to sing. Chapter 4 will review relevant literature on auditory development, and will discuss general developmental principles that can be exploited by studying juvenile songbirds. Finally, in Chapter 5 I will present data demonstrating the effects of developmental vocal learning on the coding properties of auditory cortical neurons in the juvenile songbird.

Chapter 2: Anesthetic state modulates intrinsic excitability but not spectral tuning or neural discrimination in the songbird midbrain

2.1 Abstract

The majority of sensory physiology experiments have used anesthesia to facilitate the recording of neural activity. Current techniques allow researchers to study sensory function in the context of varying behavioral states. To reconcile results across multiple behavioral and anesthetic states, it is important to consider how and to what extent anesthesia plays a role in shaping neural response properties. The role of anesthesia has been the subject of much debate, but the extent to which sensory coding properties are altered by anesthesia remains unknown. Here we ask how urethane, an anesthetic commonly used for avian and mammalian sensory physiology, affects the coding of complex communication vocalizations (songs) and simple artificial stimuli in the songbird auditory midbrain. We measured spontaneous and song-driven firing rates, spectrotemporal receptive fields, and neural discriminability from single auditory midbrain neuron responses to songs. In the same neurons, we recorded responses to pure tone stimuli ranging in frequency and intensity. Finally, we assessed the effect of urethane on population-level representations of birdsong. Results showed that intrinsic neural excitability is significantly depressed by urethane, but spectral tuning, single neuron discriminability and population representations of song do not differ significantly between unanesthetized and anesthetized animals.

2.2 Introduction

The majority of studies examining cellular and systems level processing in auditory (Knudsen and Konishi, 1978; Nelken et al., 1999; Read et al., 2001; Wehr and Zador, 2005; Woolley et al., 2005; Woolley et al., 2006) and visual neurons (Hubel and Wiesel, 1962; Kuffler, 1953; Rust et al., 2006; Weliky et al., 1996) have used anesthetized animals. Current techniques, however, allow a greater number of neurophysiological experiments to be conducted in awake animals, where neural processes involved in attention and behavior can be studied (Atiani et al., 2009; Fritz et al., 2010; Keller and Hahnloser, 2009; Wang et al., 2005; Xie et al., 2007). Because current experiments and conclusions are informed by the results of previous studies and because future studies will likely be conducted using a variety of anesthetic states, it is important to determine whether and to what extent anesthesia alters neural response properties. Accordingly, the effects of anesthesia on sensory neural function have been under considerable debate (Capsius and Leppelsack, 1996; Franks and Lieb, 1994; Hara and Harris, 2002; Sceniak and MacIver, 2006; Ter-Mikaelian et al., 2007). But few studies directly compare the complex neural coding properties of sensory neurons in anesthetized and awake animals, and even fewer include natural stimuli, which are processed differently from artificial stimuli (Rieke et al., 1995; Vinje and Gallant, 2000; Woolley et al., 2006). Of those few studies, none have tested the effects of anesthesia on spectrotemporal (auditory) or spatiotemporal (visual) tuning. Here, we conducted a detailed comparison of the coding of communication vocalizations by auditory midbrain neurons to understand if and how anesthesia alters subcortical excitability, spectral coding and temporal response properties.

Urethane is a common anesthetic for acute electrophysiological recordings in the sensory systems of mammals and birds. In the auditory system, urethane has been used for electrophysiology in the midbrain (LeBeau et al., 2001; Nakamoto et al., 2008; Schneider and

Woolley, 2010; Woolley and Casseday, 2005; 2004; Woolley et al., 2005; Woolley et al., 2006), primary forebrain (Cruikshank and Weinberger, 1996; Sen et al., 2001; Wang et al., 2007; Woolley et al., 2005; Woolley et al., 2009), higher-order forebrain regions (Gentner and Margoliash 2003; Gill et al., 2008; Nishikawa and MacIver, 2000; Rutkowski et al., 2002) and sensorimotor regions (Coleman et al., 2007; Margoliash, 1983; 1986). While urethane has been hypothesized to affect synaptic activity less than barbiturates (Franks and Lieb, 1994; Nishikawa and MacIver, 2000; Pittson et al., 2004; Scholfield, 1980), it depresses spontaneous and evoked firing rates (Albrecht and Davidowa, 1989; Capsius and Leppelsack, 1996), leaving open the possibility that urethane influences sensory tuning. While the mechanisms of urethane-induced depression have been explored at the cellular and molecular levels (Sceniak and MacIver, 2006) it remains unknown to what extent stimulus coding properties are altered by urethane.

To test how the auditory encoding of complex natural and simple synthetic sounds varies depending on anesthetic state, we recorded *in vivo* electrophysiological responses of single auditory neurons in the midbrain nucleus mesecephalicus lateralis pars dorsalis (MLd) to songs and pure tones, in urethane-anesthetized and unanesthetized zebra finches. Songbirds are model organisms for understanding the neural encoding of acoustically complex, learned communication vocalizations (Doupe and Kuhl, 1999; Konishi, 1989; Nottebohm, 1970), and their auditory systems are well characterized (Theunissen and Shaevitz, 2006). We measured spontaneous and stimulus-evoked firing rates, spectrotemporal receptive fields (STRFs), and neural discrimination from midbrain responses to conspecific song. In the same neurons, we recorded responses to pure tone stimuli to test whether spectral tuning, stimulus thresholds, and temporal response properties were altered under urethane. Lastly, we compared the representations of individual songs between anesthetized and awake neuronal populations. Our

results indicate that urethane depresses intrinsic neural excitability, but leaves spectral tuning and neural discriminability intact in single neurons.

2.3 Materials and Methods

All procedures were done in accordance with the NIH and Columbia University Animal Care and Use Policy. Adult male zebra finches (*Taeniopygia guttata*) were used, and were either purchased from a bird farm (Canary Bird Farm, Old Bridge, NJ) or were bred and raised in the Columbia University zebra finch colony. Prior to electrophysiological recordings, birds lived in a large aviary with other male zebra finches, where they received food and water *ad libitum*, as well as vegetables, eggs, grit and calcium supplements.

Surgery

Two days prior to recording, birds were anesthetized with a single intramuscular injection of 0.04 cc Equithesin (0.85 g chloral hydrate, 0.21 g pentobarbital, 0.42 g MgSO4, 8.6 ml propylene glycol, and 2.2 ml of 100 percent ethanol to a total volume of 20 ml with H_2O). Following lidocaine application, feathers and skin were removed from the skull and the bird was placed in a custom-designed stereotaxic holder with its beak pointed 45 degrees downward. For anesthetized recordings, small openings were made in the outer layer of the skull directly over the electrode track locations. For unanesthetized recordings, full craniotomies were made over the electrode tracks. To guide electrode placement during recordings, ink dots were applied to the skull at stereotaxic coordinates (2.7 mm lateral and 2.0 mm anterior from the bifurcation of the sagittal sinus). A small metal post was then affixed to the skull using dental acrylic, and a grounding wire was cemented in place with its end just beneath the skull, approximately 5 to 10

mm lateral to the junction of the midsagittal sinus. After surgery, the bird recovered for two days.

Stimuli

Song stimuli consisted of samples of the songs recorded from 20 different adult male zebra finches sampled at 48,828 Hz and frequency filtered between 250 and 8000 Hz. Songs were presented from a free field speaker at an average intensity of 72 dB SPL and in pseudorandom order for a total of 10 trials each (Fig. 2.1). All songs were balanced for RMS intensity. Songs ranged in duration between 1.62 and 2.46 seconds, and a silent period of 1.2 to 1.6 seconds separated the playback of subsequent songs. All songs were unfamiliar to the bird from which electrophysiological recordings were made.

Pure tone stimuli (0.5 – 8.0 kHz) were presented at sound levels between 20 and 90 dB. Tones were 220 ms in duration, including 10 ms cosine ramps at the beginning and end. Tone stimuli were separated by silent periods of 0.4 to 0.5 seconds.

Recordings

The recording chamber was a walk-in sound attenuation booth (Industrial Acoustics Company). Single neuron activity was recorded extracellularly in MLd using either tungsten microelectrodes (FHC, Inc.) or glass pipettes filled with physiological saline (Sutter Instruments). For some recordings, pipette electrodes also contained 0.5% biotinylated dextran amine to mark electrode locations by iontophoretic injection. For both glass and tungsten recordings, electrode resistance was between 3 and 20 MOhms (measured at 1 kHz). Electrode

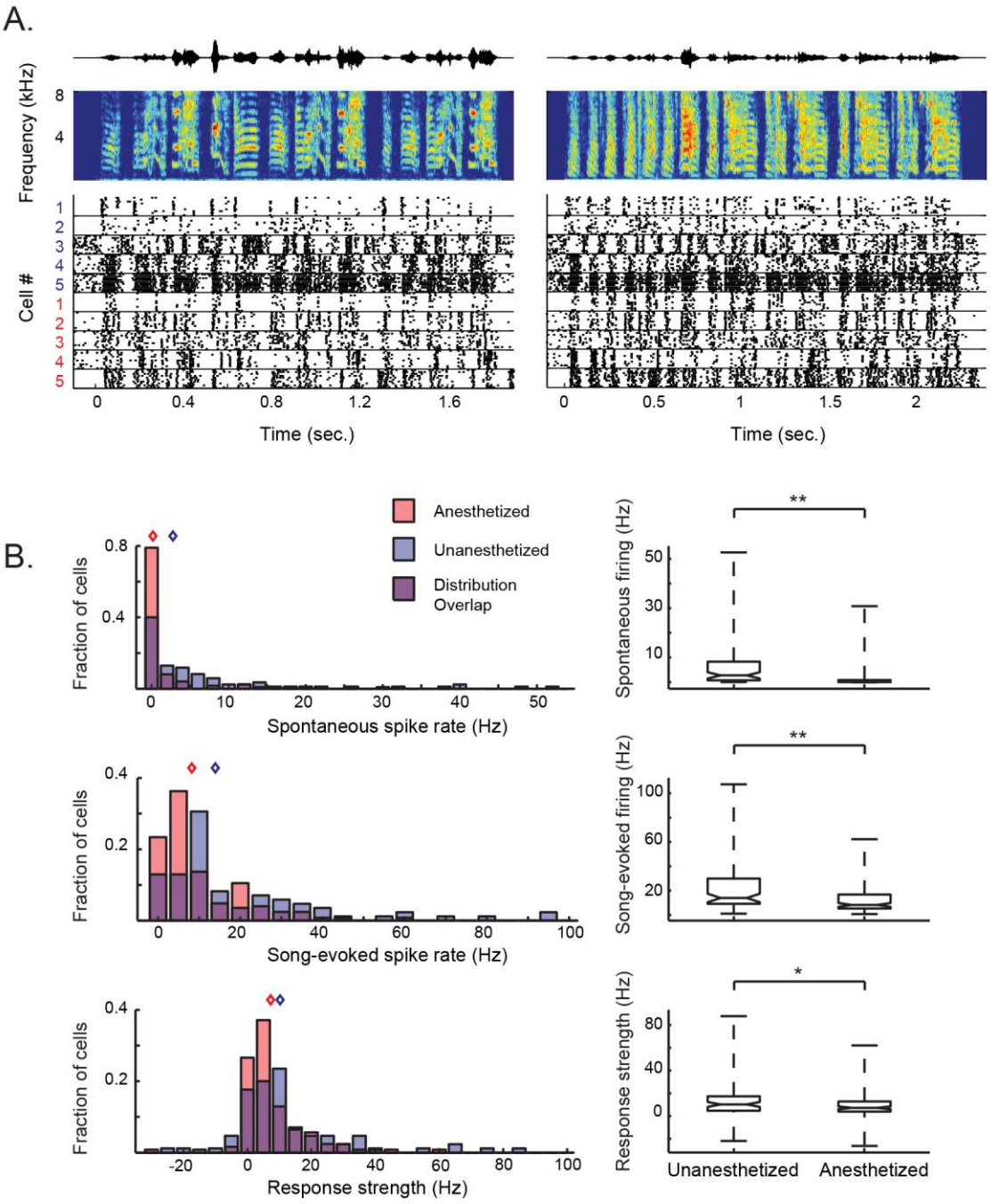

Figure 2.1 Neural responses to conspecific song vary across cells and are depressed in anesthetized neurons. **A.** Stimulus waveforms (top), song spectrograms (middle) and raster plots representing 10 cells' responses to 10 presentations of 2 conspecific songs. Unanesthetized (blue) and anesthetized (red) units each produce robust spiking responses, and show variable levels of spontaneous and song-evoked firing. **B.** Distributions and box plots of spontaneous firing rates (top), song-evoked firing rates (middle), and response strength (bottom) plotted as overlapping histograms. Blue histograms indicate unanesthetized units, red histograms indicate anesthetized units, and purple areas show distribution overlaps. Blue and red diamonds indicate median values for unanesthetized and anesthetized groups, respectively. Anesthetized units (n =

(**Figure 2.1, cont.)** 124) had significantly lower spontaneous firing rates, song-evoked firing rates, and response strength than unanesthetized units (n = 85). * $P < 0.05$; ** $P < 0.0001$

signals were amplified (1000x) and filtered (300-5000 Hz; A-M Systems). During recording, voltage traces and action potentials were monitored using an oscilloscope (Tektronix), custom software (Python; Matlab, The Mathworks), and an audio amplifier and loudspeaker. Spike times were detected using a threshold discriminator and spike waveforms were saved for offline sorting and analysis. For offline sorting, spike waveforms were upsampled 4x using a cubic spline function (Joshua et al., 2007). Action potentials were separated from non-spike events by waveform analyses and cluster sorting using the first three principal components of the action potential waveforms (custom software; Matlab, The Mathworks).

In preparation for anesthetized electrophysiological recordings, the bird was given three intramuscular injections of 0.03 ml of 20 percent urethane, separated by 20 minutes. All birds were wrapped in a blanket and then head-fixed in a custom stereotaxic device. For anesthetized recordings, the bird's body temperature was monitored by placing a thermometer underneath the wing and was maintained between 38 and 40 degrees Celsius using an electric heating pad (A-M Systems). Restrained birds were placed on a table near the center of the room and a single speaker was located 23 cm directly in front of the bird. Neurons were recorded bilaterally and were sampled throughout the extent of MLd, which is located approximately 5.5 mm ventral to the dorsal surface of the brain. We recorded from all neurons within MLd that were driven or inhibited by any of the search stimuli. Isolation was ensured by calculating the signal-to-noise ratio of action potential and non-action-potential events and by monitoring baseline firing rate throughout the recording session.

Amplitude-modulated (AM) white noise was used as a search stimulus while approaching MLd. When background multiunit activity was detected, electrode depths were recorded as an approximation of the depth of the dorsal surface of MLd. Search stimuli including conspecific songs, modulation limited noise, and AM white noise were then used to isolate individual neurons.

Data analysis

Spectrotemporal receptive field estimation. We calculated spectrotemporal receptive field (STRF) by fitting a generalized linear model (GLM), a generalization of the classical linear-nonlinear-Poisson cascade model (Paninski, 2004). This approach has been described previously (Calabrese et al., 2010). Briefly, the GLM describes a neuron's response as a function of the stimulus and three sets of fitted parameters: 1) the stimulus filter, or STRF; 2) a post-spike filter which captures the dependency of the neural response on spiking history (e.g. refractoriness or burstiness); and 3) an offset term that captures the baseline firing of the model. For each neuron, a static nonlinear function (exponential) is applied to the filtered stimulus to obtain an instantaneous spike rate (Paninski et al., 2007; Truccolo et al., 2005). To fit the model parameters, stimuli were computed as log spectrograms (Gill et al., 2006) and responses were binned at 3 ms resolution. The spectral domain of the stimulus was divided into 20 equally spaced bins, which spanned frequencies from 250 to 8000 Hz. Model parameters were fit to the resampled stimuli and responses using custom maximum penalized likelihood algorithms (Calabrese et al., 2010).

STRF tuning measures. To compare spectrotemporal tuning under unanesthetized and anesthetized conditions, we measured four STRF tuning properties (Fig. 2.2) commonly used to

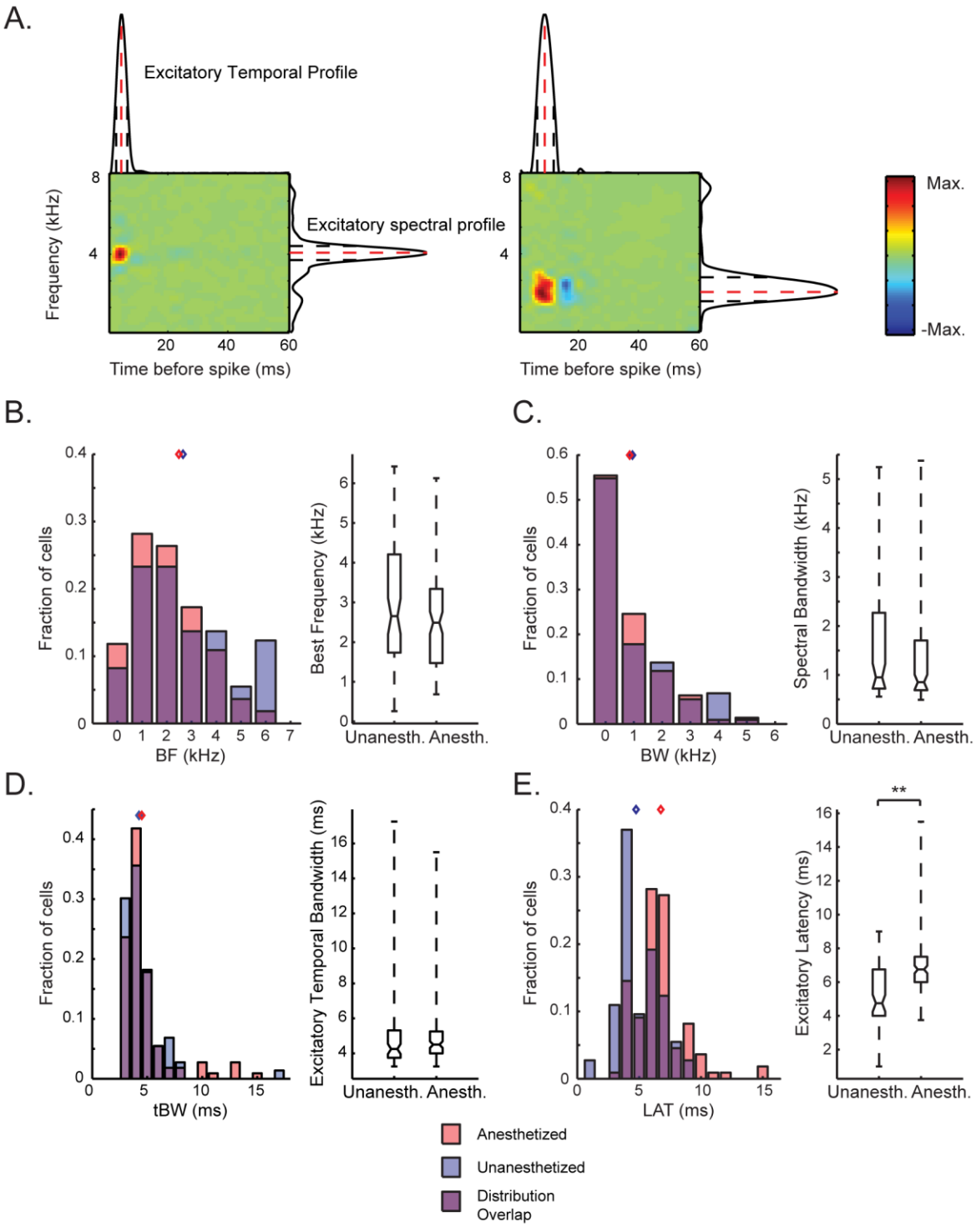

Figure 2.2 STRF tuning properties. **A.** STRF tuning measures are plotted along the axes of representative STRFs estimated from unanesthetized (left) and anesthetized (right) responses to conspecific song. Color denotes excitatory (red) and inhibitory (blue) regions of the STRFs, normalized to the peak value of each STRF. Dashed black lines demarcate the bandwidths calculated from spectral (BW) and temporal (tBW) axes. Red dashed lines illustrate BF and

(Figure 2.2, cont.) LAT relative to the spectral and temporal axes, respectively. **B-E.** Tuning parameters are displayed as overlapping histograms (unanesthetized = blue; anesthetized = red; overlap = purple). Blue and red diamonds indicate median values for unanesthetized and anesthetized groups, respectively. **B.** BF. **C.** BW. **D**. tBW. **E.** LAT was shorter in unanesthetized neurons than in anesthetized neurons, indicating longer response latencies under urethane anesthesia. ** $P < 0.0001$

characterize auditory neurons (Capsius and Leppelsack, 1996; David et al., 2009; Escabi and Read, 2003; Woolley et al., 2006): 1) best excitatory frequency (BF), the spectral frequency that evokes the strongest neural response; 2) excitatory spectral bandwidth (BW), the range of frequencies that are associated with an increase from mean firing rate; 3) excitatory temporal bandwidth (tBW), the span of time over which relevant frequencies lead to an increase from mean firing rate; and 4) latency to excitation (LAT), the time at which relevant stimulus features excite the neuron (response latency). For the tuning measures, GLM STRFs were up-sampled (3x) such that they had 1 ms temporal resolution, and 60 equally spaced spectral bins from 250 to 8000 Hz. BF was measured by setting negative STRF values to zero and averaging along the time axis. The resulting spectral tuning curve was convolved with a 5-point symmetric Hanning window, and the BF was taken to be the position (Hz) of the peak of the smoothed curve. The BW was measured from the smoothed curve as the width (Hz) at half-height of the curve. The tBW was measured by setting all negative STRF values to zero and averaging along the spectral axis. The resulting temporal tuning curve was convolved with a 5-point symmetric Hanning window, and the tBW was measured from the smoothed curve as the width (ms) at half-height. LAT was measured as the position (ms) of the peak of the smoothed curve.

Neurometric analysis. To quantify the ability of single neurons to discriminate among song stimuli, we implemented a K-means neurometric that classifies spike trains into K clusters based on their proximity to one another in a high dimensional space, where K is the number of stimuli presented (Schneider and Woolley, 2010). Briefly, as with van Rossum's (2001) spike

train distance metric, the K-means metric uses Euclidean distance to measure spike train similarity. Spike trains were smoothed using an exponential decay (t = 10 ms), and then iteratively clustered into K groups (Duda et al., 2001). Clusters were initially seeded with K randomly selected spike trains (1 randomly selected for each stimulus) as cluster centers. Each remaining spike train was assigned a cluster based on the seed with the closest proximity. After this initial clustering, cluster centers were recalculated as the geometric mean of the spike trains within that cluster. Spike trains were then re-clustered with the new cluster centers, and this process was reiterated until a set of K clusters was converged upon. A measure of percent correct discrimination was calculated by analyzing the spike trains that belonged to each of the K clusters. Clusters were assigned a song label via a voting scheme in which each spike train in the cluster voted for the song that evoked it. Each cluster was assigned to the song that cast the most votes, and if more than one cluster had the same number of votes for a song, then the cluster with the fewest spike trains from any other song was assigned to the original song, and the other cluster was assigned to the song with the second largest spike train representation. If each cluster contained spike trains from a single song, the neuron had 100% correct discrimination. If one or more spike trains were misclassified, percent correct decreased toward chance (100%/K = 5%). The K-means neurometric was iterated 100 times. K-means was seeded with a different set of spike trains in each iteration. The resulting discrimination values are the mean performance across all 100 iterations. On a given iteration, if a spike train was equally similar to two or more templates, that spike train was scored as misclassified even if one of the templates represented the appropriate song category. We used this assignment criterion because ambiguity suggests poor discriminability.

We also calculated *d'* as a measure of discriminability that provided no upper bound to the estimate of a neuron's discrimination performance. To calculate *d'*, we first smoothed each spike train with an exponential decay (τ = 10 ms) and projected the spike trains from two stimuli onto a single vector that connected the average neural response for each stimulus, which is equal to the average smoothed spike train in response to that song. We then fit a normal distribution to each of the clusters and measured the *d*' between the clusters, which is the distance between the cluster means normalized by the variance of the clusters (Schneider and Woolley, 2010). For each neuron we calculated *d'* for every pair of clusters, and averaged across all pairs.

Population analysis. We assessed neural population-level response properties under unanesthetized and anesthetized conditions by constructing neurograms and population PSTHs (pPSTHs). Each row of a neurogram consisted of the log of the time-varying PSTH of a single neuron for a single stimulus (10 trials per stimulus). Unanesthetized and anesthetized neurograms were matched for BF and contain the same number of cells (73), and neurogram rows were ordered by BF.

The pPSTHs were calculated for each song stimulus as the average PSTHs for the neural responses represented in the neurograms. For each of the unanesthetized and anesthetized neuronal populations, there were 20 pPSTHs because there were 20 song stimuli. To evaluate the degree of similarity or difference between unanesthetized and anesthetized pPSTHs for a given stimulus, we first estimated the time lag between the two by taking the cross-correlation of the unanesthetized and anesthetized pPSTHs:

$$R_{xy}(t) = \sum_{t=0}^{N-t-1} x_{t+t} y_t \qquad \textbf{[1],}$$

where x and y are, respectively, the unanesthetized and anesthetized pPSTHs during the duration of the stimulus. The time lag between x and y is then computed as the value of t that maximizes

R_{xy}. Negative values of t indicate that y lags behind x, positive values of t indicate that x lags behind y, and t equal to zero indicates no time lag between the two. We calculated correlation coefficients between unanesthetized and anesthetized pPSTHs after correcting for the optimal time lag.

We assessed stimulus discriminability performance at the population level by again calculating *d'*, however rather than computing *d'* within a single cell, we calculated stimulus discriminability by comparing the PSTHs between individual neurograms.

Frequency response area and tone tuning estimation. For a subset of the recorded neurons, we calculated frequency response area (FRA) functions from responses to repeated presentations of pure tones ranging from 500 to 8000 Hz (500 Hz increments) and intensities from 20 to 90 dB SPL (10 dB increments), for a total of 128 frequency-intensity combinations. These frequency-intensity ranges and increments were chosen based on previous work on tone tuning in the auditory midbrain (Woolley and Casseday, 2004). Frequency-intensity combinations were presented in pseudorandom order for 10 repetitions or until enough data were collected to acquire well defined FRA plots. FRA plots depict the average response at each frequency-intensity combination.

FRAs were upsampled 3X along the frequency and intensity dimensions to increase tone tuning resolution. To derive tone tuning curves from upsampled FRAs, we defined a significant excitatory response threshold as being equal to the spontaneous firing rate plus 20% of the peak driven firing rate (Sutter and Schreiner, 1991). Responses to frequency-intensity combinations that met this criterion were considered to fall within the tuning curve of the neuron. We measured four response properties from the pure tone tuning curves: 1) characteristic frequency (CF) was defined as the frequency (Hz) at which the lowest sound pressure level was necessary

to evoke a significant excitatory response; 2) best frequency (BF) was defined as the frequency that evoked the largest response when summed across all levels; 3) threshold was defined as the minimum intensity to evoke a significant excitatory response; 4) bandwidth (BW) was defined as the width in Hz of the tuning curve at 70 dB SPL, 90 dB SPL, and 20 dB above threshold.

Matching for BF. We matched unanesthetized and anesthetized units for BF for our analysis of tone tuning response properties. First, we compared the distributions of unanesthetized and anesthetized BFs using a Mann-Whitney U test. If this test showed significantly different distributions of BFs between groups, then we used this information to remove a single data point at random from a specified bin of either the unanesthetized or anesthetized populations, depending on the disparity between the two distributions. This iterative process was repeated until the Mann-Whitney U test had a non-significant *P* value.

Temporal response patterns. We determined temporal response patterns of individual neurons by averaging the PSTHs at the BF of the FRA at intensities that evoked a significant excitatory response. We defined the onset period of the response as the first 50 ms of the stimulus presentation, and the sustained period of the response as the second 100 ms of the stimulus presentation (modified from Wang et al., 2005). Neurons were then classified into three categories: 1) onset neurons responded strongly at the stimulus onset, but fired no or few action potentials during the sustained period; 2) primary-like neurons fired robustly in the onset period, and significantly but less during the sustained period; 3) sustained neurons had consistent firing rates during the onset and sustained periods.

To quantify the temporal response patterns, we used an onset index, O_{index}, defined as the onset firing rate minus the sustained firing rate, divided by the sum of the onset and sustained firing rates:

$$O_{index} = \frac{Onset_{FR} - Sustained_{FR}}{Onset_{FR} + Sustained_{FR}}, \quad \textbf{[2]}$$

where values could range from -1 (no onset response, significant sustained response) to 1 (significant onset response, no sustained response). O_{index} values between 0 and 1 represent a spectrum of response types from sustained (O_{index} = zero), to primary-like ($0 < O_{index} < 1$), to onset ($O_{index} = 1$).

Spike latency. Because we observed a variety of spontaneous firing rates, the calculation of spike latency used a binless algorithm designed to discriminate between spontaneous and stimulus-evoked action potentials. This method has been described previously (Bair and Koch, 1996) and has been applied to spike trains collected from inferior colliculus neurons (Chase and Young, 2007). Briefly, the algorithm compares the observed spiking activity over several time windows with the activity that would be expected if the neuron were firing spontaneously with Poisson statistics. The first time at which the spiking activity significantly deviated from spontaneous Poisson activity ($P < 10^{-6}$) was considered the latency for the neuron (Bair and Koch, 1996; Chase and Young, 2007). In the event that the threshold was not exceeded in the first 50 ms, the latency was undefined. For each neuron, the value of the first spike latency was calculated using all significant

2.4 Results

Urethane depresses firing rate

We recorded extracellular action potentials from 208 MLd neurons. Eighty five neurons were from 9 unanesthetized birds, and 123 neurons were from 31 anesthetized birds. We refer to birds as unanesthetized rather than "awake" because signs of wakefulness, such as eye openings and movement, varied throughout recording sessions. To measure the response properties of these neurons to complex time-varying stimuli, we recorded spike trains in response to 10 repetitions (trials) of 20 different zebra finch songs presented in pseudo-random order. Robust stimulus-locked responses were observed in both anesthetized and unanesthetized recordings (Fig. 2.1A).

To determine the effect of urethane on auditory responses to complex, natural sounds in MLd, we measured spontaneous and song-evoked firing rates during presentations of conspecific song. Anesthetized recordings yielded lower spontaneous ($p < 0.0001$, Mann-Whitney U Test; Fig. 2.1B, top panel) and song-evoked firing rates ($p < 0.0001$, Mann-Whitney U Test; Fig. 2.1B, middle panel). Response strength, defined as the evoked rate minus the spontaneous rate, was also slightly but significantly lower in anesthetized cells ($p = 0.039$, Mann-Whitney U Test; Fig. 2.1B, bottom panel). These results are consistent with previous studies; depression of spontaneous and stimulus evoked firing rates has been widely reported in urethane-anesthetized preparations (Albrecht and Davidowa, 1989; Capsius and Leppelsack, 1996; Girman et al., 1999; Sceniak and MacIver, 2006). These results indicate that, like most other systems investigated under urethane anesthesia, neural excitability is depressed in the anesthetized songbird MLd.

Effect of urethane on spectrotemporal tuning during song coding

To determine the effects of urethane anesthesia on spectral and temporal tuning during vocal processing, we calculated STRFs from responses to 20 conspecific songs (Calabrese et al., 2010). Tuning measures were analyzed only if their GLM-predicted responses matched their actual responses with a correlation coefficient of at least 0.3 (unanesthetized n = 73, 82.4%; anesthetized n = 110, 88.7%). We then measured spectrotemporal tuning properties including BF, BW, tBW, and LAT (Fig. 2.2A).

To determine if spectral tuning to complex stimuli differed in unanesthetized and anesthetized neurons, we compared BFs and BWs between the two groups. Median values and interquartile ranges for the BF of unanesthetized and anesthetized neurons were 2.65 kHz (1.74 – 4.21 kHz) and 2.48 kHz (1.47 – 3.34 kHz), respectively, and did not differ ($p > 0.05$, Mann-Whitney U test; Fig. 2.2B). This indicates that at the population level, MLd neurons are maximally tuned to frequencies that cover most of the range of zebra finch hearing (Okanoya and Dooling, 1987) in both anesthetized and unanesthetized birds. While BF did not differ between unanesthetized and anesthetized neurons, Figure 2.2B shows that we recorded a larger proportion of neurons tuned to 6 kHz or higher in unanesthetized units. This is most likely due to an anatomical sampling bias; because global activity in MLd is much higher in unanesthetized birds, single cell isolation was easiest in ventral regions where cell density is sparsest and neurons are tuned to higher frequencies (Woolley and Casseday, 2004). Median values and interquartile ranges for the BW of unanesthetized and anesthetized neurons were 0.95 kHz (0.72 - 2.27 kHz) and 0.85 kHz (0.69 – 1.71 kHz), respectively, and were not significantly different ($p = 0.22$, Mann-Whitney U test; Fig. 2C). These results indicate that the spectral tuning MLd neurons is not altered by urethane anesthesia.

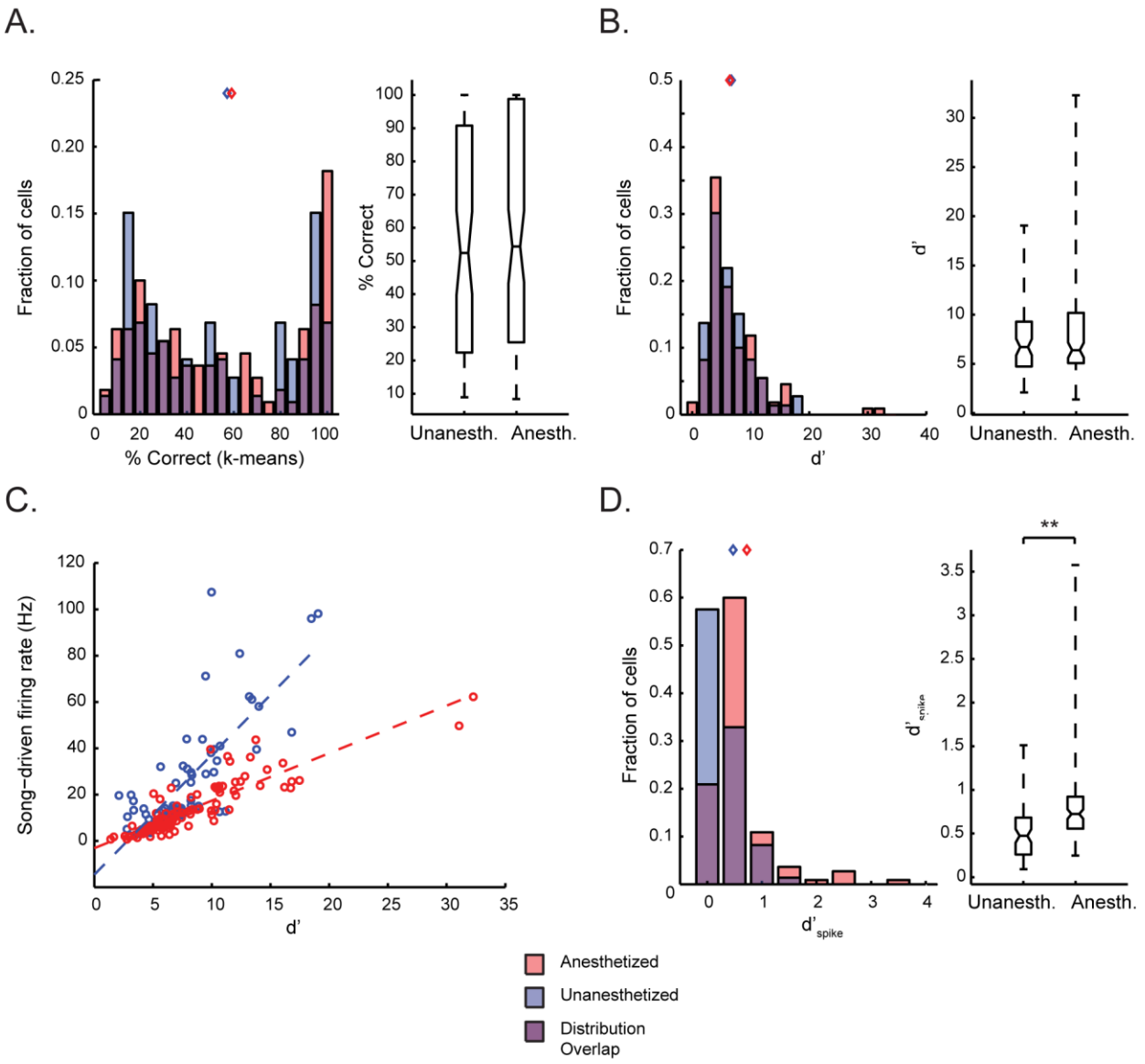

Figure 2.3 Neural discriminability performance is not affected by urethane anesthesia. Distributions of performance from discriminability metrics are plotted as overlapping histograms. Blue and red diamonds indicate median values for unanesthetized and anesthetized groups, respectively. **A.** K-means % correct did not differ between unanesthetized and anesthetized recordings. **B.** d' values for single neuron discriminability did not differ between unanesthetized and anesthetized recordings. **C.** The relationship between d' performance and driven firing rate is highly linear in both unanesthetized ($P < 0.0001$; r-square = 0.63) and anesthetized ($P < 0.0001$; r-square = 0.77) recordings, but the two groups share different slopes with respect to this relationship. **D.** Rate normalized d', d'spike, was higher for anesthetized MLd neurons, indicating that discriminability is more efficient under urethane anesthesia. ** $P < 0.0001$

Next we asked if temporal tuning measured from responses to song was affected by anesthetic state. Median values and interquartile ranges for unanesthetized and anesthetized tBW were 4.25 ms (3.75 – 5.31 ms) and 4.5 ms (4 – 5.25 ms), respectively, and were not significantly different ($p = 0.52$, Mann-Whitney U test; Fig. 2.2D). This suggests that the time frames over which acoustic stimuli are integrated into excitatory responses are indistinguishable for unanesthetized and anesthetized MLd neurons. However, LAT did differ ($p < 0.0001$, Mann-Whitney U test; Fig. 2.2E), indicating that unanesthetized MLd neurons typically responded faster to the onset of excitatory acoustic features. Median values and interquartile ranges for unanesthetized and anesthetized neurons were 4.75 ms (4 – 6.75 ms) and 6.75 ms (6 – 7.5 ms), respectively, suggesting that intrinsic excitability was depressed in anesthetized neurons.

Urethane does not affect neural discrimination of songs in single MLd neurons

To quantify the ability of single neurons to discriminate among song stimuli, we used the K-means neurometric and computed *d'* for the neurons used in the STRF analysis. Median K-means performance values and interquartile ranges for unanesthetized and anesthetized neurons were 52.43% (22.37% - 90.80%) and 54.36% (25.49% - 98.83%), respectively, and were not significantly different ($p = 0.31$, Mann-Whitney U test, Fig. 2.3A). Similar results were obtained with the *d'* metric, where median values and interquartile ranges for unanesthetized and anesthetized neurons were 6.71 (4.74 – 9.28, a.u.) and 6.39 (5.08 – 10.18, a.u.), respectively. These distributions were not significantly different ($p = 0.75$, Mann-Whitney U test, Fig. 2.3B).

We observed that *d'* had a strong positive correlation with song driven firing rate in unanesthetized (linear regression: $p < 0.0001$, $r^2 = 0.63$) and anesthetized (linear regression: $p <$

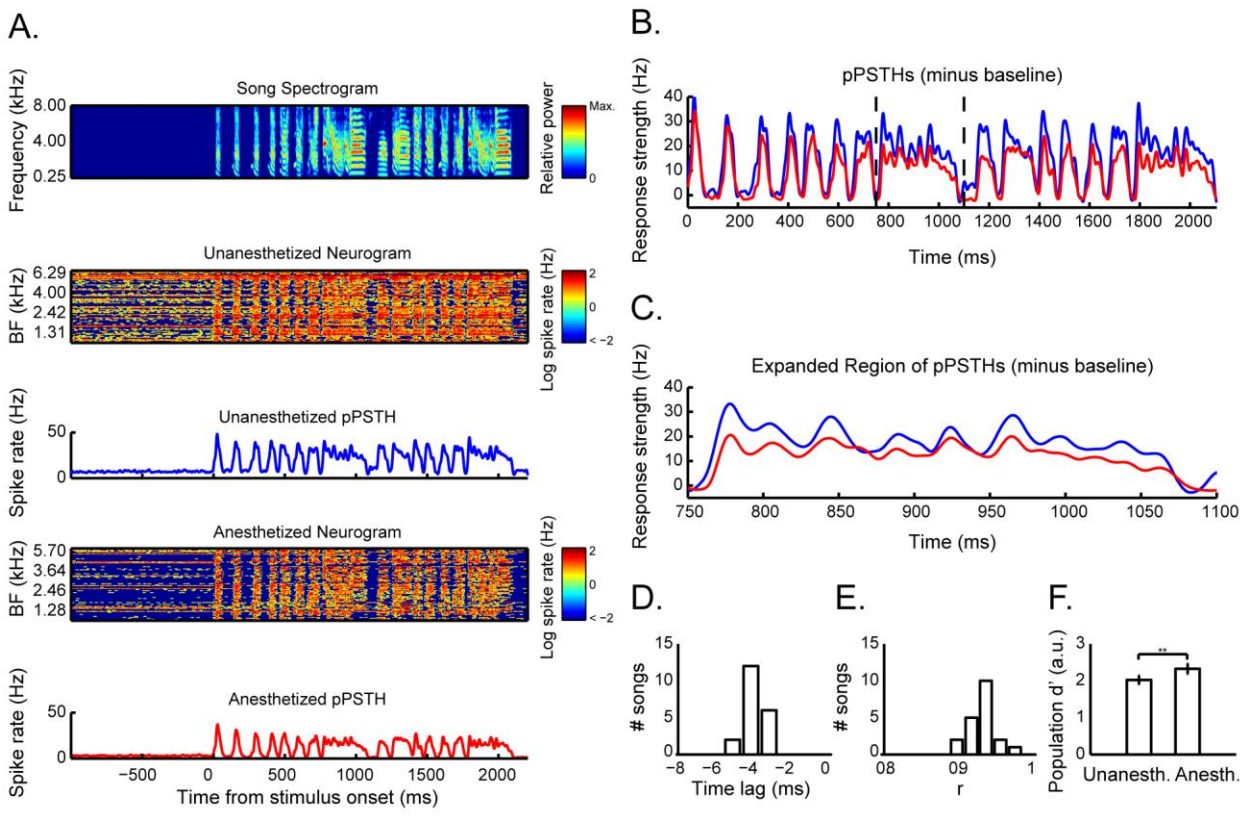

Figure 2.4 Population responses are time-lagged but show conserved temporal structure under anesthesia. **A.** A sample song spectrogram (top; color denotes relative power) is aligned with unanesthetized and anesthetized neurograms and their corresponding pPSTHs (blue and red, respectively). Each row of each neurogram represents the log of the instantaneous firing rate of an individual neuron (n = 73 per neurogram), arranged in order of their STRF BFs. Spontaneous and driven responses are distributed across the frequency range in both unanesthetized and anesthetized units. The unanesthetized neurogram is characterized by strong driven firing on top of considerable noise. **B.** Unanesthetized (blue) and anesthetized (red) pPSTHs for the same song shown in A are aligned by subtracting mean spontaneous firing rate. The red trace follows the blue trace with an apparent time lag. **C.** The region delimited by black dashed lines in **B** is expanded. **D.** The distribution of t values corresponding to the lags in the cross correlation of pPSTHs for the 20 song stimuli is entirely below zero, and has a median t of -4 ms ($p < 0.0001$, Wilcoxon signed rank test for zero median). **E.** The distribution of lag-corrected correlation coefficients, with a mean of 0.9346 (±0.02 s.d.), indicates that the temporal patterns of the average neural responses to songs are highly similar in unanesthetized and anesthetized populations. **F.** Median d' values for the unanesthetized population were significantly lower than in the anesthetized population, indicating that stimulus representations are more easily distinguishable in anesthetized neurons. ** $P < 0.0001$

0.0001, $r^2 = 0.77$) neurons, but the individual "firing rate/ *d'* " regressions had visibly different slopes (Fig 3C). Although neural discrimination did not differ between the two groups, we reasoned that this change in slope could indicate differential coding efficiency between groups. Figure 2.3C shows that increases in firing rate lead to minimal gains in *d'* discriminability in the unanesthetized cells compared to anesthetized cells. To quantify this relationship further, we calculated a metric of neural discrimination efficiency, d'_{spike}, in which *d'* was normalized by driven firing rate. Median d'_{spike} values and interquartile ranges for unanesthetized and anesthetized neurons were 0.47 (0.26 – 0.68, a.u.) and 0.72 (0.56 – 0.92, a.u.), respectively, and the difference was highly significant ($p < 0.0001$, Mann-Whitney U test; Fig. 2.3D). This indicates that, in the context of neural discrimination, unanesthetized neurons are less efficient than anesthetized units; the firing of action potentials is metabolically costly for a neuron and for unanesthetized neurons. Interestingly, despite this diminished efficiency in unanesthetized comparable levels of spiking activity yield greater discriminability for anesthetized neurons than neurons, their higher firing rates lead to no overall difference in neural discrimination performance when compared to anesthetized neurons.

Urethane preserves temporal response patterns while inducing a time lag and enhancing stimulus discrimination in neural populations

We tested whether urethane anesthesia alters the neural representation of communication vocalizations at the population level. We computed BF- and sample size-matched neurograms and pPSTHs for unanesthetized and anesthetized populations (Methods, Fig. 2.4A). Unanesthetized neurograms appear noisier, and reflect the higher spontaneous and evoked firing

rates reported above. The average temporal patterns of activation depicted by the pPSTHs were strikingly similar between the unanesthetized and anesthetized populations, but anesthetized pPSTHs showed visible time lags (Fig. 2.4B, 2.4C). We computed the time lag, t, that maximizes the correlation between unanesthetized and anesthetized pPSTHs for each stimulus using cross-correlation (Methods). The median value of the optimal t was -4 ms ($P < 0.0001$, Wilcoxon signed rank test for zero median; Fig. 2.4D). These results correspond with the shorter spike latencies observed in anesthetized STRFs (Fig. 2.2E). For each unanesthetized-anesthetized pPSTH pair, we computed the correlation coefficient, *r*, after correcting for the corresponding time lag. The mean lag-corrected *r*-value was 0.9346 (±0.02 s.d.) indicating that populations of anesthetized and unanesthetized midbrain neurons produce highly similar neural representations of communication vocalizations.

To quantify stimulus discriminability at the population level, we calculated the *d*' values between pairs of neurograms within the unanesthetized and anesthetized populations. Our estimate of population *d*' was essentially identical for single unit *d*', substituting single trials within a single cell with PSTHs across multiple cells. Median and interquartile range values for population *d*' in unanesthetized and anesthetized populations were 2.02 (1.94 - 2.12) and 2.33 (2.24 - 2.42) and were significantly different ($P < 0.0001$; Mann-Whitney U test, Fig. 2.4E), indicating that midbrain neural discriminability is enhanced by urethane anesthesia at the population level. This seemingly contrasts with our finding that unanesthetized and anesthetized single neurons have comparable neural discriminability at the single unit level, but may indicate that aggregate neural activity in unanesthetized birds is noisier than in urethane-anesthetized birds. This is consistent with our finding of differential discrimination efficiency in single units.

Urethane does not affect spectral bandwidth in responses to pure tones

We asked if the decreased firing rates in response to song stimuli corresponded to changes in responsiveness to simple pure tone stimuli. For a subset of neurons (65 out of 85 unanesthetized and 115 out of 124 anesthetized), we recorded responses to pure tones (Methods). Responses to pure tones yielded well-defined FRAs for both unanesthetized and anesthetized MLd neurons (Fig. 2.5A). We then used the responses to tones to measure tone tuning (Fig. 2.5B, 2.6), temporal response profiles (Fig. 2.5C, 2.7A), and spike latencies (Fig. 2.8). Because of the known tonotopy of MLd along the dorsal-ventral axis (Woolley and Casseday, 2004), the anesthetized and unanesthetized groups were first matched for BF (Methods) to account for a potential anatomical sampling bias between the two groups. The process of matching for BF then reduced our data set to 63 unanesthetized and 91 anesthetized units. After matching for BF across the two populations of single neurons, BF and CF (by design) did not differ between unanesthetized and anesthetized neurons ($p > 0.05$, Mann-Whitney U test; Fig. 2.6A, 2.6B). Medians and interquartile ranges for unanesthetized and anesthetized tone BFs were 3 (2.33 – 4) and 2.5 (2 – 3.63) Hz, respectively. Median and interquartile range values for unanesthetized and anesthetized CFs were 3 (2.33 – 4.17) and 2.5 (2 – 3.75) Hz, respectively.

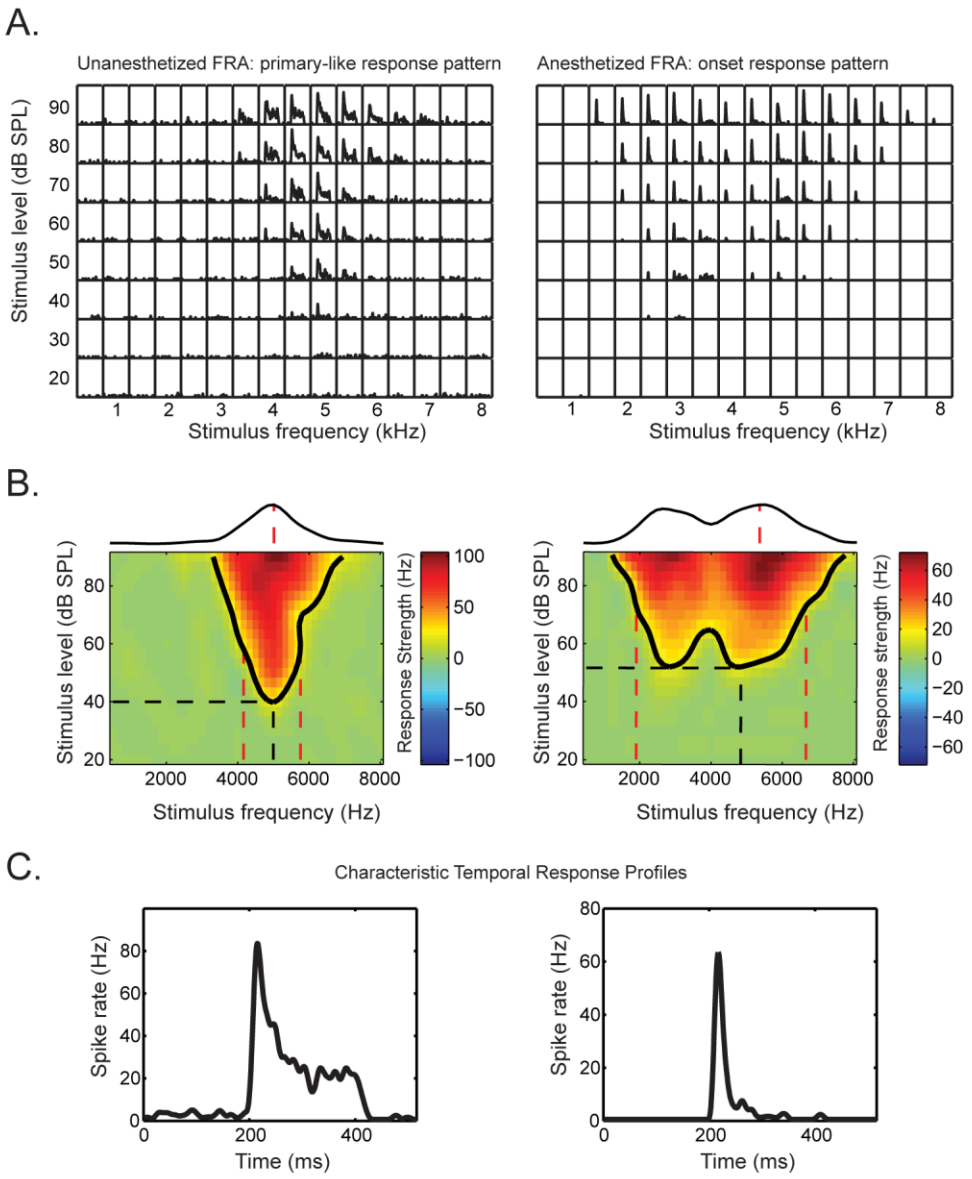

Figure 2.5 Frequency-response area tuning and temporal response profiles in single neurons. **A.** Representative FRA plots for a single unanesthetized (left) and a single anesthetized unit (right). Neurons were presented with 220 ms pure tone stimuli at 128 frequency (0.5 to 8 kHz) and intensity (20 to 90 dB SPL) combinations. **B.** FRAs were computed as color maps of response strength and were upsampled 3x in the frequency and intensity dimensions. Black contour lines mark boundaries of significant response strengths (at least 20% of the maximum evoked spike rate, above baseline). Color map FRAs from **A** are displayed with their measured tuning properties. CF and intensity threshold are plotted as dashed black lines along their respective axes. Spectral bandwidth at 20 dB above threshold is the distance between the two dashed red lines in the FRA. The normalized sum of the FRA along the intensity axis is above the FRA. A dashed red line at the peak along the frequency axis indicates BF**. C.** Characteristic temporal patterns of the two neurons were calculated as the average PSTH at BF.

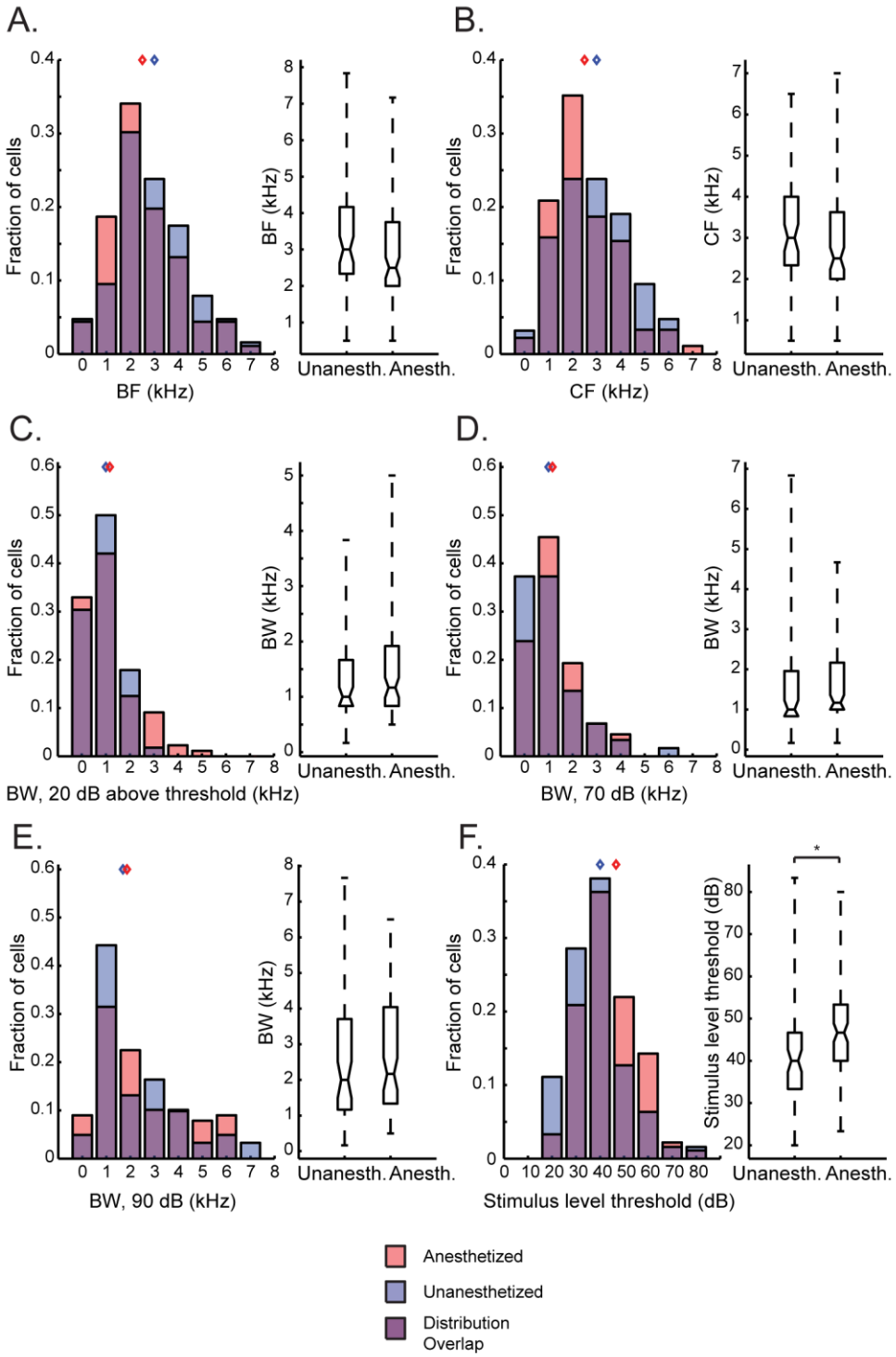

Figure 2.6. Pure tone tuning properties of BF-matched samples of anesthetized (n = 91) and unanesthetized (n = 63) MLd neurons. Tuning property distributions are displayed as overlapping histograms and box plots; red histograms indicate anesthetized units, blue

(Fig. 2.6 cont.) histograms indicate unanesthetized units, and the purple area indicates overlap in the distributions. Blue and red diamonds indicate median values for unanesthetized and anesthetized groups, respectively. **A.** BF. **B.** CF. **C.** BW at 20 dB above threshold. **D.** BW at 70 dB. **E.** BW at 90 dB. Tuning properties in **A – E** did not differ between unanesthetized and anesthetized units in the BF-matched samples**. F.** The average stimulus intensity threshold was lower for unanesthetized units than anesthetized units indicating that unanesthetized cells can respond to weaker inputs than anesthetized cells. * $P < 0.01$

BW at 20 dB above threshold did not differ between unanesthetized and anesthetized neurons ($P = 0.25$ Mann-Whitney U test; Fig. 2.6C), with median and interquartile range values of 1 (0.83 – 1.67) and 1.17 (0.83 – 1.92) Hz, respectively. This was not dependent on the method for estimating BW, as neither BW at 70 ($P = 0.19$) nor 90 dB ($P = 0.49$) differed between unanesthetized or anesthetized neurons. This is consistent with our finding that the spectral BW derived from STRFs did not differ significantly between anesthetized and unanesthetized neurons. These results indicate that urethane anesthesia did not alter the ranges of tone frequencies that drive MLd neurons to fire. Stimulus level threshold was significantly lower in unanesthetized neurons than in anesthetized neurons ($P < 0.01$, Mann-Whitney U test; Fig. 2.6D), indicating that the stimulus intensity required to drive MLd neurons is increased by urethane. Median and interquartile ranges for the threshold in unanesthetized and anesthetized units were 40 (33.33 – 46.67) and 46.67 (40 – 53.33) dB, respectively.

Urethane enhances response onsets relative to sustained firing

Consistent with previous results (Woolley and Casseday, 2004), we observed a variety of temporal response patterns in unanesthetized and anesthetized neurons (Fig. 2.5C, 2.7A). We examined the temporal response patterns at BF (Methods) to determine whether urethane alters the proportions of onset, primary-like, and sustained responses in MLd neurons (Fig. 2.7A).

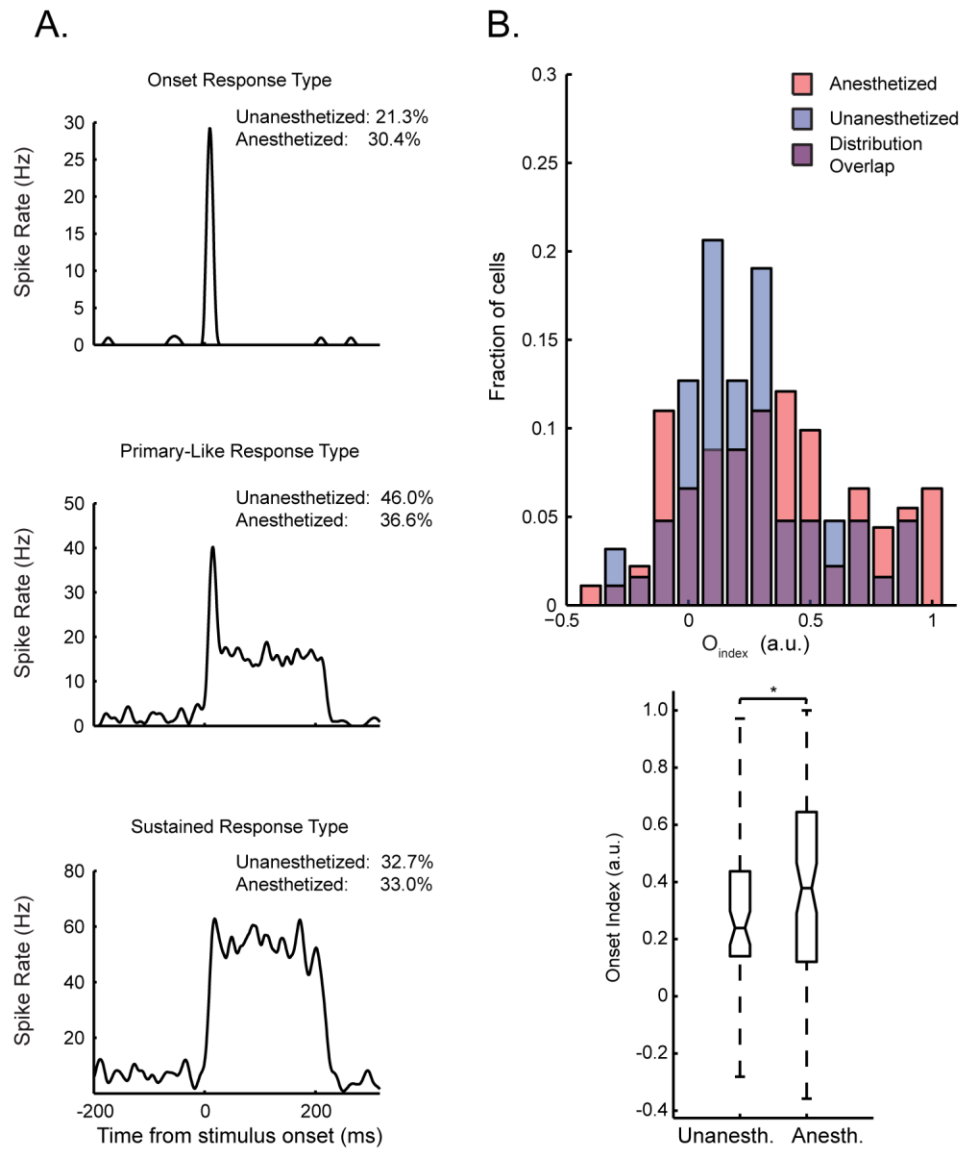

Figure 2.7. Unanesthetized MLd neurons show fewer onset type responses than anesthetized neurons. **A.** Representative examples of three temporal response types. MLd neurons that had a characteristic temporal response across intensities at BF were assigned to one of three response type groups: onset, primary-like, or sustained. Onset neurons (top) showed a strong onset response to pure tones, followed by little or no response. Primary-like neurons (middle) showed an onset response, followed by a lower firing rate sustained response. Sustained neurons (bottom) show a constant firing rate throughout the stimulus presentation. **B.** Onset index (the difference divided by the sum of the first and second halves of the characteristic temporal response pattern) distributions of BF-matched samples of anesthetized and unanesthetized neurons are displayed as overlapping histograms. Blue and red diamonds indicate median values for unanesthetized and anesthetized groups, respectively. The onset index was typically smaller in unanesthetized neurons than anesthetized neurons indicating that anesthetized units have slightly more transient temporal response patterns. * $P < 0.05$

Neurons that did not show a consistent response type across intensities at BF were not classified (unanesthetized, 6.2%; anesthetized, 13.2%). Of the remaining classifiable neurons, unanesthetized neurons were comprised of 21.3% onset responders, 46.0% primary-like responders, and 32.7% sustained responders. Anesthetized neurons were comprised of 30.4% onset responders, 36.6% primary-like responders, and 33.0% sustained responders. These proportions indicate an apparent trade-off between onset and primary-like responders across anesthetic states, but sustained responders were similarly represented between the two groups.

This qualitative classification scheme is useful for capturing the tendencies of neurons to show particular response types, but does not fully quantify differences among temporal response profiles. To quantify onset and sustained response characteristics, we used an onset index, O_{index}, as a metric for onset responsiveness (Methods). Anesthetized neurons had significantly higher O_{index} values than unanesthetized neurons ($p < 0.05$, Mann-Whitney U test) indicating that urethane enhances onset responses relative to the sustained portions of responses in MLd (Fig. 2.5B). Median and interquartile range values for O_{index} in unanesthetized and anesthetized cells were 0.24 (0.14 - 0.44) and 0.39 (0.12 - 0.65) respectively.

Urethane increases first spike latency

Results showing that urethane depressed spontaneous and evoked firing rates, increased response thresholds and enhanced onset responses suggested that urethane reduces the intrinsic excitability of MLd auditory neurons. To further explore this possibility, we calculated the first spike latency to tone stimuli that evoked significant excitatory responses (Methods). We hypothesized that if urethane depresses intrinsic neural excitability, then neurons should take

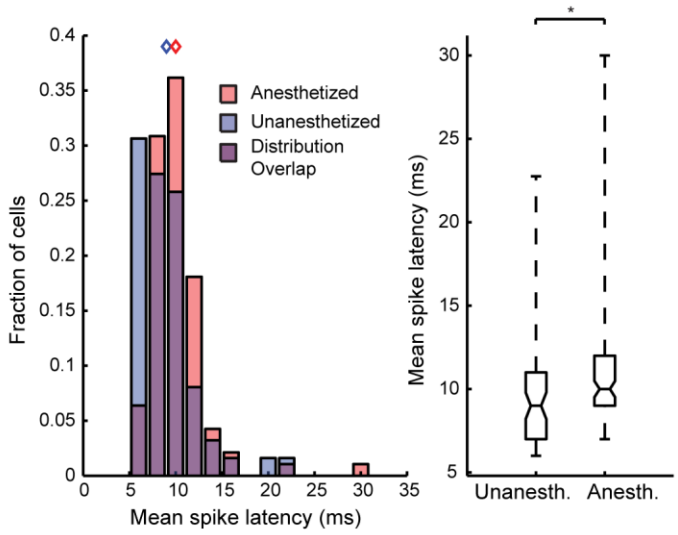

Figure 2.8. Anesthesia increases spike latencies to pure tone stimuli. Average spike latencies for BF matched samples of unanesthetized and anesthetized MLd neurons. Spike latencies were calculated for pure tone stimuli that generated response strengths that were at least 20% of the maximum song-driven firing rate. Distributions of spike latencies are depicted as overlapping histograms and box plots. Blue and red diamonds indicate median values for unanesthetized and anesthetized groups, respectively. Unanesthetized units had significantly lower spike latencies than anesthetized units. * $P < 0.01$

longer to reach spike threshold in response to a given stimulus. Anesthetized neurons had significantly longer first spike latencies than unanesthetized neurons ($p < 0.01$, Mann-Whitney U test; Fig. 2.8). Median and interquartile ranges of spike latencies for unanesthetized and anesthetized cells were 9 (7 – 11) and 10 (9 – 12) ms, respectively. This indicates that the time to reach spike threshold was slightly but significantly increased by urethane, and is consistent with our observation of longer STRF latencies and a pPSTH lag in anesthetized units. Combined, these results provide strong evidence that intrinsic excitability is decreased by urethane.

2.5 Discussion

Understanding the impact of anesthesia on neural coding is crucial for interpreting neurophysiological data. We compared the response properties of unanesthetized and urethane-anesthetized auditory midbrain neurons in the processing of communication vocalizations and pure tones in songbirds. An ideal data comparison would have incorporated cells in which recordings were made before and after treatment with urethane. Due to the time course of systemic urethane injections, the time required to hold a single cell under our experimental conditions would have increased approximately three fold, and complete data recordings would not have been likely. Furthermore, the irreversible effects of systemic urethane treatments preclude a washout period in which to verify neural recovery, a standard control for pharmacological manipulations.

Similar to previous results in other systems, we found that anesthetized neurons had significantly lower spontaneous and sound-evoked firing rates, suggesting a decrease in general excitability in anesthetized neurons. Despite decreased excitability in anesthetized neurons, we found no effects of anesthesia on spectral tuning or neural discriminability at the single neuron level, although discrimination efficiency was higher in anesthetized neurons. Neural discrimination at the population level was sensitive to differences in firing between unanesthetized and anesthetized neurons, and was higher for anesthetized neurons. Small shifts in temporal response latency between unanesthetized and anesthetized neurons were consistent in single neurons and neuronal populations, as well as in song and tone responses. Temporal response patterns to tones also showed small, significant differences in the magnitude of response onsets relative to sustained responses. Furthermore, we observed an apparent trade-off between the proportions of onset and primary-like responders across anesthetic states, but the

proportion of sustained responders was consistent in unanesthetized and anesthetized populations. Despite these differences, population representations of vocalizations were highly similar in unanesthetized and anesthetized animals, though population song discrimination was enhanced under anesthesia. These findings are consistent with a urethane-induced decrease in membrane resistance, which has been shown to be urethane's primary mechanism of action *in vitro* (Sceniak and MacIver, 2006). Increases in membrane resistance could result in increased response latencies and intensity thresholds without inducing changes in the stimulus frequency ranges to which neurons respond. This study is the first to compare spectrotemporal tuning to complex sounds in unanesthetized and anesthetized neurons and shows that, while intrinsic excitability may be depressed by urethane, the midbrain encoding of complex communication sounds and simple, synthetic sounds remains largely intact with urethane treatment.

Effects of anesthesia on auditory coding

Despite its widespread use in neurophysiology, the suitability of anesthesia for collecting neural responses to sensory stimuli has been called into question, particularly in the context of auditory processing. Others have suggested that anesthesia causes large changes in auditory response properties such as spectral tuning (Gaese and Ostwald, 2001; Zurita et al., 1994), temporal response patterns (Wang et al., 2008; Wang et al., 2005), and temporal modulation tuning (Goldstein et al., 1959; Wang et al., 2008). For example, while we found comparable proportions of sustained responding neurons in unanesthetized and anesthetized neurons, Wang et al. (2005) found a prevalence of sustained responses to preferred time-varying stimuli in the auditory cortex of awake marmosets, and observed that previous studies in other anesthetized

animals reported primarily transient responses (deCharms and Merzenich, 1996; DeWeese et al., 2003; Schnupp et al., 2001). This may have led to the conclusion that anesthesia limits what can be learned about auditory coding by significantly altering neural tuning properties away from the properties that underlie normal auditory perception. The effects of anesthesia on auditory coding depend on the brain regions that are studied, however. A recent study comparing the response properties of unanesthetized and barbituate-anesthetized inferior colliculus (IC) and A1 neurons demonstrated that the effects of anesthesia are highly dependent on the brain area under investigation (Ter-Mikaelian et al., 2007). Pentobarbitol/ketamine anesthesia decreased trial-to-trial variability in minimum spike latency in A1, and reduced response reliability. This effect was not observed in the anesthetized IC, indicating that subcortical structures may be relatively more resistant to anesthesia than cortex. Thus, concerns regarding the use of anesthetized preparations should depend on the neural population under investigation. While our study did not compare the influence of anesthesia in forebrain and midbrain neurons, we also found that midbrain auditory representations are surprisingly stable regardless of anesthetic state; spectral tuning, neural discrimination, and the temporal response patterns evoked by songs were not altered by urethane in single neurons.

Because different anesthetics have different mechanisms of action, some are likely to have larger effects on sensory responses than others. The studies that have shown large effects of anesthesia on auditory coding used barbiturates, and frequently used ketamine. For example, Gaese and Ostwald (2001) showed that Equithesin entirely eliminated responses to pure tones in a majority of A1 neurons, but cells that still had well defined tone responses under anesthesia showed a decrease in tuning curve sharpness. Zurita et al. (1994) found that ketamine and pentobarbital treatment led to changes in tone tuning bandwidth, in a subset of A1 and thalamic

recordings. We did not observe changes in frequency bandwidths, in STRFs or in pure tone tuning curves. This difference may be explained by the use of different anesthetics. Barbiturates alter the kinetics of synaptic transmission. For example, pentobarbital lengthens the open time of GABA-mediated chloride channels (Macdonald et al., 1989; Nicoll et al., 1975). Ketamine is a noncompetitive NMDA receptor antagonist (Franks and Lieb, 1994), and reduces AMPA-mediated depolarization (Leong et al., 2004; Ter-Mikaelian et al., 2007). These effects are not observed under other anesthetics, such as urethane. Sceniak and McIver (2006) demonstrated that urethane induced depressions in firing rate by decreasing membrane input resistance in neurons *in vitro*. Changes in membrane resistance were caused by an increase in tonic background K^+ conductance, mediated specifically by the selective opening of Ba^{2+}-sensitive K^+ leak currents, and no influence on excitatory or inhibitory synaptic transmission was found using relevant concentrations of urethane. Because anesthesia is advantageous for some intracellular and long-duration recordings and is important for maintaining consistent behavioral states in some experiments, eliminating anesthesia is not feasible for many in neurophysiology studies. The irreversible effects of urethane force experiments to be terminal, and therefore cannot be used if repeated recording sessions are required over multiple days from a single animal. In other cases, urethane is advantageous for sensory coding studies that require anesthesia because it affects auditory coding less than do other anesthetics.

Comparisons to previous auditory coding studies using urethane

The effects of urethane anesthesia on vocalization coding may to be species-dependent. Consistent with our findings, Capsius and Leppelsack (1996) observed substantial urethane-

induced changes in firing rate and spike latency in subregions of the starling primary auditory forebrain (avian homolog of A1). Narayan et al. (2006) found no differences in neural discriminability performance among urethane-anesthetized and unanesthetized responses to songs in zebra finch primary forebrain neurons. But, Huetz et al. (2009) found that spike-timing reliability was higher in unanesthetized than in anesthetized neurons in responses of guinea pig thalamic and cortical neurons to vocalizations. Because spike timing reliability and neural discriminability are comparable measures, our finding that unanesthetized and anesthetized neurons show similar levels of neural discriminability appears contrary to their findings. The differences between the findings of Huetz et al. (2009) and those from songbird studies may be attributable to species differences.

The use of urethane anesthesia has played an important role in studies on vocal learning and sensorimotor integration in songbirds. Urethane-anesthetized neural recordings in the vocal control nuclei HVC and RA show response selectivity for a bird's own song (BOS), compared to conspecific song or reversed BOS (Dave et al., 1998; Doupe and Konishi, 1991; Lewicki, 1996; Margoliash, 1983; 1986; Margoliash and Fortune, 1992). However, this BOS selectivity is suppressed when birds are awake (Schmidt and Konishi, 1998). The gating of HVC BOS responses by behavioral state is mediated by the release of norepinephrine in the sensorimotor nucleus NIf, which is high in awake conditions and low in anesthetized or sedated conditions (Cardin and Schmidt, 2004a; b; 2003). This implicates attentional mechanisms in mediating the flow of auditory information into the song system. Because the representation of auditory information at is stable across anesthetic states in MLd, it is not likely that such attentional mechanisms would be triggered by changes in neural activity at the level of MLd or lower

brainstem auditory regions, implicating higher order regions in the triggering of attention to gate the flow of auditory information to the song system.

Conclusions

Our results are consistent with previous studies suggesting that urethane decreases the intrinsic excitability of sensory neurons through changes in membrane electrical properties, and that compared to other anesthetics, urethane has minimal effects on synaptic transmission. Despite significant changes in spike rates and response latencies under urethane anesthesia, single neuron spectral tuning and neural discriminability performance were not affected. To our knowledge, this is the first study to explore the influence of urethane on receptive field structure, response reliability, and temporal response properties. Our results indicate that urethane is suitable for studying complex auditory response properties, but important considerations must be made when comparing results from studies using different anesthetics and brain regions.

Chapter 3: Noradrenergic modulation of auditory coding in the songbird auditory forebrain

3.1 Abstract

Social communication requires that sensory systems extract and encode behaviorally meaningful information from complex environments. During the processing of complex signals, sensory coding can be modulated by behavioral or attentional state. These states may affect neural coding through the action of neuromodulators, such as norepinephrine (NE), the release of which is linked to arousal and alertness. The songbird auditory cortex contains markers for NE-related activity, but it remains unclear if auditory coding in these neurons is sensitive to local NE. To determine if the response properties of single neurons in the songbird auditory cortex are sensitive to changes in local NE, we recorded single unit spontaneous and auditory-evoked responses while simultaneously varying the local concentration of NE via iontophoretic microinjections near the recording electrode tip. Spiking during injections of NE or vehicle were compared for firing rates, temporal coding performance, spike timing precision and reliability, and neural song discriminability. We found that Field L neurons are sensitive to local NE, and that NE largely had a suppressing effect on excitability. This suppression was associated with increases in phase-locking, decreases in trial-to-trial spike reliability, and diminished neural discrimination performance. Together, these results indicate that arousal-related release of NE may have a strong impact on the coding properties of Field L neurons.

3.2 Introduction

The noradrenergic system is important in regulating neural processes involved in optimizing perception and action (Berridge and Waterhouse, 2003; Aston-Jones and Cohen, 2005). Noradrenergic activity is mediated via a number of g-protein coupled receptors, and the development, projections and receptor distribution of this system are conserved across vertebrates (Smeets and Gonzalez, 2002). As in mammals, the songbird noradrenergic system (reviewed in Castelino and Schmidt, 2009) originates from the locus coeruleus (LocC) and the subcoeruleus (SCv) in the brainstem. NE is the signature neurotransmitter of the noradrenergic system, and its synthesis from dopamine is catalyzed by the enzyme dopamine-beta-hydroxylase (DBH), which is present in all noradrenergic neurons and provides an accurate marker of noradrenergic activity. LocC projects to several song system nuclei that control the acquisition, production, and perception of song. Tract tracing experiments have identified ipsilateral LocC projections throughout motor nuclei collectively known as the song control system (Appeltants et al., 2000; Appeltants et al., 2002; Castelino et al., 2007). Measured levels of NE, noradrenergic receptor and enzyme distribution reveal LocC projections to forebrain auditory regions Field L, NCM, and CMM (Barclay et al. 1992, 1996; Sockman and Salvante 2008; reviewed in Castelino and Schmidt, 2009). Furthermore, DBH-immunoreactivity is high in MLd, Ov, and Field L suggesting a noradrenergic component to neural processing in these auditory areas (Mello, 1998; Waterman and Harding, 2008). However, it remains to be seen whether and to what extent NE alters the coding properties of auditory neurons in the songbird.

Most data relating to noradrenergic action come from experiments in mammals that are trained to perform behavioral tasks that have little ethological relevance (Berridge and Waterhouse, 2003; Aston-Jones and Cohen, 2005). However, songbirds offer a model system

that is well suited for studying the role of noradrenergic action in a more naturalistic setting: during the production and perception of species-specific communication sounds. Here we asked whether the excitability and coding properties of Field L auditory neurons are sensitive to the local concentration of NE, which we measured and manipulated using multibarrel pipettes attached to carbon fiber recording electrodes.

3.3 Materials and Methods

All procedures were done in accordance with the NIH and Columbia University Animal Care and Use Policy. Subjects were adult male zebra finches (*Taeniopygia guttata*) that were either purchased from a bird farm (Canary Bird Farm, Old Bridge, NJ) or were bred and raised in the Columbia University zebra finch colony. Prior to electrophysiological recordings, birds lived in a large aviary with other male zebra finches, where they received food and water *ad libitum*, as well as vegetables, eggs, grit and calcium supplements.

Surgery

Two days prior to recording, birds were anesthetized with a single intramuscular injection of 0.04 cc Equithesin (0.85 g chloral hydrate, 0.21 g pentobarbital, 0.42 g MgSO4, 8.6 ml propylene glycol, and 2.2 ml of 100 percent ethanol to a total volume of 20 ml with H_2O). Following lidocaine application, feathers and skin were removed from the skull and the bird was placed in a custom-designed stereotaxic holder with its beak pointed 45 degrees downward. For anesthetized recordings, small openings were made in the outer layer of the skull directly over the electrode track locations. For unanesthetized recordings, full craniotomies were made over the electrode tracks. To guide electrode placement during recordings, ink dots were applied to

the skull at stereotaxic coordinates (2.7 mm lateral and 2.0 mm anterior from the bifurcation of the sagittal sinus). A small metal post was then affixed to the skull using dental acrylic, and a grounding wire was cemented in place with its end just beneath the skull, approximately 5 to 10 mm lateral to the junction of the midsagittal sinus. After surgery, the bird recovered for two days.

Stimuli

Song stimuli consisted of samples of the songs recorded from 20 different adult male zebra finches sampled at 48,828 Hz and frequency filtered between 250 and 8000 Hz. Songs were presented from a free field speaker at an average intensity of 72 dB SPL. All songs were balanced for RMS intensity. Songs ranged in duration between 1.62 and 2.46 seconds, and a silent period of 1.2 to 1.6 seconds separated the playback of subsequent songs. All songs were unfamiliar to the bird from which electrophysiological recordings were made.

Pure tone stimuli (0.5 – 8.0 kHz) were presented at sound levels between 20 and 90 dB. Tones were 220 ms in duration, including 10 ms cosine ramps at the beginning and end. Tone stimuli were separated by silent periods of 0.4 to 0.5 seconds.

Click train stimuli were 1.5 seconds long and consisted of broadband white-noise clicks separated by a wide range of inter-click intervals (ICIs: 5 to 30ms in 2.5ms intervals, 30 to 100ms in 10ms intervals, 100 to 200ms in 50ms intervals, and 200 to 500ms in 100ms intervals). Individual clicks were 5ms white noise bursts with 1ms cosine ramps (10 – 90%).

Neural Recordings

The recording chamber was a walk-in sound attenuation booth (Industrial Acoustics Company). Single neuron activity was recorded extracellularly in Field L using cabon fiber electrodes attached to multibarrel pipettes (Carbostar-4). For some recordings, pipettes also contained 0.5% biotinylated dextran amine to mark electrode locations by iontophoretic injection. Electrode resistance was between 3 and 20 MOhm. Electrode signals were amplified (1000x) and filtered (300-5000 Hz; A-M Systems). During recording, voltage traces and action potentials were monitored using an oscilloscope (Tektronix), custom software (Python; Matlab, The Mathworks), and an audio amplifier and loudspeaker. Spike times were detected using a threshold discriminator and spike waveforms were saved for offline sorting and analysis. For offline sorting, spike waveforms were upsampled 4x using a cubic spline function (Joshua et al. 2007). Action potentials were separated from non-spike events by waveform analyses and cluster sorting using the first three principal components of the action potential waveforms (custom software; Matlab, The Mathworks).

In preparation for recordings, birds were wrapped in a blanket and then head-fixed in a custom stereotaxic device. Restrained birds were placed on a table near the center of the room and a single speaker was located 23 cm directly in front of the bird. Neurons were recorded bilaterally and were sampled throughout the extent of Field L. We recorded from all neurons within Field L that were driven or inhibited by any of the search stimuli. Isolation was ensured by calculating the signal-to-noise ratio of action potential and non-action-potential events and by monitoring baseline firing rate throughout the recording session. Search stimuli including conspecific songs, modulation limited noise, and AM white noise were then used to isolate individual neurons.

Neural Data analysis

Vector strength analysis. To assess temporal reliability to periodic click-train stimuli, we calculated the vector strength of the neuronal response at each ICI,

$$Vector\ Strength = \left(\frac{1}{n}\right) * \sqrt{\sum\left(\cos\left(\frac{2\pi t_i}{T}\right)\right)^2 + \sum\left(\sin\left(\frac{2\pi t_i}{T}\right)\right)^2}$$

Where n is the number of spikes, t_i is the time of the i-th spike from click onset, and T is the click period. Statistical significance was assessed using the Rayleigh statistic $2n(VectorStrength)$, which also takes into account the number of spikes evoked by the stimulus (Bartlett and Wang, 2007). A threshold Rayleigh statistic value of 13.8 was considered significant at the $p < 0.001$ level. Neurons were considered phase-lockers if they exhibited significantly locked responses to one or more click-train stimuli, and a characteristic vector strength was assigned to each neuron by averaging the vector strength for all significant click-trains within a neuron.

Spike timing and reliability analysis. To quantify trial-to-trial statistics relating to spike timing reliability and precision in phase-locking neurons we used previously described measures of spike timing jitter, neural precision, and reliability (Berry et al., 1997; Butts et al., 2007). Reliability to click-train evoked spikes was computed by first aligning all neural responses to their time relative to the period of significantly phase-lock-evoking stimuli. First spike jitter was defined as the standard deviation of 1st spike times relative to click onset. Spiking event timescales were computed as the width of the central peak of the PSTH autocorrelation at half height. Finally, spiking event reliability was computed as the fraction of clicks that evoked spikes within the timescale of each neuron's spiking events.

Neurometric analysis. To quantify the ability of single neurons to discriminate among song stimuli, we implemented a K-means neurometric that classifies spike trains into K clusters based on their proximity to one another in a high dimensional space, where K is the number of stimuli presented (Schneider and Woolley, 2010). Briefly, as with van Rossum's (2001) spike train distance metric, the K-means metric uses Euclidean distance to measure spike train similarity. Spike trains were smoothed using an exponential decay (τ = 10 ms), and then iteratively clustered into K groups (Duda et al., 2001). Clusters were initially seeded with K randomly selected spike trains (1 randomly selected for each stimulus) as cluster centers. Each remaining spike train was assigned a cluster based on the seed with the closest proximity. After this initial clustering, cluster centers were recalculated as the geometric mean of the spike trains within that cluster. Spike trains were then re-clustered with the new cluster centers, and this process was reiterated until a set of K clusters was converged upon. A measure of percent correct discrimination was calculated by analyzing the spike trains that belonged to each of the K clusters. Clusters were assigned a song label via a voting scheme in which each spike train in the cluster voted for the song that evoked it. Each cluster was assigned to the song that cast the most votes, and if more than one cluster had the same number of votes for a song, then the cluster with the fewest spike trains from any other song was assigned to the original song, and the other cluster was assigned to the song with the second largest spike train representation. If each cluster contained spike trains from a single song, the neuron had 100% correct discrimination. If one or more spike trains were misclassified, percent correct decreased toward chance (100%/K = 5%). The K-means neurometric was iterated 100 times. K-means was seeded with a different set of spike trains in each iteration. The resulting discrimination values are the mean performance across all 100 iterations. On a given iteration, if a spike train was equally similar to two or more

templates, that spike train was scored as misclassified even if one of the templates represented the appropriate song category. We used this assignment criterion because ambiguity suggests poor discriminability.

We also calculated *d'* as a measure of discriminability that provided no upper bound to the estimate of a neuron's discrimination performance. To calculate *d'*, we first smoothed each spike train with an exponential decay (t = 10 ms) and projected the spike trains from two stimuli onto a single vector that connected the average neural response for each stimulus, which is equal to the average smoothed spike train in response to that song. We then fit a normal distribution to each of the clusters and measured the *d*' between the clusters, which is the distance between the cluster means normalized by the variance of the clusters (Schneider and Woolley, 2010). For each neuron we calculated *d'* for every pair of clusters, and averaged across all pairs.

3.4 Results

NE application depresses neuronal firing rates in Field L.

To assess whether auditory forebrain neurons are sensitive to local NE, we performed single unit recordings (n = 35) in field L of unanesthetized male zebra finches. During presentations of song, click-train stimuli, and tones (section 4.5, Methods and Materials), we measured spontaneous and driven firing rates while, in separate trials, iontophoretically injecting high concentrations of NE (100 or 200 mM), or saline vehicle only. Figure 1 depicts a representative cell that was presented with 50 playbacks of a single conspecific song bout (Fig. 3.1a). After the first 10 trials of vehicle injection, the ejection current (50 nA) was switched to a pipette barrel containing 200mM NE. Both spontaneous and driven firing rates immediately become

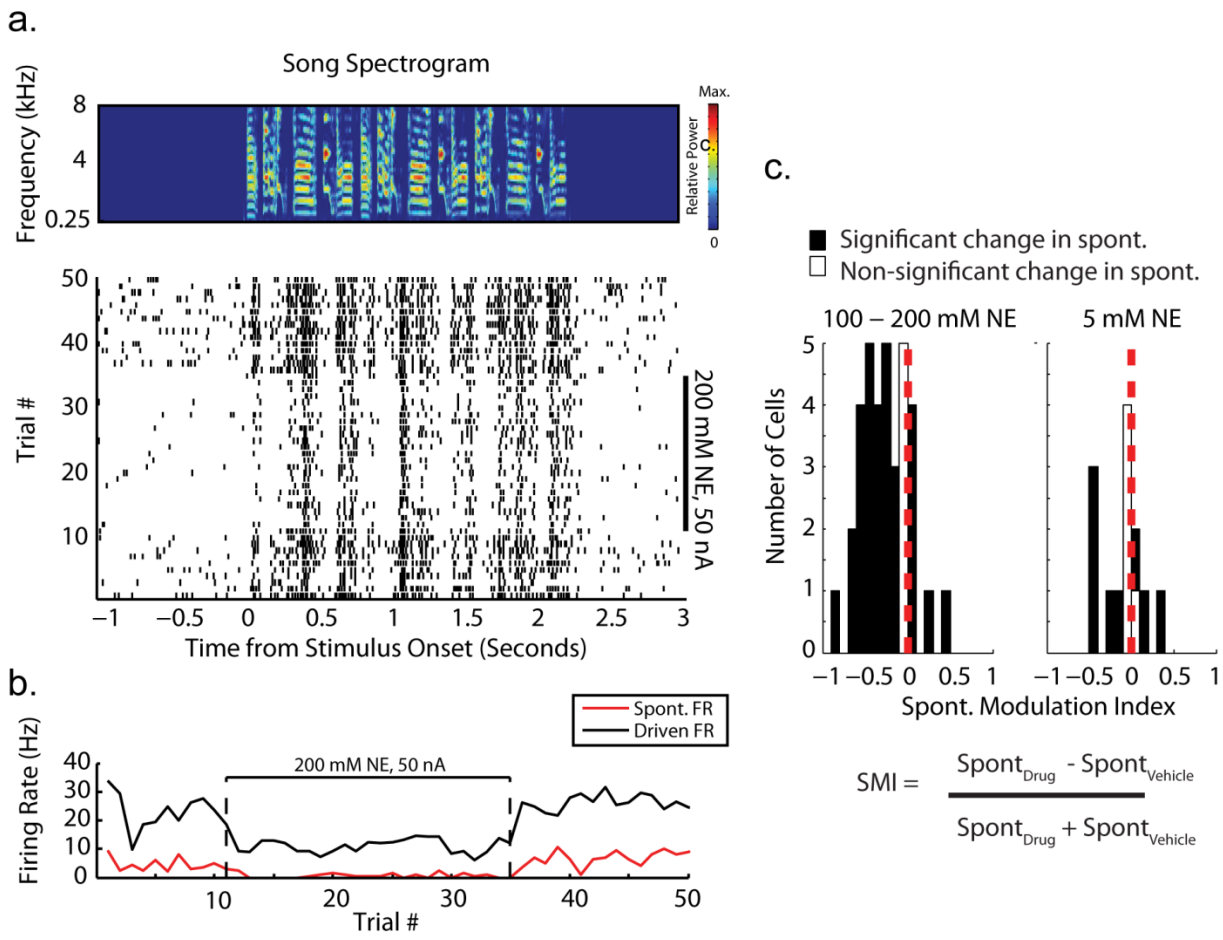

Figure 3.1: NE application depresses firing rates in a dose-dependent manner. **a.)** An example neuron demonstrates the effect of a prolonged 200 mM NE injection. A single unfamiliar bird's song (top) was repeated 50 times while recording responses (bottom). Trials 1 through 10 (baseline) and 36 through 50 (wash) were recorded during vehicle injection. Trials 11 through 35 were recorded during NE injection. **b.)** Spontaneous and driven firing rates of the same neuron are depicted across trials, demonstrating the NE-dependent suppression of excitability. **c.)** Across our population of recordings, high doses of NE (100 or 200 mM) significantly suppressed spontaneous firing rates, while low doses (5 mM) did not systematically alter excitability. ***$p < 0.0001$

suppressed throughout the duration of the injection, and recover within a single trial following a switch back to the vehicle injection (Fig. 3.1b). The population of recordings (n = 35) show that this suppressive effect is characteristic of 100 to 200 mM NE injections. Changes in baseline neuronal excitability are summarized by calculating a Spontaneous-Firing Modulation Index

(SMI), equal to the difference in NE and vehicle spontaneous firing rates, divided by their sum. Ranging from -1 to 1, negative SMI values correspond to cells for which NE suppressed spontaneous spiking activity (Fig. 3.1c). High doses of NE significantly suppressed SMI values in field L neurons to less than zero ($p<0.0001$, Students t-test). In a smaller population of recordings made during low concentrations of NE (5mM), SMI values were not significantly different from zero ($p=0.34$, Students t-test), indicating that this dose was not sufficient to systematically drive significant changes across neurons. These results indicate that field L neurons are sensitive to the presence of local NE, but this sensitivity is concentration-dependent.

NE-dependent changes in excitability are correlated to changes in phase locking performance.

To assess the functional role of NE-induced changes Field L neuronal firing rates, we compared phase-locking performance of a subset of cells (n = 17) in response to repeated playbacks of click-train stimuli in the presence and absence of high NE doses (Fig 3.2). An additional 7 cells failed to phase lock to click-trains under any condition, and were excluded from these analyses. Click-trains were 1.5 seconds long and had interclick intervals ranging from 5 to 500 ms (Fig 3.2a.).

We assessed phase locking performance by calculating vector strength, a measure of a neurons firing precision relative to the phase of the stimulus (section 4.3), Methods and Materials). Phase-locking neurons typically followed the periodicity of click train stimuli significantly (as measured by Rayleigh statistics) for multiple click train stimuli (Fig. 3.2b.). We quantified the effect of NE injections on vector strength using a vector strength modulation index (VMI), which is analogous to the SMI and is equal to the difference in baseline and drug induced

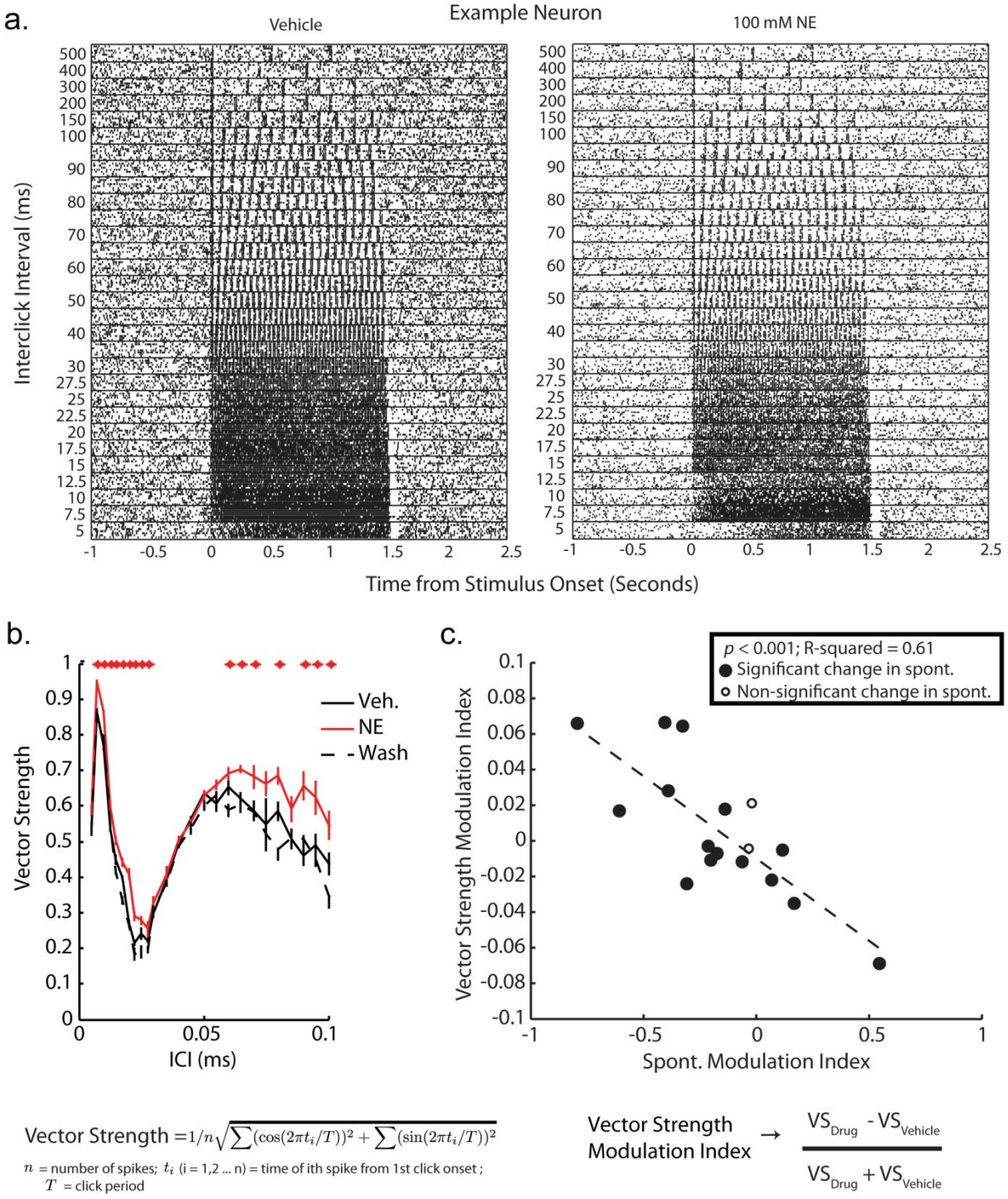

Figure 3.2: NE-mediated changes in neural excitability are correlated with changes in phase locking performance. a.) Robust responses to click-train stimuli with varied in ICIs in a single representative Field L neuron are sensitive to local a NE injection. During vehicle injection (left) the neuron exhibits a high spontaneous firing rate, which is suppressed during injection of 100 mM NE (right). b.) Phase locking as measured by vector strength in the example neuron from a.

(**Figure 3.2, cont.)** is enhanced for specific ICIs during NE injection (red) compared to baseline and washout vehicle injections (black). c.) Modulation of vector strength is strongly correlated with SMI for 17 phase-locking Field L neurons.

vector strength divided by the sum of baseline and drug vector strength. Following injections of 100 mM NE, VMI values varied as a function of each cell's SMI (Fig. 3.2c.; $p < 0.001$; r-square = 0.61). The example neuron in Figure 3.2a and 3.2b demonstrates the effect of enhancing vector strength in tandem with a decrease in spontaneous noisy spiking. These results indicate that NE-induced suppression or enhancement of spontaneous firing had a direct functional impact on the neuron's ability to track the periodicity of the stimulus.

NE suppresses reliability in evoked activity without altering the temporal precision of neural spiking events.

We found that auditory neurons were sensitive to local concentrations of NE, and that NE-induced changes in neural excitability were correlated with changes in a neuron's ability to phase-lock as measured by vector strength. We then asked whether NE specifically induces changes in in the precision of neural spiking events and/or the reliability of evoked spiking across trials. In the same subpopulation of phase-locking neurons, spike times were aligned to the period of each click-train that significantly evoked phase locking. We then computed 1st spike jitter as the standard deviation of the distribution of 1st spike times for each trial. NE did not significantly change 1st spike jitter relative to control (Fig. 4.3a).

We then estimated the precision of evoked spiking by computing the autocorrelation of the click period PSTH, and measured the width of the central peak of the autocorrelation

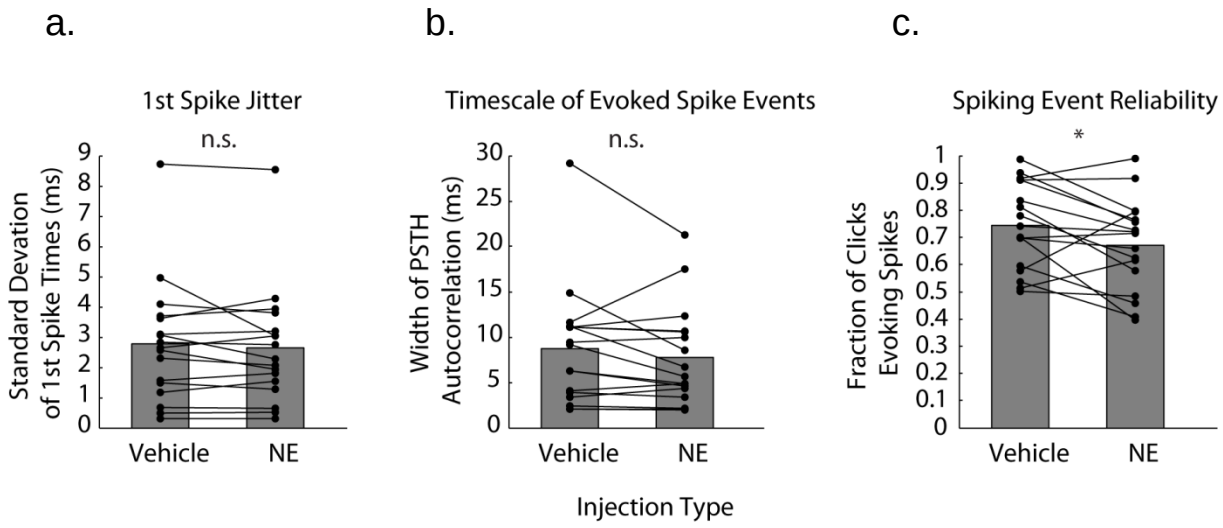

Figure 3.3 Spike timing reliability, but not precision, is altered by NE injections. a.) 1st spike jitter, as measured by the standard deviation of first spike times following a click, was not significantly different between vehicle or NE injections. b.) The timescale of neural precision, as measured by the width of the click-aligned PSTH autocorrelogram, was not different for vehicle or NE injections. c.) Spiking event reliability was significantly reduced during NE injections compared to vehicle injections in 17 phase locking neurons. * $P < 0.01$.

function at half height. Similar to 1st spike jitter, NE did not systematically alter PSTH autocorrelation width relative to vehicle injections, indicating that the timescale of neural precision is preserved in the presence of local NE (Fig. 4.3b). To assess whether trial to trial reliability was altered in the presence of NE, we measured the fraction of clicks that evoked a spike in phase-locking trials. Here we found that in the presence of NE injections, the fraction of clicks that evoked a spike was significantly decreased relative to vehicle (Wilcoxon signed rank test, $p<0.05$). This indicates that the spike depressing effects of NE are substantial enough to suppress driven firing, in addition to noisy, spontaneous firing.

NE-mediated suppression impairs neural discriminability of birdsongs

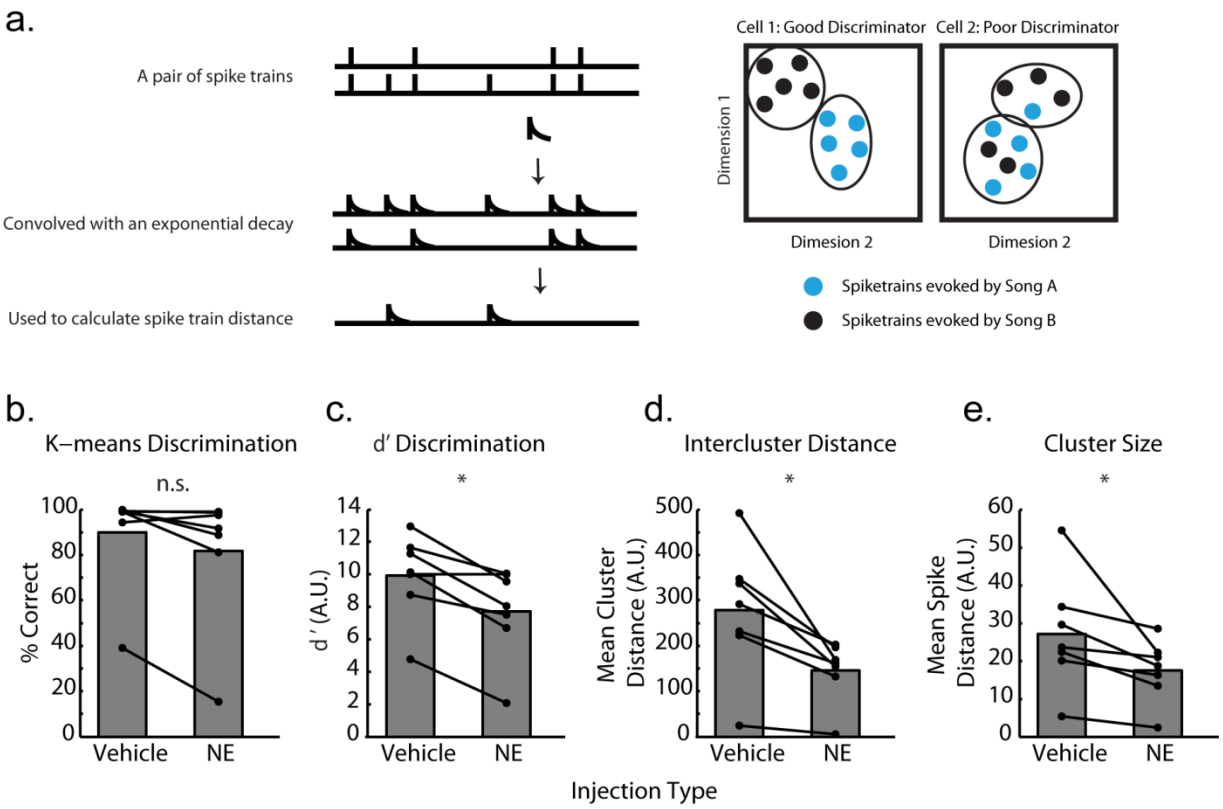

Figure 3.4: Neural discriminability of birdsong stimuli is diminished during NE injections. a.) This schematic illulstrates how spike train distance metrics measure the discriminability of individual sounds. First, a pair of spike trains is convolved with an exponential decay, and then subtracted to determine their inter-spike train distance (left). Neighboring clusters of spike trains in a high dimensional "spike train space" can be homogeneously comprised of spike trains from an individual song, or heterogeneously comprised of spike trains from different songs. The cartoon example on the left illustrates a good discriminator, while the example on the right illustrates a poor discriminator. b.) K-means discrimination performance did not differ between vehicle or NE injection, while c.) d' discrimination was significantly reduced during NE injection. d.) Decreased d' discrimination was likely due to decreases in intercluster distance, which would inhibit discrimination performance. e.) Spike train cluster size, as measured by average spike train distance within clusters, also decreased, but was not sufficient to overcome reductions in intercluster distance seen in d.).

The observed decrease in spiking reliability led us to hypothesize that increases in local NE would influence song discrimination ability in single neurons. To quantify the ability of single neurons to discriminate among song stimuli, we used spike-distance based discrimination metrics (Fig. 3.4) including the K-means neurometric and *d'* for a subset of 7 Field L neurons. K-means

performance did not significantly differ between NE and vehicle injections (Fig. 3.4b). However, the *d'* metric, and unbounded estimate of neural discrimination, was significantly lower for NE injection trials than vehicle trials (Wilcoxon signed rank test, $p<0.05$), and coincided with decreases in both spike train intercluster distance and cluster size (Wilcoxon signed rank test, $p<0.05$). These results indicate that, along with NE-mediated suppression of excitability, the ability of single neurons to distinguish between songs based on the structure of their evoked spike trains is diminished during NE injections.

3.5 Discussion

Here we tested whether Field L neurons were sensitive to varying the local concentration of NE via iontophoretic injections. High concentrations in the range of 100 to 200 mM NE were sufficient to suppress excitability in a majority of Field L neurons. In phase locking cells, this suppression was correlated with changes in stimulus tracking, but did not alter the precision of neural spiking events. Trial-to-trial reliability was diminished by NE injections, as was single neuron discrimination of unfamiliar conspecific songs. These results indicate that arousal related neurotransmission is sufficient to alter the excitability and coding properties of neurons in the songbird auditory cortex.

The presentation of song evokes states of arousal and aggressive (male) or sexual (female) behavior in songbirds (Catchpole and Slater, 1995). If social context influences arousal states and the coding properties of auditory neurons are state-dependent, then it is possible that changes in social context lead to changes in the coding properties of auditory neurons. There is reason to hypothesize that a functional link may exist between auditory processing and socially-driven affective mechanisms. For instance, pharmacological degradation of the noradrenergic system,

commonly thought to regulate arousal and modulate sensory processing (Berridge and Waterhouse, 2003), changes the patterns of song-induced IEG expression, a marker for neural activity, in songbird auditory forebrain areas (Lynch and Ball, 2008). Furthermore, noradrenergic degradation diminishes behavioral responses to presentations of birdsong, and alters song preference and discrimination (Appeltants et al., 2002). These observations implicate NE as a potential affective mediator of sensory processing.

The noradrenergic system has an important role in modulating behavioral state transitions. Locus coeruleus is most active when an animal is awake and is least active during REM sleep (Cirelli and Tononi, 2000). LocC also regulates the expression of several genes related to the regulation depression and other state-dependent disorders (Cirelli and Tononi, 2004). NE plays an important role in modulating sensory responsiveness across behavioral states. Increased levels of NE can increase the signal-to-noise ratio of sensory responses by increasing evoked sensory responses while decreasing spontaneous activity (Hasselmo et al., 1997; reviewed in Berridge and Waterhouse, 2003). NE can also increase sensitivity by increasing the probability of neural responses to subthreshold stimuli (Waterhouse et al., 1998; reviewed in Berridge and Waterhouse, 2003).

Activity in LocC shows drastic changes across behavioral states, increasing during wakefulness and decreasing during rest, sleep, and anesthesia. These changes are strongly correlated with the release of NE in other parts of the brain (Devilbiss et al., 2006), and this noradrenergic activity is involved in attentional modulation (reviewed in Aston-Jones and Cohen, 2005). In mammalian studies, attention-demanding tasks increase locus coeruleus firing, and the resulting increase in NE levels is thought to influence sensory responsiveness and representations in cortex (reviewed in Berridge and Waterhouse, 2003). Cortical representations

of attended features are often enhanced, while the representations of competing features are suppressed. This phenomenon, known as biased competition (Buehlmann and Deco, 2009), has been demonstrated in the visual system (Desimone and Duncan, 1995), auditory cortex (reviewed in Fritz et al., 2007), and barn owl auditory spatial maps (Winkowski and Knudsen, 2007). Studies have shown rapid task-dependent STRF plasticity that resembles biased competition (Fritz et al., 2005), but a relationship with NE has yet to be determined.

Previous work on the role of NE in regulating auditory responsiveness has been shown in the song system. A famous characteristic of song system neurons is their preferential response to a bird's own song (BOS). For instance, HVC neurons respond robustly to BOS, but not as much to reversed or rearranged BOS, or conspecific vocalizations (Margoliash, 1986). This BOS selectivity is strongly influenced by a bird's behavioral state. Sleeping or anesthetized birds reveal strong multiunit BOS responses in HVC (Schmidt and Konishi, 1998; Nick and Konishi, 2001; Dave et al., 1998; Cardin and Schmidt, 2003; 2004a), but awake birds show more variable BOS responses. Awake BOS responses are often weaker or are absent, and are generally not stronger than responses elicited by other stimuli (Schmidt and Konishi, 1998; Dave et al., 1998; Cardin and Schmidt, 2003). Neurons in NIf, a sensorimotor input to HVC, show a similar pattern, and have been shown to have a strong impact on the auditory responsiveness of HVC (Cardin and Schmidt, 2004a).

NE regulates behavioral state-dependent transitions in the sensory processing of mammals (Aston-Jones and Bloom, 1981; Devilbiss et al., 2006; reviewed in Aston-Jones and Cohen, 2005), and strong evidence supports the role of NE in songbird sensory processing as well. Cardin and Schmidt (2003; 2004b) conducted a series of studies in which arousing stimuli (air puffs) presented before the onset of BOS presentations were shown to suppress auditory

responses in NIf and HVC. Infusions of NE into NIf mimicked this effect in a dose dependent manner. Low concentrations of NE increased auditory responsiveness, while high concentrations had a suppressing effect. This mimics inverted U-shaped response profile of LocC activity in mammals, suggesting that LocC-NE release may modulate this state-dependent neural coding.

Other areas that might show noradrenergic-dependent auditory responsiveness include MLd and Field L, both of which have high DBH labeling and/or measured levels of NE. As central auditory nuclei, Field L and MLd are critical to the perception and representation of the acoustic environment, including birdsong. Noradrenergic projections to these areas could play a role in shaping the auditory representation of social signals. Although, Cardin and Schmidt (2003) did not find behavioral-state dependent modulation of BOS responsiveness in Field L across the sleep-wake transition, this not surprising considering that Field L is not thought to be BOS-selective under any contextual state (Theunissen, 2008). Together with the studies reviewed above, our findings confirm that the songbird auditory cortex is indeed sensitive to arousal-related neurotransmission mediated by the noradrenergic system. Future studies will be required to determine if these effects are consistent for a wide range of NE concentrations, and whether different concentrations can yield varying coding manipulations, as seen in mammals.

Part 2: Assessing developmental properties of the songbird auditory cortex.

Chapter 4: Dynamic structure and function in the developing auditory system

4.1 The role of experience in the developing brain

Early postnatal experience has lifelong impact on health and behavior in humans and other animals. In rare cases dating from the 14th century to modern time, humans raised apart from natural rearing environments, so-called feral children, demonstrate severe behavioral abnormalities. Child psychologists of the early to mid-twentieth century formally demonstrated that perceptual and social experiences were required for cognitive development. Inspired by the work of Sigmund Freud, Rene Spitz (1945) conducted a study comparing infants reared in either a nursing home attached to a woman's prison, or a foundling hospital for abandoned children. The rearing conditions provided infants with equal nutritional and medical care, but differed in that the nursing home infants received parental affection each day and had visual and acoustic access to other children from their cribs. At four months of age, infants in the foundling home scored better on developmental tests than those in the prison homes. However, after the first year of life, the children in the prison homes far outscored the foundlings in motor and perceptual abilities. Foundling children developed a withdrawn and depressed phenotype which Spitz referred to as hospitalism (now known as anaclitic depression), while the prison children developed at a rate consistent with normally reared children. This case study is an early demonstration of the human developmental reliance on social and sensory stimulation, and it illustrates that healthy developmental trajectories in children emerge over long timescales (Sanes and Jessell, 2013). Studies such as Spitz's have shaped modern ethical perspectives in science, which prohibit social deprivation in a child's environment.

Over the past several decades it has become feasible to use animal models to probe the neural basis of experience-dependent developmental plasticity in sensory systems. Neurophysiological and anatomical studies of the role of experience in sensory development have shaped our understanding of the functional properties of sensory neurons. Here I discuss experimental approaches for probing the functional ontogeny of sensory systems, with an emphasis on auditory neural processing and perception. I begin with an overview of behavioral assessments of perceptual development, and then provide an overview of sensory development from the periphery to the cortex.

4.1.1 Development of perceptual skills

Human studies of auditory development demonstrate that: 1) perceptual maturation occurs well into adolescence; 2) adult-like perceptual abilities emerge at different ages depending on the skill; and 3) individual perceptual skills emerge with the maturation of neural coding properties in the auditory system (review: Sanes and Woolley, 2011). For instance, frequency resolution (tone detection in the presence of a tone of similar frequency) reaches peak maturity by 6 months of age (Spetner and Olsho, 1990; Hall and Grose, 1991), corresponding to the timescale of cochlear development. On the other hand, frequency discrimination does not fully mature for over a decade (Maxon and Hochberg, 1982; Moore et al., 2011). Similarly, human perception of temporal cues displays a wide range of developmental timelines. Sound duration discrimination matures at six years of age (Elfenbein et al., 1993; Jensen and Neff, 1993), while detection of amplitude modulations such as those in speech, matures at up to 12 years of age (Banai et al., 2011). Together these studies indicate that developmental changes in neural coding mechanisms

underlie perceptual maturation, and that studies using animal models may lead to the identification of these mechanisms (Sanes and Woolley, 2011).

4.1.2 Development of functional auditory circuits

Auditory developmental timelines vary among species. Rodent auditory systems develops over the first postnatal month (review: Sanes and Bao, 2009); hearing onset occurs in rats and mice around postnatal day P11 (Geal-Dor et al., 1993) while the human auditory system is functional before birth. A mother's voice and other auditory stimuli evoke motor responses and changes in heart rate *in utero* (Moore and Fred H Linthicum, 2009). Heart rate responses also demonstrate frequency discrimination in fetal infants (Shahidullah and Hepper, 1994). Auditory development in most animals that have been studied occurs over a prolonged postnatal period of neural and perceptual maturation that is thought to allow central auditory neurons and circuits to develop under the influence of experience (Keuroghlian and Knudsen, 2007).

Subcortical Development

Many subcortical auditory structures in the rodent mature in the first few postnatal weeks. The cochlear microphonic is detectable in rats as early as P8 (Uziel et al., 2009), and cochlear hair cells are spontaneously active between P0 and P10 (Tritsch and Bergles, 2010). Brainstem nuclei that process interaural differences between level (ILD) and timing (ITD), the two principal cues used for sound localization, require experience to develop normal stimulus coding properties. For example, gerbils reared in the presence of omnidirectional noise show abnormal

ITD coding in the dorsal nucleus of the lateral lemniscus (DNLL) that is likely caused by a postnatal failure of inhibitory axons to form precise spatial connections (Seidl and Grothe, 2005).

The vast majority of auditory projections ascending from the lower brainstem converge on the inferior colliculus (IC), along with descending projections from cerebral cortex (Brunso-Bechtold and Henkel, 2005a). The mammalian IC generally consists of a central nucleus (CNIC) that is surrounded by a dorsal (DIC) and external (EIC) nuclei. Many of the axonal projections to these regions also develop postnatally. Cells in the CNIC are born at E14 in the rat, 3 weeks before hearing starts (Altman and Bayer, 1981). Lateral superior olive (LSO) and DNLL projections are diffuse throughout the IC in the first week after birth and form banded axonal terminations are also present in rats several days before hearing (Gabriele and Brunso-Bechtold, 2000). This anatomical development illustrates that mammalian subcortical auditory processing is immature at birth, but begins to form functional circuit properties before the onset of sound detection.

The pre- and postnatal maturation of anatomical organization in the IC is paralleled by development of functional coding properties such as frequency tuning (Aitkin and Moore, 1975), binaural tuning (Aitkin and Reynolds, 1975). For example in kittens, CNIC tuning curves are broadly tuned with high intensity thresholds from P6 to P11, but sharpen, map tonotopically, and have lower intensity thresholds by day 21 (Aitkin and Moore, 1975).

Ascending auditory activity plays a central role in the formation of hindbrain auditory and IC circuits. Studies on the role of sensorineuronal hearing loss (e.g. removing the cochlea) or conductive hearing loss (e.g. ossicle removal or ear plugging) indicate that anatomical and functional properties of IC depend on experience-dependent brainstem activity to mature properly (Brunso-Bechtold and Henkel, 2005b). Early unilateral cochlear ablation in gerbils and

ferrets decreases ipsilateral CN volume and increases the strength of the projection from CN to IC on the contralateral side (Moore and Kowalchuk, 1988). In contrast, bilateral cochlear removal does not result in abnormal CN to IC projections, indicating that competition between activity from each ear plays a role in developing projections to IC (Moore, 1990). This binaural competition may also play a role in ascending DNLL projections, as early unilateral cochlear ablation alters the banding of contralateral and ipsilateral DNLL afferents in IC (Gabriele et al., 2000).

The findings reviewed above suggest that the development of the IC is driven by activity in ascending and converging auditory pathways during early postnatal life. The IC also demonstrates strong experience-dependent plasticity during development. This is well characterized in the barn owl. Owls raised with prism lenses that shift the visual field show a remapping of the auditory spatial map of ITDs in the IC (Brainard and Knudsen, 1993). Spectral processing in IC is also sensitive to experience. Juvenile rats exposed to a single tone develop an over-representation of that tone in the IC (Poon and Chen, 1992), and mouse pups exposed to repeated broadband clicks have broadened IC receptive fields (Sanes and Constantine-Paton, 1983; 1985).

The role of activity in the brainstem is both trophic (for developing projections) and refining (for synaptic specificity). Interestingly, the synaptic mechanisms responsible for activity-dependent changes vary across brain regions (review: Sanes and Bao, 2009). For example, auditory neurons throughout the CNS tend to exhibit enhanced excitability following bilateral hearing loss. Studies in congenitally deaf mice show that in the cochlear nuclei this excitability increase is mediated by enhanced excitatory synaptic currents, but in the medial nucleus of the trapezoid body (MNTB) this excitability increase is mediated by the down

regulation of a potassium channel (Oleskevich and Walmsley, 2002; Leao et al., 2004). In the LSO, inhibitory axon terminals refine their synapses in two stages: 1) a decrease in connectivity before hearing; and 2) an elimination of terminal boutons after hearing onset (Anon, 1993; Kim and Kandler, 2003). This second stage of refinement is activity dependent, and may depend on inhibitory synaptic long-term depression (Kotak and Sanes, 2000; Kandler and Gillespie, 2005; Sanes and Bao, 2009).

As for hindbrain projections to the IC, projections from the medial geniculate nucleus of the thalamus to primary auditory cortex (A1) emerge in the first postnatal week, and mature through P12 (Fathke and Gabriele, 2009). The development of subcortical auditory circuitry during the perinatal period becomes established to a degree that is sufficient for strong tone-evoked responses in A1 by P14, with cortical development extending well beyond this point.

Cortical Development

The development of A1 has largely been explored with respect to neonatal critical period plasticity (Hensch, 2005; Sanes and Bao, 2009; Froemke and Jones, 2011). Rather than being poorly structured before maturation, recent evidence suggests that A1 is mapped tonotopically shortly after hearing onset, and this tuning becomes somewhat less precise over time (Bonham et al., 2004; Insanally et al., 2009). As described above, neonatal auditory responses in subcortical regions become more sharply tuned during development, suggesting that a gradual broadening of tuning in cortex reflects cortical developmental processes (Sanes and Bao, 2009).

Several important studies demonstrate the critical role of acoustic experience in the development of auditory coding. Merzenich and colleagues report that repeated presentations of a given tone led to expanded anatomical representations of that tone in juvenile rodents (Zhang

et al., 2001; Chang et al., 2005; de Villers-Sidani et al., 2007). Han et al. (2007) also showed that this experience-dependent, tone-specific cortical expansion is correlated with a decreased ability to behaviorally discriminate nearby tones. They also found that discrimination within neighboring tone regions was enhanced, and suggest that early over-exposure results in a neural basis for categorical perception (Han et al., 2007).

Tonotopic maps emerge with the development of individual tone receptive fields at the single neuron level. In juvenile rats, frequency-intensity tuning is considered adult-like by roughly P21 (Froemke and Jones, 2011). Other response properties emerge over longer periods. GABA-mediated, inhibitory sidebands have been reported to be stronger in juveniles than adults, with broad two-tone suppression remaining until P45 (Chang et al., 2005).

In addition to displaying spectral tuning plasticity, auditory cortical neurons are developmentally sensitive to temporally modulated sounds. In the absence of experiencing rapidly repeating sounds, or with over-exposure to slowly modulated sounds, cortical neurons show diminished entrainment to high rate stimuli (Chang and Merzenich, 2003; Zhou and Merzenich, 2008). This is also seen in spectrotemporally modulated stimuli; rats reared in the presence of repeated frequency sweeps develop A1 neurons with selectivity for those specific FM sounds (Insanally et al., 2009).

Evidence that the acoustic characteristics of over-exposed sounds alter the timing of A1 critical periods adds an additional layer of complexity to the story of developmental plasticity in A1. Rearing in continuous white noise, rather than periodic bursts of noise, not only degrades cortical tuning, but extends the critical period for plasticity (Chang and Merzenich, 2003; Speechley and Hogsden, 2007). Exposure to a continuous tone stimulus also extends the critical

period (Zhou and Merzenich, 2008), while modulated stimuli appear to sufficient to close the critical period (Dorrn et al., 2010).

In addition to sound evoked activity, development of A1 receptive fields has been studied at the synaptic level. *In vitro* recordings of rodent A1 demonstrate a maturation of intrinsic cellular and synaptic properties in glutamatergic cells, with large changes in postsynaptic conductances between P12 and P21, corresponding to the timeline of changes in rodent A1 frequency tuning (Oswald and Reyes, 2008; Insanally et al., 2009). Recordings *in vivo* demonstrate that excitatory inputs are tuned to characteristic frequencies by P14, while inhibitory inputs remain poorly tuned (Dorrn et al., 2010; Sun et al., 2010). After three weeks of acoustic experience, the tuning of A1 inhibition becomes tuned and scales across stimuli with excitatory conductances (Wehr and Zador, 2003; Froemke et al., 2007; Dorrn et al., 2010). This balance of excitation and inhibition may be critical in establishing mature receptive fields (Froemke and Jones, 2011).

4.2 Discussion: limitations and future directions in experimental frameworks for probing functional auditory development

The research outlined above demonstrates that development throughout the central auditory system is sensitive to experience. Multiple forms of hearing loss are sufficient to induce anatomical and functional developmental abnormalities from CN to A1, and continuous over-exposure to sound reorganize tonotopic maps in the IC and A1. These developmental manipulations can also be observed at the synaptic level, where depending on the region, auditory deprivation can modify and refine the strength of synapses or change the intrinsic electrical properties of neurons.

It is clear that the timecourse of auditory development varies across auditory regions and species, and the development of human perceptual abilities (months to years) does not coincide with the auditory properties observed in model systems (days to weeks). It is also clear that the principal manipulations used to probe development in the auditory system are environmental disruptions of normal development, either through the over-representation of artificial stimuli in postnatal rearing conditions, or the deprivation of sound evoked activity through surgical, genetic, or experiential means. Sanes and Bao (2009) importantly point out that the experiments that use these methods have likely provided insights into general principles of normal development, but they are limited to the extent that they are: 1) largely performed in anesthetized animals or brain slices; and 2) nowhere near representing natural rearing or behavioral conditions that the nascent nervous system is likely to encounter. It is up to experimentalists to derive new frameworks for probing auditory development in the context of natural behavior.

One promising avenue of research that is already providing significant contributions to developmental neurobiology is the interaction between vocal behavior and auditory coding. Vocal communication is a specialized behavior shared by many species, and neural response selectivity for species-specific vocalizations have been observed in several vertebrate groups including primates (Glass and Wollberg, 1983; Wang, 2000), bats (Klug et al., 2002), guinea pigs (Šuta et al., 2003), frogs (Elliot et al., 2011) and songbirds (Margoliash, 1986; Doupe and Konishi, 1991; Grace et al., 2003). A subset of these model systems, including bats and songbirds, learn to communicate vocally during early development. In these two groups, experience with vocalizations shapes auditory response properties during development, and plays an important role in the emergence of vocal selectivity.

Bat IC and A1 neurons respond selectively to downward FM sweeps that are intrinsic to their echolocation calls, and this is in part mediated by the complex timing of GABA-ergic inputs to these cells (Andoni et al., 2007; Fuzessery et al., 2011). This selectivity emerges several weeks after the onset of hearing and experience with sonar behavior, and young bats that are vocally impaired and deprived of hearing normal echolocation have diminished FM direction selectivity (Razak et al., 2008). Bats make an ideal system for studying how natural behavioral contexts influence neural development, in large part because the circuitry mediating FM sweep coding is largely worked out.

Songbirds provide a model system in which the neural substrate governing the acquisition and production of a learned social behavior is well characterized. Birdsong, like speech, is acquired over multiple sensory and sensorimotor critical periods that have distinct temporal windows (Doupe and Kuhl, 2003). The natural rearing conditions of the songbird feature an abundance of complex vocalizations and social experience, and provides a surprisingly simple framework to test whether vocal learning experience influences auditory coding in juveniles and adult birds. Neurons in the primary auditory cortex of songbirds (Field L) have firing rate selectivity for conspecific song over artificial stimuli, and this selectivity is stronger in adults than juveniles (Grace et al., 2003; Amin et al., 2004; Amin et al., 2013). Early isolation from song exposure also results in diminished response selectivity as measured by multiunit recordings and fMRI (Cousillas et al., 2004; Maul et al., 2010).

Future studies could continue to test how natural communication signals influence songbird auditory development by manipulating the vocal learning conditions in which songbirds are raised. Woolley et al. (2010) found that single auditory neurons displayed higher information coding capacities in male zebra finches tutored with conspecific song, compared with male zebra

finches tutored with Bengalese finch song. The mechanisms leading to song selectivity and coding capacity remain unknown. Cross-fostering studies probing the development of receptive field properties will provide an answer as to whether the statistics of vocally learned signals become preferentially encoded in the auditory system. Furthermore, chronic recording techniques will allow experimenters to probe the physiology of auditory neurons throughout the course of vocal learning in juvenile birds, and will provide insights into how natural behavioral experience during development is linked with the development of auditory circuits that underlie learned vocal communication. Data presented in chapter 5 will address this topic directly.

Chapter 5: Vocal learning drives experience dependent changes in the coding properties of auditory cortical neurons in a region and cell-type specific manner.

5.1 Abstract

Auditory neural circuit development relies on experience-dependent mechanisms that operate during critical periods. This enables auditory neurons to optimally encode the acoustic environment by acting as matched filters for relevant sound features in the world. This process is important in shaping the coding and perception of sound later in life. In animals that communicate vocally, auditory cortex encodes the complex acoustic features of conspecific vocalizations. Some animals, such as songbirds, learn vocalizations during development by imitation. To facilitate vocal learning, early social communication experience may shape auditory cortical response properties to accurately encode the acoustic features of the imitated model. Here we tested whether the onset of song tutoring during a critical developmental period for vocal communication induces changes in the response properties of auditory cortical neurons in juvenile male zebra finches. We performed longitudinal neural recordings along single electrode tracks through the auditory cortex before and during song tutoring using chronically implanted miniature motorized microdrives. Here we show that the onset of tutoring is sufficient to drive shifts in the temporal and spectral coding properties of auditory cortical neurons in a cell-type and region specific manner. Furthermore, we demonstrate a functional specialization in dorsal, but not ventral subregions of the auditory cortex for processing auditory feedback.

5.2 Introduction

In humans, vocal learning during childhood plays a major role in speech perception throughout life. Native speakers of a language are more adept at discriminating between and recognizing their speech sounds than non-native speakers and prolonged training of non-native speaking adults fails to overcome this deficit (reviewed in Kuhl, 1994; Iverson et al., 2003; Kuhl, 2010). It is therefore likely that developmental vocal learning modifies the central auditory circuits that underlie vocal communication.

Auditory neural circuit development relies on experience-dependent mechanisms that operate during critical periods (Sanes and Bao, 2009). This is presumed to allow auditory neurons to encode the acoustic environment by acting as matched filters for relevant sound features in the world. This process is also important in shaping the coding and perception of sound later in life. Disorders of auditory development have profound consequences in the lives of both children and adults, and have a complex etiology including genetic factors, prematurity and low birth weight, infection, trauma, and epilepsy (Bamiou et al., 2001). It is therefore important to explore the physiology of developing organisms, identify critical periods during which functional properties are modifiable, and determine which functional properties are modified by experience.

Current studies of auditory physiology in juvenile animals are limited. Juvenile vertebrates are often delicate, and are not suitable for many experimental manipulations. As a result, most juvenile physiology data are collected in anesthetized preparations, which alter certain neural response properties (Schumacher and Woolley, 2010). Moreover, the role of auditory experience in neural circuit development has been studied primarily in extreme non-natural contexts, such deafening or over-exposure to noise or other sounds (Zhang et al., 2001; Chang et al., 2005; de Villers-Sidani et al., 2007; Han et al., 2007; Insanally et al., 2009). These studies certainly demonstrate the role of experience in neural development, but it remains unclear how natural

behavioral contexts that occur during development shape the coding properties of auditory neurons. This is at least in part due to the scarcity of suitable model systems for studying the development of complex perceptual or sensorimotor behaviors.

Like humans, and unlike the vast majority of animals, songbirds learn to vocalize during development by imitating a model, or tutor bird, through observation and vocal practice (Kuhl and Doupe, 1999). In juvenile male zebra finches, forebrain premotor and motor nuclei undergo rapid anatomical and physiological changes following exposure to a song model (Roberts et al., 2010, Shank and Margoliash, 2009). Previous studies have shown that auditory cortical neurons in adult zebra finches have higher firing rates to natural song stimuli than artificial noise stimuli, and that this song selectivity emerges developmentally (Grace et al., 2003; Amin et al., 2014). It remains to be seen what, if any, physiological properties of auditory neurons develop in concert with periods of vocal learning, and over what timescales those changes may take place. Songbirds have well characterized critical periods for sensory acquisition/memorization of a song model and for vocal motor practice. Yet it remains unknown if songbird auditory cortical developing occurs in tandem with known song learning critical periods. To answer these questions, we examined the response properties of auditory cortical neurons in juvenile male zebra finches before and throughout vocal learning. Juveniles were raised in the absence of a song tutor and implanted with miniature, motorized microdrives carrying extracellular recording electrodes to allow chronic recording of auditory neural response properties. Following 10 days of baseline recordings to simple tone stimuli in naïve, untutored birds, experimental subjects were given access to a tutor everyday while we continued to record neural responses to tones, as well as repeated playbacks of the tutor bird's song.

5.3 Methods

Animal Care and Use

All procedures were done in accordance with the NIH policies on animal care and were approved by the Columbia University Animal Care and Use Committee. Adult zebra finch breeders and tutors (*Taeniopygia guttata*) were either bred and raised in the Columbia University zebra finch colony or purchased from a bird farm (The Finch Farm). Breeders lived in a large aviary with other zebra finches before mating and producing offspring for this study. Both parents raised juvenile subjects in sound proof booths until juveniles were posthatch age (P) 10 days, when male parents was removed from booths to prevent juvenile exposure to song. Subjects were raised by their mother until feeding independently (P32-36), and were then housed in singly until implantation with recording microdrives. All birds had free access to food, water, grit, and cuttlebone, and were given supplements of egg and lettuce twice weekly.

Subjects were implanted with miniature motorized microdrives (Keller and Hahnloser, 2008) between days P40 and P5, and then placed in a chronic recording enclosure that allowed daily presentation of tones and vocalizations and simultaneous recording of sing neurons responses along the dorsal-ventral axis of the auditory cortex. Baseline tone responses were measured up to P50, requiring the birds to be teathered for 4 to 10 hours per day. Subjects were allowed free access to food and water, and recordings were suspended during periods of eating or movement.

Tutoring of experimental pupils began after day P50. Tutoring sessions occurred at midday for up to two hours. Tutors were separated from juveniles by a plastic mesh partition, but both birds had visual and acoustic access to one another. Rare cases in which the tutor would not direct singing to the juveniles were remedied by adding a quiet female to the tutor's cage.

Both pupil-directed and female-directed singing were both sufficient to drive song learning in pupils.

Surgery and Electrophysiology

Surgical procedures were similar to what we've previously described (Schumacher et al., 2011), but with minor alterations. Birds were anesthetized with a single intramuscular injection of 0.03 ml Equithesin. Craniotomies were approximately 0.5 by 0.5 mm squares above the intended electrode track (relative to the midsagital sinus: 1.2 to 1.3 mm medial-lateral, 1.2 to 1.3 mm anterior posterior). A slight tear in the dura was made with a hypodermic needle, and the microdrive was positioned over the center of the surgical area. Minutien pins were threaded through the skull anterior to the surgical area to serve as anchors for dental cement. A fine platinum iridium reference wire was implanted lateral to the electrode, and a ground wire was implanted beneath the skull posterior to the implant. The entire exposed skull and microdrive were sealed with dental cement. Birds typically resumed normal behavior within 8 hours and were considered recovered within 24 hours.

The recording chamber was contained within a custom sound proof booth (ETS-Lindgren), calibrated to feature a flat frequency response at its center. The recording cage was equipped with a 12 channel commutator to carry electrode, ground, and reference signals to custom TDT recording software. The teather featured a custom headstage with a two channel op-amp in a unity gain buffer configuration, which provided initial signal conditioning for the electrode and reference channels. Electrodes (Thomas Recording Co.) were glass coated with impedences of 6 to 10 MOhms.

When recordings were finished, we made electrolytic lesions by passing 15uA currents through the electrode to ground for 15 seconds (Fig. 1). Multiple lesions along a single track allowed for identification of the coordinates of recordings sites.

Stimuli

All stimuli were presented from a free-field speaker (JBL), calibrated to have a flat frequency response at the center for the recording chamber. Pure tone stimuli (0.5 – 8.0 kHz) were presented at sound levels between 10 and 90 dB SPL. Tones were 220 ms in duration, including 10ms cosine ramps at the beginning and end. Tone stimuli were separated by silent periods of at least 0.4 s. Song stimuli consisted of multiple renditions of each subjects tutor song, as well as renditions of the subject's own song, sampled at 24,414 Hz and frequency filtered between 250 and 8,000 Hz. Songs were initially presented at varying sound intensities (10 to 90 dB SPL) to gauge the importance of sound level on neural responses, but for most birds the tutor song playback was presented at specific intensities around the natural intensity of song (70 +/- 10 dB SPL).

Song Analysis

We quantified song copy performance using similarity scores generated by Sound Analysis Pro 2011 (SAP2011) from fifteen asymmetric pairwise comparisons between the pupil's largest common song motif with the tutor's song motif. Songs were recorded in the pupil's recording chamber with a directional microphone (Sennheiser, ME2).

Neural Data Analysis

Spike sorting. Spikes were sorted offline using the WaveClus automated sorting algorithm (Quiroga et al., 2004). Signal-to-noise was increased prior to sorting using a nonlinear filter applied to the bandpass-viltered voltage trace (Hill et al., 2011). To quantify the electrical isolation of each cell, we computed the signal-to-noise ratio comparing spike waveform peaks to baseline voltage values (Hill et al., 2011).

Frequency response area and tone tuning estimation. For a subset of the recorded neurons, we calculated frequency response area (FRA) functions from responses to repeated presentations of pure tones ranging from 500 to 8000 Hz (500 Hz increments) and intensities from 10 to 90 dB SPL (10 dB increments), for a total of 144 frequency-intensity combinations. These frequency-intensity ranges and increments were chosen based on previous work on tone tuning in the auditory midbrain (Woolley and Casseday 2004). Frequency-intensity combinations were presented in pseudorandom order for 10 to 20 repetitions or until enough data were collected to acquire well defined FRA plots. FRA plots depict the average response at each frequency-intensity combination. FRAs were upsampled 3X along the frequency and intensity dimensions to increase tone tuning resolution. From the upsampled FRA we measured best frequency (BF), which we defined as the frequency that evoked the largest response when summed across all levels.

Temporal response patterns. We determined temporal response patterns of individual neurons by averaging the PSTHs of frequency/intensity combinations that drove a significant excitatory. We defined the onset period of the response as the first 50 ms of the stimulus presentation, and the sustained period of the response as the second 100 ms of the stimulus presentation (modified from Wang et al., 2005). To quantify the temporal response patterns, we

used an onset index (Schumacher et al., 2011), O_{index}, defined as the onset firing rate minus the sustained firing rate, divided by the sum of the onset and sustained firing rates:

$$O_{index} = \frac{Onset_{FR} - Sustained_{FR}}{Onset_{FR} + Sustained_{FR}}, \quad \textbf{[2]}$$

where values could range from -1 (no onset response, significant sustained response) to 1 (significant onset response, no sustained response). O_{index} values between 0 and 1 represent a spectrum of response types from sustained (O_{index} = zero), to primary-like ($0 < O_{index} < 1$), to onset ($O_{index} = 1$).

FRA tuning coherence. We measured the structure of tone receptive fields using Geary's Contiguity (C) ratio (Geary, 1954), a measure of spatial autocorrelation within a matrix. FRA tuning coherence was calculated as

$$C = \frac{(n-1)\sum_i \sum_j w_{ij}(x_i - x_j)^2}{(2\sum_i \sum_j w_{ij})\sum_i (x_i - \overline{x})^2}$$

where *n* is the number of spatial units indexed by *i* and *j*, *x* is the variable of interest (in this case tone evoked firing rates), $\overline{x}$ is the mean of *x*, and w_{ij} is an element of an *n*x*n* matrix of spatial weights where *w* for nearest neighbors equals 1, and all other w_{ij} elements are equal to zero.

The statistical significance of *C* is given by a z score:

$$z = \frac{(C - E_C)}{\sqrt{Var_C}}$$

where E_c is the expectation of *C* under randomization (E_c = 1 for *n*! samples), and Var_C is the variance of *C* under randomization given by:

$$Var_C = \frac{[S_1(n-1)(n^2 - 3n + 3 - k(n-1)]}{n(n-2)(n-3){S_0}^2}$$

$$+ \frac{\left[{S_0}^2(n^2 - 3 - (n-1)^2 k)\right]}{n(n-2)(n-3){S_0}^2}$$

$$-\frac{\left[\frac{1}{4}\left((n-1)S_2\langle n^2+3n-6-(n^2-n-2)k\rangle\right)\right]}{n(n-2)(n-3){S_0}^2}$$

with variables in the variance equation defined as:

$$S_0 = \sum_{i=1}^{i=n}\sum_{j=1}^{j=n} w_{ij}$$

$$S_1 = \frac{\sum_{i=1}^{i=n}\sum_{j=1}^{j=n}\left(w_{ij}+w_{ji}\right)^2}{2}$$

$$S_2 = \sum_{i=1}^{i=n}(w_{i\cdot}+w_{\cdot i})^2$$

$$k = \frac{\left[\sum_{i=1}^{i=n}(x_i-\overline{x})^4/n\right]}{\left[\sum_{i=1}^{i=n}(x_i-\overline{x})^2/n\right]}$$

Finally, reported *C* values are subtracted from 1 to yield a measure varying from 1 (maximal positive autocorrelation) to approximately -1 for high negative autocorrelation, however in our data set the floor value for *C* is approximately zero. We also report z scores multiplied by -1, so that positive z scores indicate significant spatial clustering of response strengths in the FRA.

5.4 Results

Juvenile zebra finches learn to accurately copy tutors in a compressed learning paradigm for chronic electrophysiology.

Juvenile male zebra finches were raised under conditions that heavily constrained their access to vocal tutoring. (Fig. 5.1a). Subjects were 13 male zebra finches that were nest-reared by their both of their biological parents in sound isolation boxes (IAC Acoustics) until posthatch age (P)

12 to 14, at which point hearing sensitivity is weak and male zebra finches are not yet acquiring a song template from their fathers (Grace et al., 2003). Fathers were then removed from their nest boxes and chicks were reared by their mothers until feeding independently (P31 to P36), at which point they were moved into social isolation. At P40, subjects were implanted with miniature motorized microdrives that delivered extracellular recording electrodes through the extent of the avian auditory cortex (Fig 5.1b,c). The implants provided stable, high signal-to-noise electrophysiological recordings for up to twenty-five days, and allowed for longitudinal sampling from single electrode tracks across days (Fig. 5.1c). From implantation through the duration of recordings, subjects lived in a chronic recording booth where neural responses to pure tones were recorded daily. At P50, subjects were split into two groups. 7 birds (Tut. group) were given two hours of access to a song tutor per day, while 6 birds continued to live in social isolation without tutoring (Ctrl. group), and served as age-matched controls for effects of natural maturational processes involved in the development of auditory cortical neuronal physiology.

Pupils produced accurate copies of their tutor's song (Fig 5.2), even with limited access to tutoring. Song similarity scores (Sound Analysis Pro 2011) were computed between tutor birds and juveniles from multiple rearing conditions. Similarity scores did not differ between our experimental pupils and pupils raised in unconstrained conditions in our zebra finch colony by the same tutors. As expected, isolate reared juveniles did not form copies of our experimental tutors, indicating that common, species typical song components do not account for the copy accuracy of our experimental pupils. One experimental pupil from the Tut. group did not learn the tutor's song, and had a song similarity score comparable to isolate reared birds. As a result this bird is not considered in our analysis of the neural data. In general we find a main effect for

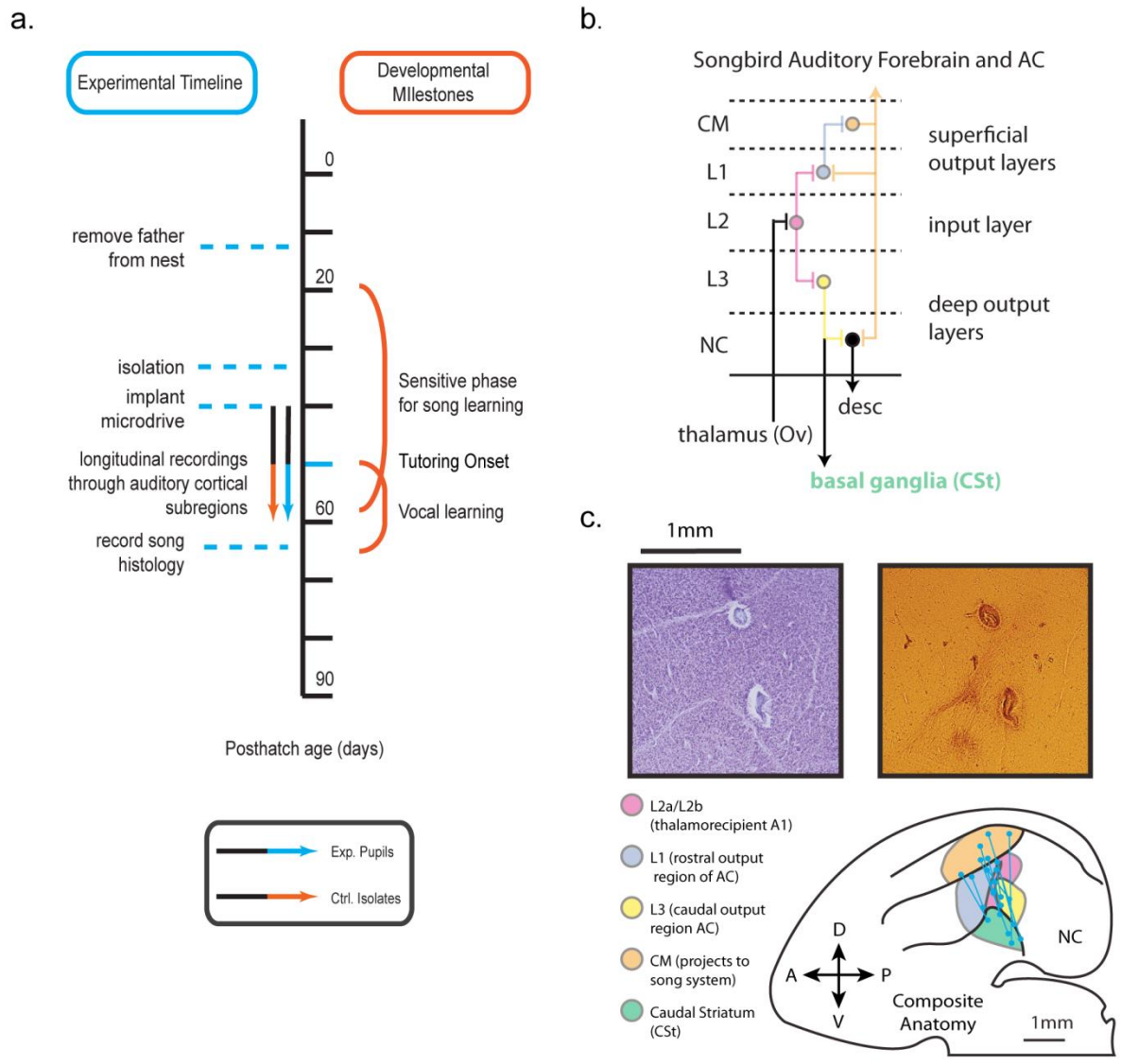

Figure 5.1: Testing the sensitivity of auditory cortical coding to the onset of sensory learning. **(a.)** We developed an experimental paradigm that allows us to control for the onset of vocal learning in juvenile songbirds while recording longitudinally throughout the AC. **(b.)** A schematic of the songbird auditory forebrain shows the basic connectivity of the songbird AC. **(c.)** Representative reconstructions of electrode paths show electrolytic lesions, indicating an electrode track through multiple auditory subregions. Nissl stained sections (top left) and fresh wet tissue (top right) reveal relevant lamina and anatomical features for delineating subregions. Composite anatomy of recording subjects (bottom) shows individual electrode tracks and lesion locations (blue lines).

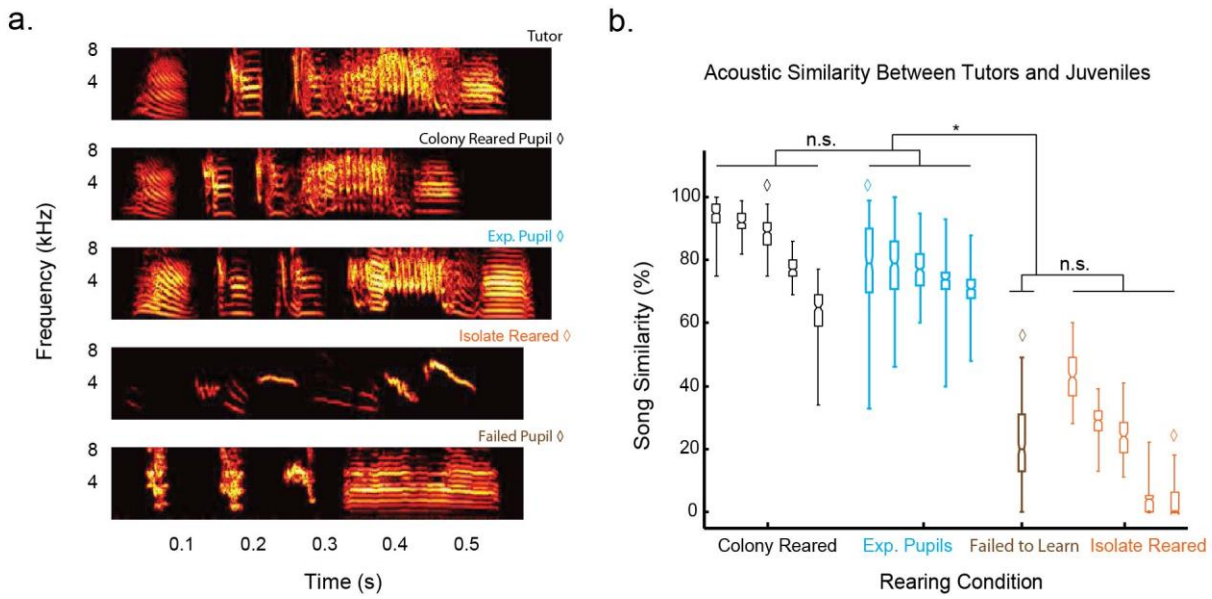

Figure 5.2: Experimental pupils form accurate copies of their tutor's song. **a.)** Sample song spectrograms from subjects in various rearing categories, including one of the subject tutors (top). Colony-reared and experimental pupil spectrograms visually resemble their tutors. Isolate-reared pupils and a single failed experimental pupil demonstrate abnormal song learning. **b.)** Song copy similarity scores for individual subjects in four rearing categories. Box plots denote ranges of similarity scores between pairs of song motifs from each tutor and pupil. Colony-reared and experimental pupils show comparable levels of song copying, while isolate-reared and a single failed pupil demonstrate no motif copying. ANOVA reveals a significant main effect for rearing condition ($p<0.0001$), and post-hoc analysis indicates that colony-reared and experimental pupils show enhanced learning compared to isolates and the single failed learner (*$p<0.01$).

rearing condition (ANOVA; $p<0.0001$), and post-hoc analysis reveals significantly higher learning for colony-reared and experimentally tutored pupils than for isolates and the single failed pupil (Tukey HSD; $p<0.01$).

Thalamorecipient area L2: rapid song learning coincides with changes in the temporal structure of neural responses to tones

To assess whether auditory cortical neurons were sensitive to the onset of vocal learning, we longitudinally recorded along single electrode tracks in juvenile male songbirds before and after

inducing vocal learning. Our single unit recordings in 1124 neurons reproduced a previously observed bimodal distribution of action potential types (Fig 5.3a). Action potential width was used to separate fast-spiking (FS, putative inhibitory cells) and regular spiking units (RS, putative excitatory cells), which are analyzed separately. Much of our analysis compares cell types across multiple subregions of the AC during different recording epochs relating to the vocal learning conditions of the subjects. A summary of our recording populations is available in Table 5.1.

We presented 220ms pure tones varying in frequency (0.5 to 8 kHz) and intensity (10 to 90 dB SPL) while recording from single units. Frequency response area (FRA) plots were constructed by assessing response strength at each frequency intensity combination (Fig. 5.3b). FRAs depict regions of the neurons receptive field that excite of suppress firing in each neuron, and are used to compute the features to which each neuron is tuned. Furthermore, each neural step response had a characteristic temporal profile in the peristimulus time histogram (PSTH), which we quantified using an onset index (OI), defined as the difference in onset and sustain firing rates divided by their sum (Fig. 5.3c.). To determine if the temporal response dynamics were sensitive to the onset of vocal learning, we compared the OI of neurons recorded 10 to 6 days prior to tutoring (Pre-T1), 5 to 1 day prior to tutoring (Pre-T2), post-tutor onset (Tut.), and in control isolate birds that were age matched to the Tut. group (Ctrl.). In thalamorecipient region L2, Tut. FS neurons had significantly higher OI measures than PreT1, PreT2, and Ctrl. FS neurons (Fig. 5.3d; $p<0.01$, Tukey-HSD), indicating that the temporal dynamics of the neural

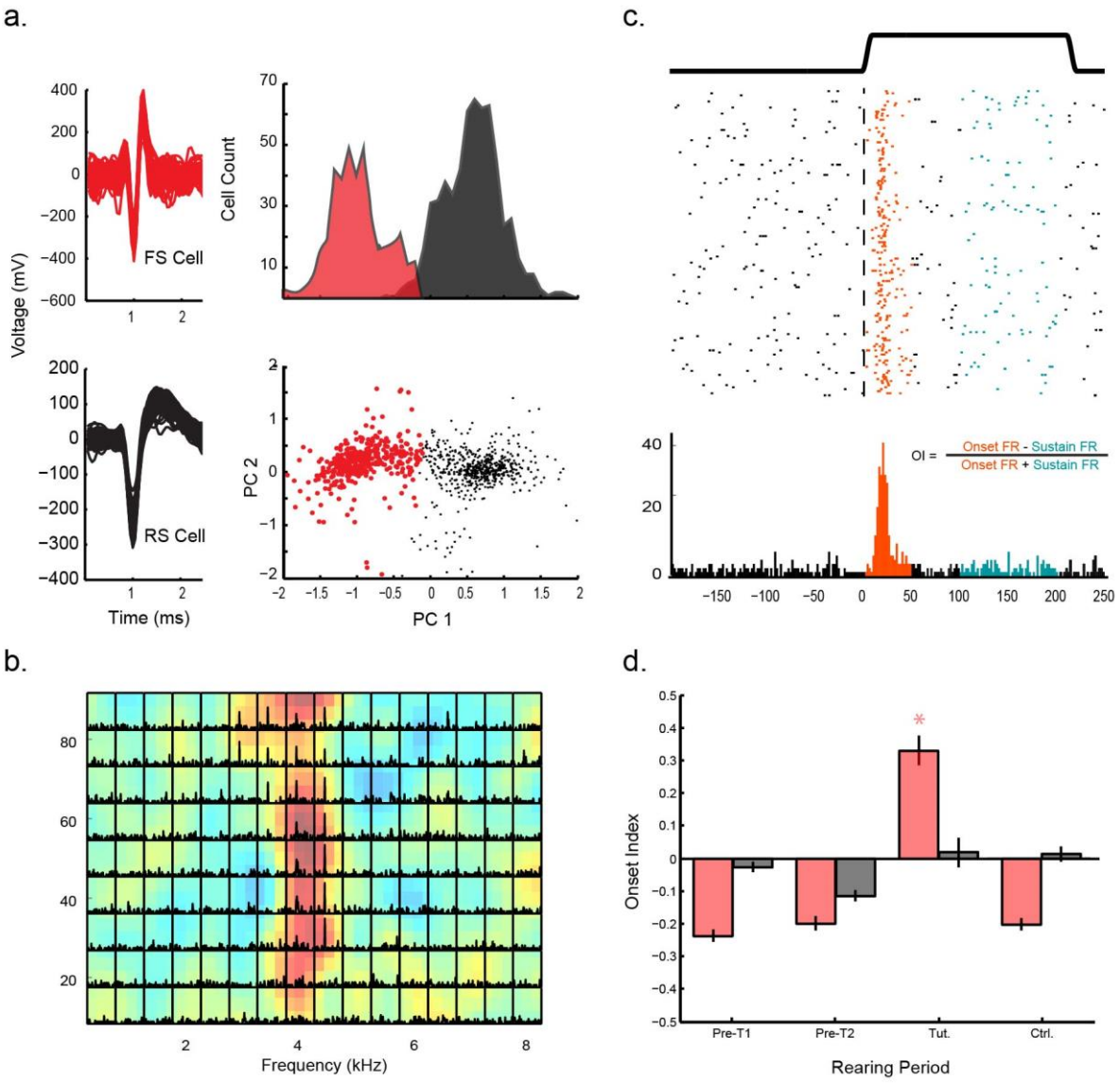

Figure 5.3: Fast-spiking (FS) neurons in L2 show enhanced onset responses following the onset of song learning. **(a.)** Two distinct cell types, delineated by their action potential shapes, are found in all regions of songbird AC. FS neurons are characterized by narrow action potentials and high firing rates. Regular spiking (RS) neurons are characterized by sparse firing and broad action potential shapes. **(b.)** Example FRA for an onset neuron tuned to 4 kHz. PSTH plots for each frequency/intensity combination, overlaying an interpolated heat map of neural response strengths at each frequency intensity combination. **(c.)** We quantified the temporal structure of each neuron's tone step response (top) using an onset index (OI). Raster plot of tone-evoked activity (middle) and the PSTH (bottom) of the fast spiking cell from **(b.)** shows strong onset responses (orange) and a deminished sustained response (aqua) with an OI of 0.95. **(d.)** FS neurons in L2 have higher OI following the onset relative to early in the pretutoring phase, late in the pretutoring phase, and compared to age matched Ctrl. birds (red bars). This is not the case in RS cells. Bars indicate mean values +/- S.E.M. *p<0.01

Region	Pre-T1	Pre-T2	Tut.	Ctrl.
CM	RS = 78; FS = 31	RS = 55; FS = 16	RS = 40; FS = 34	RS = 25; FS=15
L1	RS = 28; FS = 8	RS = 36; FS = 7	RS = 12; FS = 6	RS = 13; FS = 4
L2	RS = 40; FS = 33	RS = 36; FS = 25	RS = 18; FS = 12	RS = 37; FS = 27
L3	RS = 31; FS = 19	RS = 40; FS = 22	RS = 26; FS = 27	RS = 20; FS = 9
CST	18	11	30	23

Table 5.2: Summary of the number of each type of cell recorded during each rearing condition. Pre-T1 corresponds to days 10 to 6 prior to tutor onset at P50. Pre-T2 corresponds to days 5 to 1 prior to tutor onset. Tut. corresponds to all recording days following the onset of tutoring. Ctrl. corresponds to days P50+ in age-matched control birds that were never tutored. In each region, other than CSt, we divide our cells into RS and FS subpopulations, with corresponding n's reported. Neurons in the "other" region were recorded in hippocampus, or anterior to the auditory forebrain.

response are sensitive to the onset of vocal learning in this region and cell type. We did not observe temporal changes in OI for RS cells in L2 (Fig 5.3d), or in other subregions.

Spike timing reliability to tutor song playback gradually increases following tutoring onset in L2 FS neurons

The observed increase in OI values for L2 FS cells following the onset of tutoring indicates that the onset portion of the step response becomes stronger relative to the sustained portion of the response. We hypothesized that one functional consequence of this would be an enhancement of spike timing precision in response to complex stimuli. To test this hypothesis, we presented repeating playbacks of multiple renditions of each Tut. bird's tutor song to neurons throughout the AC (n = 124) following the onset of tutoring.

Of the 124 neurons for which tutor song responses were recorded, 20 were identified as L2 FS neurons. Figure 5.4a shows 5 representative cells recorded between post-tutor days 2 and 8. As vocal learning experience increased across days, we found a refinement of spike timing

a.

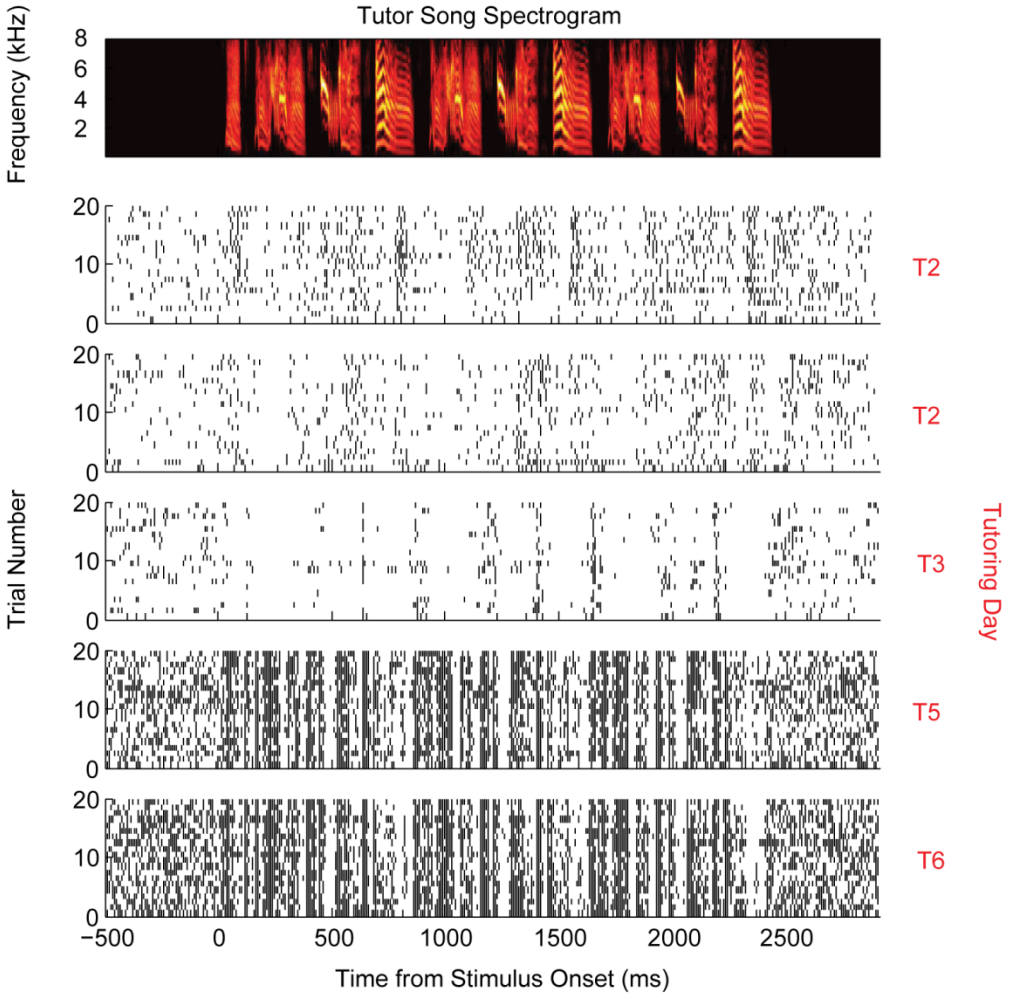
Tutor Song Spectrogram
Frequency (kHz)
8
6
4
2
Trial Number
T2
T2
T3
T5
T6
Tutoring Day
−500
0
500
1000
1500
2000
2500
Time from Stimulus Onset (ms)

b.

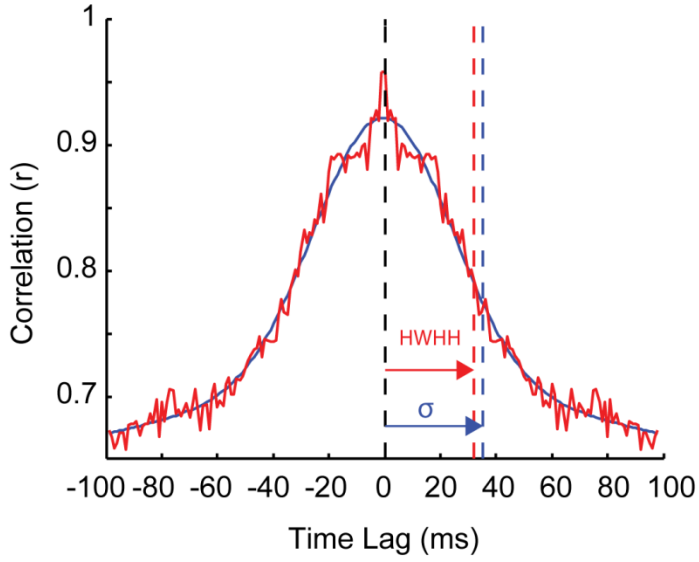
Correlation (r)
1
0.9
0.8
0.7
HWHH
σ
-100 -80 -60 -40 -20 0 20 40 60 80 100
Time Lag (ms)

c.

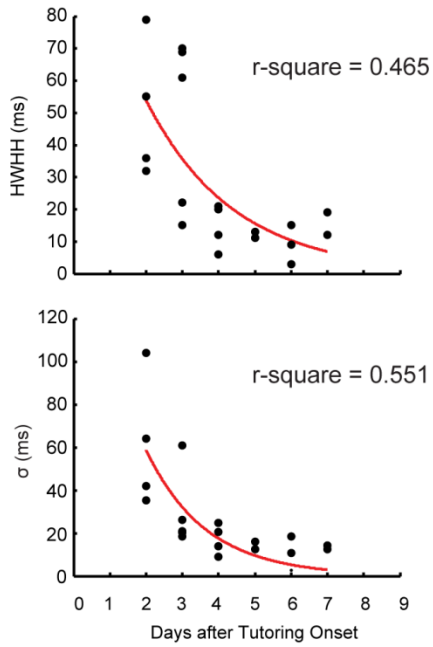
HWHH (ms)
r-square = 0.465
σ (ms)
r-square = 0.551
0 1 2 3 4 5 6 7 8 9
Days after Tutoring Onset

Figure 5.4: Spike timing precision to tutor song playback increases following tutor onset. a.) Raster plots from 5 different L2 FS neurons recorded across multiple post-tutoring days (red) to 20 repetitions of the same tutor song (top spectrogram). As post-tutor days progress, spike timing precision in L2 FS cells appears more refined. b.) The PSTH autocorrelogram function (red) for the top raster from a. (day T2) is fit with a Gaussian curve (blue). The Gaussian curve is used to measure the half width at half height (HWHH, red dotted line) and sigma (blue dotted line). c.) 20 L2 FS neurons recorded in the days post-tutor onset show an exponential decay in both HWHH and sigma, indicating that spike timing precision rapidly increases following the onset of tutoring.

precision within this neural subpopulation. We quantified neural precision by measuring the width of the central peak of each cell's PSTH autocorrelogram. Our method for assessing autocorrelogram width has been described previously, but briefly, we compute a neurons autocorrelation function by first averaging spike rates across trials in 1 ms bins (PSTH), and then computing the PSTH autocorrelation for time lags extending from -100 to 100 ms. The width of the central peak is assessed as the half width at half height (HWHH) or the standard deviation (σ) of a gaussian curve fit to the autocorrelation (Figure 5.4b). These two measures provide similar estimates of the timescale over which neural spiking events occur for each neuron.

Both the HWHH and σ of the autocorrelation demonstrate an exponential increase in spike-timing precision in the first week following the onset of tutoring in L2 FS neurons (Fig. 5.4c). Two to three days following the onset of tutoring, precision measures are highly variable, but on subsequent days the autocorrelation widths decrease to around 10ms, indicating that the timescale of individual firing events gradually becomes compressed with increased vocal learning experience. This is consistent with our finding of enhanced tone onset responses, and suggests that increasing exposure to vocal communication learning leads to enhanced patterning of neural responses to acoustic stimuli.

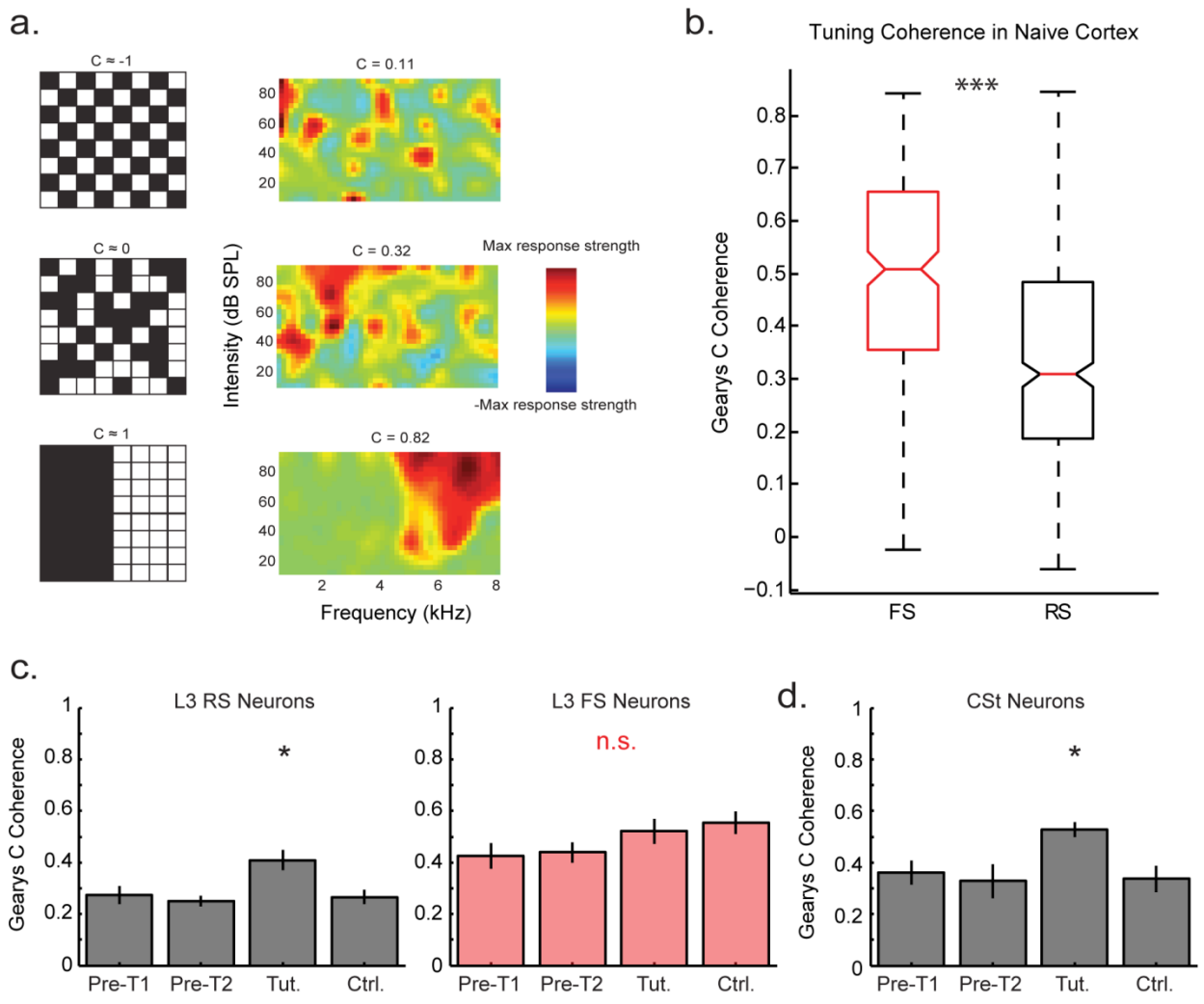

Figure 5.5. Tuning coherence increases following tutoring onset in L3 RS cells, and in CSt cells. a.) FRA tuning coherence is measured using Geary's contiguity (C) ratio. Black and white binary matrices illustrate potential Geary's C values for dispersed values (top left, C = -1), randomly scattered values (middle left, C = 0), and clustered values (bottom left, C = 1). Representative FRAs are depicted in the right column with their corresponding C values and range from randomly arranged (top) to coherently arranged (bottom). FRAs are plotted in a 3X upsampled form, but actual C values are computed on raw FRAs. b.) Geary's C values for all auditory neurons across all subregions in naïve, untutored birds are shown split in to FS (n = 161) and RS (n = 344) cells. FS cells had significantly higher C values across all regions. c.) L3 RS cells (left, black bars) display experience-dependent increases in tuning coherence. Neurons recorded following tutor onset (Tut.) were higher than those recorded 10 to 6 days prior to tutoring (Pre-T1), 5 to 1 day prior to tutoring (Pre-T2), and in age-matched control birds following the day 50 onset of tutor exposure (Ctrl.). No differences were observed for different rearing conditions in L3 FS cells. d.) CSt neurons had an experience-dependent increase in coherence following the onset of tutoring compared to Pre-T and Ctrl. neurons. Bars in c.) and d.) indicate mean values +/- S.E.M. *P<0.01, ***P<0.0001

Downstream areas L3 and Caudal Striatum: rapid song learning coincides with enhancement of receptive field structural coherence in L3 RS cells striatal neurons.

In addition to measuring experience-dependent changes in the temporal coding properties of cortical neurons, we asked if the auditory cortical representation of spectral information was sensitive to vocal learning by comparing receptive field structure before and after the onset of tutoring. Receptive field structure was assessed by computing FRA plots (Fig. 5.3b) for each of our recorded single units. Figure 5.5a shows three representative FRAs for neurons recorded in the pre-tutoring phase of the experiments. We found a variable degree to which these cells were coherently tuned to a specific subset of frequencies and intensities, and hypothesized that incoherently tuned neurons could represent an immature feature of AC neurons that could be refined with experience. We quantified receptive field structural coherence using Geary's contiguity ratio (C statistic), a measure of spatial autocorrelation within a matrix (see Methods and Materials). Geary's C statistic is an index that quantifies similarity or difference between local values within a spatially organized matrix. This is illustrated in Figure 5a, where binary (black and white) matrices illustrate potential values for C. Perfectly dispersed binary values yield a C measure of -1 (Fig. 5.5a, top checkerboard), randomly scattered binary values yield a C measure of 0 (Fig. 5.5a, middle checkerboard), and perfectly clustered values yield a C measure of approximately 1 (Fig. 5.5a, bottom checkerboard). The floor value for neural FRA matrices is approximately 0, as neurons tend to range from noisy to coherent (Fig. 5.5a, right column).

To assess the general coherence of receptive fields in the developing AC, we first compared FS and RS cells throughout the subregions of the AC in naïve, untutored birds. FS

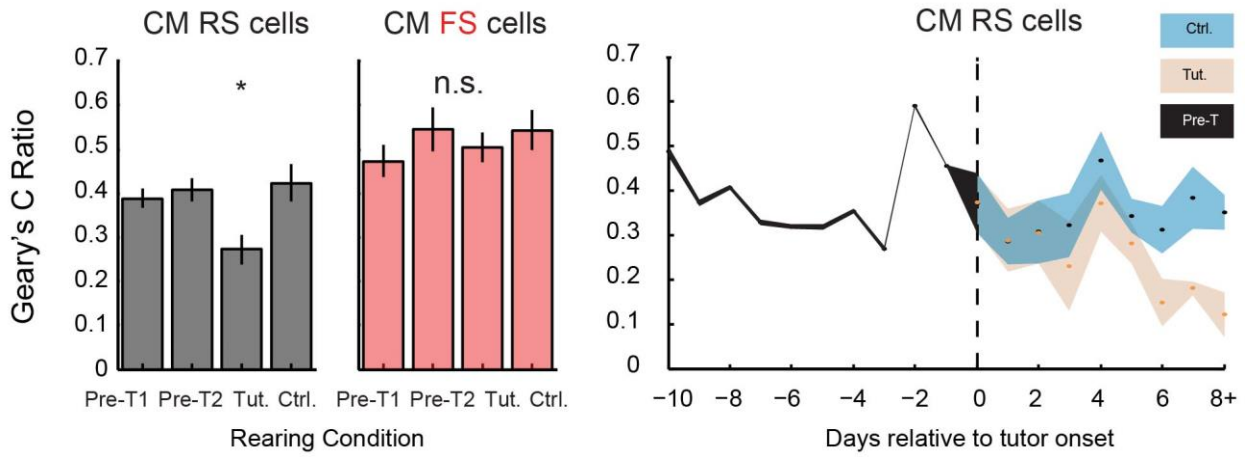

Figure 5.6: a.) CM RS neurons (left), but not FS neurons (right) undergo experience-dependent decreases in tuning coherence compared to Pre-T and Ctrl. neurons. b.) Plotting mean coherence measures (+/- S.E.M.) across days reveals an approximately week long gradual decrease in Geary's C values. * $P < 0.01$

neurons throughout the auditory cortex had high FRA coherence compared to RS cells (Fig. 5.5b). This suggests that in developing birds, FS cells may serve as a substrate for well-tuned, high fidelity auditory input, and may play an important role in early stages of song learning.

Although FRA coherence in RS cells was low in the naïve pre-tutoring phase, coherence measures showed an experience-dependent increase following the onset of tutor exposure in the ventral output region of the auditory cortex. RS cells in L3 had higher coherence in the Tut. condition compared to Pre-T1, Pre-T2, and Ctrl. cells (Fig. 5.5c; $p<0.01$, Tukey-HSD). Experience-dependent changes in coherence were not detected in L3 FS cells or other subregions of Field L, but were observed in the caudal striatum (CSt), where neurons had increased coherence following tutor onset compared to Ctrl. neurons (Fig. 5.5d, $p<0.01$ Tukey-HSD). The cell type distribution within CSt is not characterized, and so we do not distinguish between FS and RS cells in this region. CSt is a largely unexplored region in the forebrain, but it has known anatomical connectivity with Field L (Kelley and Nottebohm, 1979), and one study suggests that

it may form a functional corticostriatal loop with the L3 (Smith et al., 2006) that may be important for learning to discriminate sounds (Znameneskiy and Zador, 2013). The experience-based increase in L3 and CSt receptive field coherence during song tutoring may lend credence to this idea.

Higher order region CM: song learning coincides with a gradual decrease in tone receptive field coherence.

An experience-dependent shift in receptive field coherence also occurs in the secondary auditory region CM at the dorsal extent of the auditory forebrain axis. Unlike RS cells in L3 and neurons in CSt, RS cells in CM show progressively lower receptive field coherence following the onset of vocal learning, compared to CM RS neurons recorded from pre-tutored and untutored birds (Fig. 5.6a; $p<0.01$, Tukey-HSD). As in other regions, this effect of tutoring was not seen in CM FS cells (Fig. 5.6a).

In general, our recordings were biased toward sampling from CM because it is the most dorsal region in the auditory forebrain and spans significant depth. As a result, we recorded a large number of CM cells compared to other regions, allowing us to observe the timecourse over which changes in CM receptive field coherence decreases in RS cells. Figure 5.6b shows that compared to RS cells recorded from Ctrl. birds (grey), RS neurons in Tut. pupils (red) decrease in tuning coherence over roughly one week compared to baseline recordings. The week long change in CM tuning coherence is consistent with the timecourse of changes that we observed in neural precision in L2 FS neurons, suggesting that the mechanisms responsible for the distinct

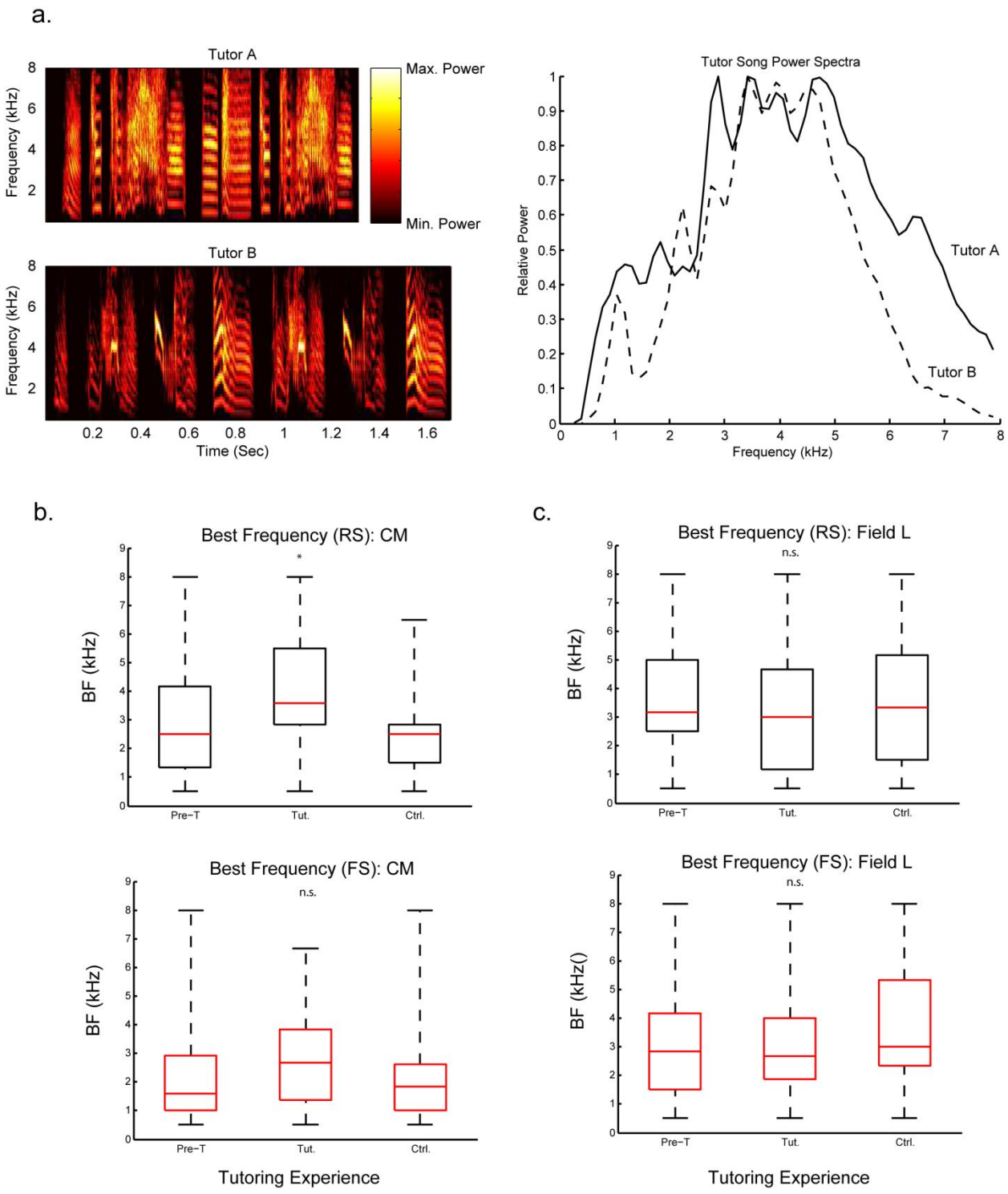

Figure 5.7: Tutoring experience shapes frequency representation in CM RS cells, but not Field L neurons. a.) Tutor song spectrograms (left) and power spectra (right) for the two experimental tutors reveal similar spectral characteristic. Peak power in the frequency distributions is centered from 3 – 5 kHz in both birds, with similar frequency roll-offs to neighboring frequencies. b.) Best frequency distributions for Pre-T, Tut., and Ctrl. conditions reveal that frequency tuning

(**Figure 5.7, cont.**) increases in CM RS cells (top) but not FS cells following the onset of tutoring. This increase in BFs shifts the frequency representation of CM RS cells into the range of peak power for the tutors' songs. c.) Neither RS cells (top) nor FS cells (bottom) across subregions of Field L have BF differences across rearing conditions. $*P < 0.01$

changes in different subpopulations of neurons are operating over similar timescales, and are stimulated by the experience of adult songs.

Frequency representation in CM, but not Field L, aligns with the acoustics of tutor song in an experience dependent way.

Vocal learning-dependent changes in L3, CSt and CM receptive field structure led us to hypothesize that experience of vocal sounds and early social learning contribute to the development of auditory coding strategies that represent important acoustic features for learning vocal communication signals. To test this hypothesis, we measured the power spectra of adult male tutor birds used in our Tut. rearing condition, and asked whether the distributions of frequency tuning in the auditory cortex matched the acoustics of the tutor song power spectra. We assessed frequency tuning for individual neurons by summing the response power of each FRA over all intensities, and assigned each neuron a best frequency (BF) based on the frequency that drove the peak response across summed intensities. For this analysis, we upsampled each FRA 3X to increase frequency resolution prior to assigning a BF (see Methods and Materials).

The songs of the two tutor birds had similar spectral acoustics (Fig. 5.7a). Frequency power spectra were computed by first calculating song spectrograms for each tutor (Fig. 5.7a, left column), and then averaging the spectrogram across all time points (Fig. 5.7a, right column). The song power spectra of the two tutors were each averaged for 5 song renditions, and then

normalized by each of their peak frequencies. In both cases, the highest power in tutors' songs was between 3 and 5 kHz, with gradual power roll-offs to neighboring frequencies.

We then compared frequency tuning for RS and FS cells in Field L and CM that were significantly, coherently tuned based on their Geary's C measures. Significant coherence was assessed by calculating z-scores for each neuron's Geary's C measurement (see Methods and Materials). Neurons with a Geary's C z-score greater than 1.96 were considered to be significantly tuned at the $p < 0.05$ level, and were included in this BF tuning analysis.

BF distributions for naïve, untutored RS and FS neurons in CM are skewed toward lower frequencies, but the BF distribution for CM RS cells increases into the range of peak tutor song power following the onset of tutoring, compared to untutored, age-matched Ctrl. birds (Fig. 5.7b, top panel). This increase in BF was not apparent in our CM FS recordings (Fig. 5.7b, bottom panel), nor were changes in BF seen in Field L, which we report here with its subregions grouped together (Fig. 5.7c). This suggests that vocal learning drives the frequency representation of well-tuned RS cells in CM to form a match of the frequency distribution of the tutor's song. Given that we see an overall decrease in the receptive field coherence of CM RS cells as a whole, this suggests that neurons tuned for lower frequencies may gradually lose their tuning coherence, leaving behind a coherent subpopulation of cells with BFs matched to the acoustics of song.

Behavioral-context dependent auditory responses reveal specialization in CM for processing vocal output.

Our observations led us to hypothesize that dorsal and ventral AC neurons may serve distinct functional roles during the vocal learning phase and into adulthood. Ventral neurons in L3 and CSt have enhanced receptive field structure following the onset of vocal learning, while dorsalneurons in CM form a tuning distribution that is gradually shaped to match the acoustics of song. Furthermore, CM is a putative input to the song premotor nucleus HVC and may act as an important conduit of auditory-vocal mapping during song learning. To test the hypothesis that dorsal output of the AC is specialized for processing vocal acoustics, we asked whether neurons on opposite poles of the auditory cortical axis responded differently to the behavioral context of auditory input. Following roughly two weeks of acclimation to the recording chamber and tutoring paradigm, Tut. birds would begin to sing while electrophysiologically teathered to their headstage. Once the birds began singing repeated motifs, we were then able to record neural responses to auditory feedback during singing and subsequently record auditory responses to recordings of the bird's own song. Previous work has shown that this varying context for a bird hearing its own vocalizations can modulate the response properties of auditory cortical neurons (Keller and Hahnloser, 2008), but whether different auditory subregions respond differently from one another remains unclear.In many cases, auditory neurons in the songbird forebrain were highly sensitive to varying the behavioral context. Figure 5.8a shows a single unit recorded in CM during live vocal practice. We aligned neural responses to repeated live song motifs by aligning the amplitude envelopes of individual songs (Fig. 5.8a, second panel). Amplitude envelopes of live song are depicted in black, while song playback is depicted in red. Despite natural variation from rendition to rendition, this alignment is sufficient to reveal rich acoustic structure in the average of the aligned song spectrograms (Fig. 5.8a, top panel). Using these

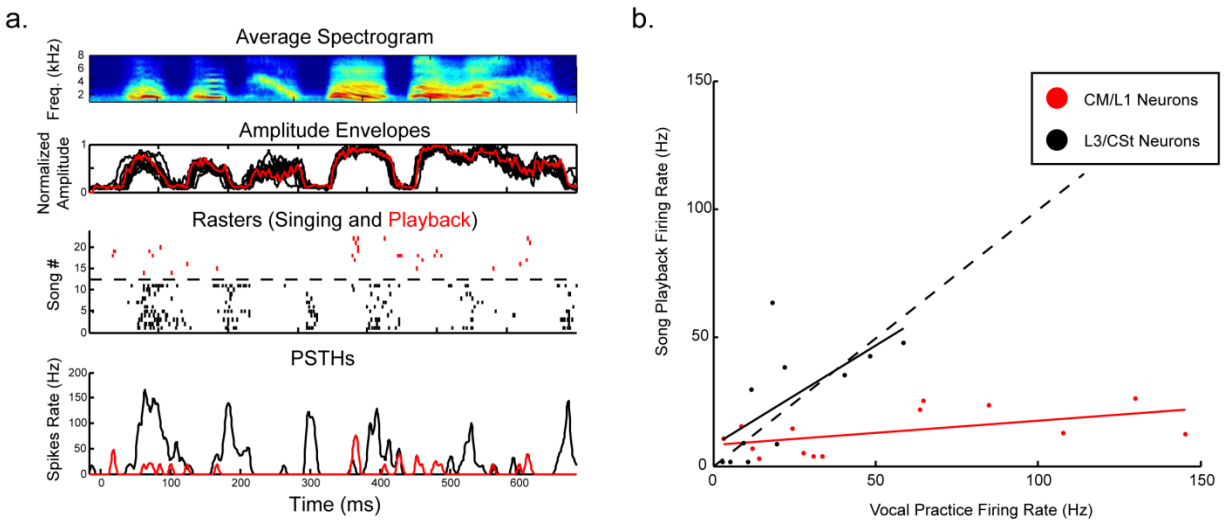

Figure 5.8: Dorsal output regions of the songbird auditory cortex are highly sensitive auditory behavioral context compared to ventral neurons. a.) An example CM neuron displays robust bursts of action potentials aligned to individual syllables of live singing motifs, but fails to respond reliably to playback of the same sounds. The average spectrogram (top) of the juvenile's live singing is aligned by the amplitude envelopes of individual live motifs (second row). Raster plots and PSTHs show profound differences in the firing pattern of vocal auditory feedback and song playback in this example neuron. b.) Groups of neurons recorded at either the dorsal extent of the auditory forebrain (CM and L1, red) or ventral extent (L3 and CSt) display different sensitivity to live singing vs. playback. As a population, dorsal neurons were highly sensitive to live singing, while ventral neurons responded more linearly between contexts.

temporally aligned songs, we were then able to compare rasters (Fig. 5.8a, third panel) and PSTHs of live singing (black) and song playback (red). In this example neuron, live singing resulted in strong bursts of action potentials corresponding to each unique syllable, while playback of the song failed to elicit strong auditory responses.

We recorded live singing and playback responses from 23 AC neurons, which we grouped into dorsal (CM/L1) and ventral (L3/CSt) cohorts. Neurons in the dorsal group were highly sensitive to behavioral context, firing much stronger to live singing than playback. Neurons in the ventral group responded similarly across these two contexts. This suggests that during vocal learning, dorsal output regions are specialized for processing vocal auditory feedback, while

ventral output regions respond more linearly. This may be consistent with differing learning-dependent effects that we see between these regions.

5.5 Discussion

Here we used a novel experimental framework to study the link between vocal communication learning and developmental plasticity in auditory cortical neurons. We found that juvenile songbirds deprived of tutoring well into the critical period for tutor song memorization showed an ability to rapidly form accurate copies of a tutor's song, whereas birds reared in isolation from adult male song but otherwise similar experimental conditions developed atypical vocalizations that did not indicate learning. This approach supports previous song learning findings (Tchernichovski et al., 2001), and shows that song learning can occur in tandem with chronic electrophysiology in the auditory forebrain.

Our neural hypotheses were driven by three previous observations. First, delayed song tutoring leads to rapid physiological changes in song vocal-motor nuclei (Roberts et al., 2010; Shank and Margoliash, 2008). Second, rapid and accurate song copying can occur with limited exposure to a tutor (Tchernichovski et al., 1999). Rapid neuronal plasticity and learning indicate that naive juvenile songbirds are capable of accurately mapping auditory information onto vocal-motor control circuits. This would suggest that neurons in the early auditory system are prepared to code for important acoustic features in the tutor song. Third, studies in mammals and zebra finches have demonstrated that the neural firing rate selectivity for salient acoustic stimuli is sensitive to developmental manipulations (Amin et al., 2007, 2014). We sought to understand these previous results by recording from naïve juveniles before exposure to song and throughout vocal learning.

We asked which auditory subregions and cell types featured stability and/or plasticity at the onset of tutoring. We found evidence for an early putative substrate for high fidelity auditory mapping into the song motor system in FS neurons, as well as an experience driven specialization of two auditory pathways in the songbird auditory cortex: a dorsal pathway for song processing, and a ventral region that becomes linearly driven by broad acoustic stimuli with experience.

We observed that L2 FS neurons develop stronger onset responses following the onset of tutoring, but not in age matched controls. The spike timing precision of these neurons during the processing of tutor song also increased in an experience dependent manner. First time exposure to tutoring brings naive juveniles into contact with strongly temporally modulated external stimuli. This finding is complementary to studies in mammals showing that development in the absence of modulated sounds, or over exposure to slowly modulated sounds, diminishes the ability of cortical neurons to lock to rapidly modulated sounds (Chang and Merzenich, 2003; Zhou and Merzenich, 2008). Together, our results and those of others demonstrate the importance of hearing temporally modulated sounds during development. We cannot say for certain whether experience-dependent shifts in spiking precision occur in Field L *de novo*, or whether they are inherited from upstream regions such as the auditory thalamus or midbrain. Future studies will be required to determine if lower auditory regions exhibit similar experience-dependent development.

We observed that FRA tuning coherence, measured by Geary's C ratio, shifted following the onset of tutoring. Ventral cortical output region L3 RS neurons and CSt neurons developed high coherence with the onset of vocal learning, while dorsal output region neurons in CM showed decreases in FRA coherence following the onset of vocal learning. This suggests a

potential functional difference in the processing of sounds in these two areas. One study used a computational model to infer functional connectivity between L3 and CSt, and the similar experience-dependent increase in receptive field structure in these regions may be parsimonious with this hypothesis. If L3 and CSt comprise a part or whole corticostriatal loop, these regions may be important for learning to discriminate between sounds. Corticostriatal connections play an important role in the performance of auditory discrimination tasks in mammals (Znamenskiy and Zador, 2013), but their role in the sensory cortex of birds remains unclear.

CLM projects to the song system premotor nucleus HVC (Bauer et al., 2008), implicating CM as an important region for mapping song acoustic information onto motor control circuits. The shift in tuning coherence in CM may indicate the development of specialization in this structure for vocal-motor imitation, and suggests that nonlinear, song-selective processing in CM emerges in an experience-dependent manner during development. Previous studies have shown that neurons in CM have higher firing rates to birdsong than synthetic tone stimuli, and that juvenile zebra finches display adult-like song selectivity in CM (Grace et al., 2003).

We cannot say for certain whether the decrease in FRA coherence corresponds to the emergence of song selectivity. However, we found that significantly tuned neurons in CM had best frequency distributions that matched the spectral acoustics of tutor songs following the onset of tutoring. This may indicate that CM takes advantage of experience-dependent plasticity to optimally represent the features of tutor songs. Furthermore, our observation that CM and L1 neurons exhibit strong behavior-context sensitivity indicates that these regions are particularly specialized for processing vocal feedback during song learning. In total, our results argue that CM exists as a higher order, non-linear processing region dedicated to sensorimotor learning.

Chapter 6: Concluding remarks

In this dissertation I showed that experimental and behavioral contexts relating to arousal are sufficient to alter neural excitability in a way that has implications for neural coding in the songbird auditory system. Urethane, a common anesthetic used in neurophysiological studies of songbird and mammalian auditory neurons, suppresses neural excitability, but does not alter spectrotemporal tuning or neural discrimination in single auditory midbrain neurons. Norepinephrine, a neurotransmitter involved mediating changes in arousal and behavioral state, similarly has an overall suppressing effect on neural excitability at certain doses. This was seen to improve phase-locking in a subset of Field L neurons, while simultaneously reducing the reliability of evoked spikes and neural discrimination of sounds.

I then reported the results of a developmental study that demonstrates experience-dependent changes in temporal and spectral tuning in the songbird auditory cortex during vocal learning. These effects were found to have region and cell-type specificity, and highlight potential functional roles for dorsal and ventral auditory cortical neurons in the songbird. This is one of the few studies to exploit naturalistic developmental conditions to probe the developing auditory system in juvenile animals.

Future studies will continue to provide insights into the effects demonstrated here. It remains to be seen if the specific experience-dependent changes observed during vocal learning persist into adulthood. One way to address this issue will be to cross-foster different species that have songs with distinct acoustic statistics, and to assess the degree to which non-natural foster parents can impart these acoustic features onto a neural representation in their foster offspring. It is conceivable that the effects observed as a result of vocal learning are temporary, and are altered during specific time points in service of vocal learning during development.

Furthermore, it remains to be seen whether experience-dependent plasticity in the songbird auditory cortex is purely a result of auditory experience, social arousal, vocal practice, or some combination of these distinct aspects of the vocal learning environment.

To address cellular and molecular level mechanisms involved in the development of the songbird auditory system, intracellular recordings of excitatory and inhibitory conductances may explain how receptive field coherence emerges over time in ventral cortical regions, while diminishing in dorsal regions. Using modern optical techniques such as 2-photon imaging will allow experimenters to track populations of identified neurons over time during development, particularly in regions near the surface of the brain, such as CM. The ability to monitor single neurons across days of recordings will add a great deal of explanatory power to the results reported in this dissertation.

In the limit of infinite recordings, it may be possible to link distinct stages of vocal learning to the development of auditory cortex. For instance, it may be possible to observe distinct auditory coding signatures associated with subsong, plastic song, and crystalized song. Such an analysis would require high temporal resolution that is not possible in limited data sets, and could make use of multi-electrode arrays to record neural populations over time, rather than single units.

Future studies into the functional connectivity of genetically distinct cell types will also inform the results reported here. It is presumed that FS and RS neurons correspond to inhibitory interneurons and excitatory principle cells, respectively, but this has not been demonstrated empirically as of yet. Despite decades of research, there remain regions of the auditory forebrain that are relatively unexplored, including the putative connections between Field L and CSt.

Finally, it will be important to try to tie the neural effects of rearing experience to perceptual performance. Birds can be readily trained to perform operant discrimination tasks, and it is therefore possible to ask whether effects of rearing conditions reveal themselves in the perceptual abilities of juvenile or adults songbirds.

Bibliography

Aitkin LM, Merzenich MM, Irvine D (1986) Frequency representation in auditory cortex of the common marmoset (Callithrix jacchus jacchus). *J Comp Neurol*, 252(2): 175-85.

Aitkin LM, Moore DR (1975) Inferior colliculus. II. Development of tuning characteristics and tonotopic organization in central nucleus of the neonatal cat. *J Neurophysio,*. 38: 1208-16.

Albrecht D, Davidowa H. (1989) Action of urethane on dorsal lateral geniculate neurons. *Brain Res Bull*, 22: 923-27.

Aitkin LM, Reynolds A (1975) Development of binaural responses in the kitten inferior colliculus. *Neurosci Letters* 1(6):315–19.

Altman J, Bayer SA (1981) Time of origin of neurons of the rat inferior colliculus and the relations between cytogenesis and tonotopic order in the auditory pathway. *Exp Brain Res* 42:411–23.

Amin N, Gastpar M, Theunissen, FE (2013) Selective and Efficient Neural Coding of Communication Signals Depends on Early Acoustic and Social Environment *PLoS one* 8(4):e61417.

Amin N, Gill P, Theunissen FE (2010) Role of the zebra finch auditory thalamus in generating complex representations for natural sounds. *J Neurophysiol*, 104(2): 784-98.

Amin N, Grace JA, Theunissen FE (2004) Neural response to bird's own song and tutor song in the zebra finch field L and caudal mesopallium. *J Comp Physiol A* 190:469–89.

Andoni S, Li N, Pollak GD (2007) Spectrotemporal receptive fields in the inferior colliculus revealing selectivity for spectral motion in conspecific vocalizations. *J Neurosci* 27:4882–93.

Appeltants, D, Absil, P, Balthazart, J, and Ball, GF (2000) Identification of the origin of catecholaminergic inputs to HVc in canaries by retrograde tract tracing combined with tyrosine hydroxylase immunocytochemistry. *Journal of Chemical Neuroanatomy*, 18(3):117-33.

Appeltants, D, Ball, GF, Balthazart, J (2002) The origin of catecholaminergic inputs to the song control nucleus RA in canaries. *Neuroreport,* 13(5):649-53.

Appeltants, D, Del Negro, C, and Balthazart, J (2002) Noradrenergic control of auditory information processing in female canaries. *Behavioral Brain Research*, 133(2):221-35.

Aronov D, Andalman AS, Fee MS (2008) A specialized forebrain circuit for vocal babbling in the juvenile songbird. *Science* 320:630–634.

Aston-Jones, G, and Bloom, FE (1981) Norepinephrine-containing locus coeruleus neurons in behaving rats exhibit pronounced responses to non-noxious environmental stimuli. *J Neurosci*, 1(8):887-900.

Aston-Jones, G, and Cohen, JD (2005) An integrative theory of locus coeruleus-norepinephrine function: adaptive gain and optimal performance. *Annual Reviews in Neuroscience*, 28: 403-50.

Atiani S, Elhilali M, David SV, Fritz JB, and Shamma SA (2009) Task difficulty and performance induce diverse adaptive patterns in gain and shape of primary auditory cortical receptive fields. *Neuron*, 61: 467-80.

Bair W, and Koch C (1996) Temporal precision of spike trains in extrastriate cortex of the behaving macaque monkey. *Neural Comput*, 8: 1185-1202.

Barclay, SR, Harding, CF, and Waterman, SA (1992) Correlations between catecholamine levels and sexual behavior in male zebra finches. *Pharmacology Biochemistry and Behavior*, 41(1):195-201.

Barclay, SR, Harding, CF, Waterman, SA (1996) Central DSP-4 treatment decreases norepinephrine levels and courtship behavior in male zebra finches. *Pharmacology Biochemistry and Behavior*, 53(1):213-20.

Banai K, Sabin AT, Wright BA (2011) Separable developmental trajectories for the abilities to detect auditory amplitude and frequency modulation. *Hear Res.* 280(1): 219-27

Bauer, EE, Coleman, MJ, Roberts, TF, Roy, A, Prather, JF, and Mooney R (2008) A synaptic basis for auditory-vocal integration in the songbird. *J Neurosci* 28(6):1509–22.

Berridge, CW, and Waterhouse, BD (2003) The locus coeruleus-noradrenergic system: modulation of behavioral state and state-dependent cognitive processes. *Brain Research Reviews*, 42(1):33-84.

Berry, MJ, Warland, DK, Meister, M (1997) The structure and precision of retinal spike trains. *Proc Nat Acad Sci USA*, 94(10): 5411-16

Bigalke-Kunz B, Rübsamen R, Dörrscheidt GJ (1987) Tonotopic organization and functional characterization of the auditory thalamus in a songbird, the European starling. *J Comp Physiol A,* 161:255–265.

Blättler F, Hahnloser R (2011) An efficient coding hypothesis links sparsity and selectivity of neural responses. *PLoS one*, 6(10),e25506.

Bonham BH, Cheung SW, Godey B (2004) Spatial organization of frequency response areas and rate/level functions in the developing AI. *J Neurophysiol*, 91(2), 841-54

Bonke DBA, Bonke D, Scheich H (1979) Connectivity of the auditory forebrain nuclei in the

Guinea Fowl (Numida meleagris). *Cell Tissue Res,* 200:101–121.

Bottjer SW, Halsema KA, Brown SA (1989) Axonal connections of a forebrain nucleus involved with vocal learning in zebra finches. *J Comp Neurol,* 279(2): 312-26

Brainard MS, Doupe AJ (2000) Interruption of a basal ganglia forebrain circuit prevents plasticity of learned vocalizations. *Nature* 404:762–66.

Brainard MS, Knudsen EI (1993) Experience-dependent plasticity in the inferior colliculus: a site for visual calibration of the neural representation of auditory space in the barn owl. *J Neurosci,* 13:4589–4608.

Brunso-Bechtold JK, Henkel CK (2005) Development of Auditory Afferents to the Central Nucleus of the Inferior Colliculus. In: *The Inferior Colliculus*, pp 537–558. Springer New York.

Buehlmann, A, and Deco, G (2008) The neuronal basis of attention: rate versus synchronization modulation. *J Neurosci*, 28(30):7679-86.

Butts, DA, Weng, C, Jin, J, Yeh, CI, Lesica, NA, Alonso, JM, and Stanley, GB (2007) Temporal precision in the neural code and the timescales of natural vision. *Nature*, 449(7158): 92-5.

Calabrese A, Schumacher JW, Schneider DM, Paninski L, and Woolley SM (2011) A generalized linear model for estimating spectrotemporal receptive fields from responses to natural sounds. *PLoS one*, 6: e16104.

Capsius B, and Leppelsack HJ (1996) Influence of urethane anesthesia on neural processing in the auditory cortex analogue of a songbird. *Hear Res,* 96: 59-70

Cardin JA, Raksin JN, Schmidt MF (2005) Sensorimotor nucleus NIf Is necessary for auditory processing but not vocal motor output in the avian song system. *J Neurophysiol,* 93:2157–66.

Cardin JA, Schmidt MF (2003) Song system auditory responses are stable and highly tuned during sedation, rapidly modulated and unselective during wakefulness, and suppressed by arousal. *J Neurophysiol,* 90:2884–99.

Cardin JA, Schmidt MF (2004a) Noradrenergic inputs mediate state dependence of auditory responses in the avian song system. *J Neurosci,* 24:7745–53.

Cardin JA, Schmidt MF (2004b) Auditory Responses in Multiple Sensorimotor Song System Nuclei Are Co-Modulated by Behavioral State. *J Neurophysiol,* 91:2148–63.

Capsius, B, and Leppelsack, HJ (1996) Influence of urethane anesthesia on neural processing in the auditory cortex analogue of a songbird. *Hear Res*, 96:59-70.

Castelino, CB, and Ball, GF (2005) A role for norepinephrine in the regulation of context-dependent ZENK expression in male zebra finches (Taeniopygia guttata). *European Journal*

of Neuroscience, 21(7):1962-72.

Castelino, CB, and Ball, GF (2006) Differences in singing behavior by zebra finches across social context are abolished by systemic depletion of norepinephrine in the song control circuit. *Abstract Viewer/Itinerary Planner,. Society for Neuroscience, Atlanta, GA (Online).*

Castelino, CB, Diekamp, B, and Ball GF (2007) Noradrenergic projections to the song control nucleus area X of the medial striatum in male zebra finches (Taeniopygia guttata). *J Comp Neurol*, 502(4)544-62.

Castelino, C, and Schmidt, M (2009) What birdsong can teach us about the central noradrenergic system. *Journal of Chemical Neuroanatomy*, 39(2): 96-111.

Catchpole, CK, & Slater, PJB (1995) Bird Song. *Cambridge University Press.*

Chang EF, Bao S, Imaizumi K (2005) Development of spectral and temporal response selectivity in the auditory cortex. *Proc Nat Acad Sci USA*, 102(45): 16460-5.

Chang EF, Merzenich MM (2003) Environmental noise retards auditory cortical development. *Science* 300:498–502.

Chase SM, and Young ED. (2007) First-spike latency information in single neurons increases when referenced to population onset. *Proc Nat Acad Sci USA*, 104: 5175-80.

Chew SJ, Mello C, Nottebohm F, Jarvis E, Vicario DS (1995) Decrements in auditory responses to a repeated conspecific song are long-lasting and require two periods of protein synthesis in the songbird forebrain. *Proc Nat Acad Sci USA*, 92:3406–3410.

Cirelli, C, and Tononi G (2000) Gene expression in the brain across the sleep-waking cycle. *Brain Research*, 885(2):303- 21.

Cirelli, C, and Tononi, G (2004) Locus ceruleus control of state-dependent gene expression. *J Neurosci*, 24(23):5410-19.

Clayton NS (1987) Song learning in cross-fostered zebra finches: a re-examination of the sensitive phase. *Behaviour.* 67-81.

Clayton NS (1989) The effects of cross-fostering on selective song learning in estrildid finches. *Behaviour,* 163-75.

Coleman MJ, Mooney R (2004) Synaptic transformations underlying highly selective auditory representations of learned birdsong. *J Neurosci*, 24:7251–7265.

Coleman MJ, Roy A, Wild JM, Mooney R (2007) Thalamic gating of auditory responses in telencephalic song control nuclei. *J Neurosci*, 27:10024–10036.

Cousillas H, Richard JP, Mathelier M, Henry L, George I, Hausberger M (2004) Experience-

dependent neuronal specialization and functional organization in the central auditory area of a songbird. *European Journal of Neuroscience* 19:3343–3352.

Cruikshank SJ, and Weinberger NM (1996). Receptive-field plasticity in the adult auditory cortex induced by Hebbian covariance. *J Neurosci* 16: 861-875

Dave AS, Yu AC, Margoliash D (1998) Behavioral state modulation of auditory activity in a vocal motor system. *Science,* 282:2250–2254.

David SV, Mesgarani N, Fritz JB, and Shamma SA (2009) Rapid synaptic depression explains nonlinear modulation of spectro-temporal tuning in primary auditory cortex by natural stimuli. *J Neurosci,* 29: 3374-3386

deCharms RC, and Merzenich MM (1996). Primary cortical representation of sounds by the coordination of action-potential timing. *Nature,* 381: 610-613

Desimone, R, and Duncan, J (1995) Neural Mechanisms of selective visual attention. *Annual Reviews in Neuroscience,* 18:193-222.

Devilbiss, DM, Page, ME, Waterhouse, BD (2006) Locus ceruleus regulates sensory encoding by neurons and networks in waking animals. *J Neurosci*, 26(39):9860-72.

de Villers-Sidani E, Chang EF, Bao S, Merzenich MM (2007) Critical period window for spectral tuning defined in the primary auditory cortex (A1) in the Rat. *J Neurosci*, 27:180–189.

Devoogd TJ, Krebs JR, Healy SD, Purvis A (1993) Relations between song repertoire size and the volume of brain nuclei related to song: comparative evolutionary analyses amongst oscine birds. *Proc R Soc Lond B,* 254:75–82.

DeWeese MR, Wehr M, and Zador AM (2003) Binary spiking in auditory cortex. *J Neurosci,* 23: 7940-7949

Dorrn AL, Yuan K, Barker AJ, Schreiner CE, Froemke RC (2010) Developmental sensory experience balances cortical excitation and inhibition. *Nature* 465:932–936.

Doupe AJ, Konishi M (1991) Song-selective auditory circuits in the vocal control system of the zebra finch. *Proc Nat Acad Sci USA,* 88:11339–43.

Doupe, AJ, & Kuhl, PK (1999) Birdsong and human speech: common themes and mechanisms. *Annual Reviews in Neuroscience,* 22:567-631.

Duda RO, Hart PE, and Stork DG (2001). *Pattern Classification*. Wiley.

Elfenbein JL, Small AM, Davis JM (1993) Developmental Patterns of Duration Discrimination. *J Speech Hear Res,* 36:842–849.

Elliot TM, Christensen-Dalsgard J, Kelley DB (2011) Temporally selective processing of communication signals by auditory midbrain neurons. *J Neurophys,* jn.00261

Escabi MA, and Read HL (2003). Representation of spectrotemporal sound information in the ascending auditory pathway. *Biol Cybern,* 89: 350-362,

Fathke RL, Gabriele ML (2009) Patterning of multiple layered projections to the auditory midbrain prior to experience. *Hear Res,* 249:36–43.

Fischer FP (1994) Quantitative TEM analysis of the barn owl basilar papilla. *Hear Res,*73:1–15.

Fortune ES, Margoliash D (1992) Cytoarchitectonic organization and morphology of cells of the field L complex in male zebra finches (Taenopygia guttata). *J Comp Neurol,* 325(3), 388-404.

Fortune ES, Margoliash D (1995) Parallel pathways and convergence onto HVc and adjacent neostriatum of adult zebra finches (Taeniopygia guttata). *J Comp Neurol,* (360)3:413-441.

Foster EF, Bottjer SW (1998) Axonal connections of the High Vocal Center and surrounding cortical regions in juvenile and adult male zebra finches. *J Comp Neurol,* 397:118–38.

Franks NP, and Lieb WR (1994) Molecular and cellular mechanisms of general anaesthesia. *Nature,* 367: 607-14

Fritz, JB, Elhilali, M, David, SV, & Shamma, SA (2007) Auditory attention – focusing the searchlight on sound. *Curr Opin Neurobiol,* 17:437-55.

Fritz, J, Elhilali, M, and Shamma, S (2005) Active listening: task-dependent plasticity of spectrotemporal receptive fields in primary auditory cortex. *Hear Res,* 206(1-2):159-76.

Fritz J, Shamma S, Elhilali M, Klein D (2003) Rapid task-related plasticity of spectrotemporal receptive fields in primary auditory cortex. *Nat Neurosci,* 6:1216–23.

Fritz JB, David SV, Radtke-Schuller S, Yin P, Shamma SA (2010) Adaptive, behaviorally gated, persistent encoding of task-relevant auditory information in ferret frontal cortex. *Nat Neurosci,* 13:1011–19.

Froemke RC, Dan Y (2002) Spike-timing-dependent synaptic modification induced by natural spike trains. *Nature,* 416:433–38.

Froemke RC, Jones BJ (2011) Development of auditory cortical synaptic receptive fields. *Neuroscience & Biobehavioral Reviews* 35:2105–13.

Froemke RC, Merzenich MM, Schreiner CE (2007) A synaptic memory trace for cortical receptive field plasticity. *Nature,* 450:425–29.

Fuzessery ZM, Pollak GD (1985) Determinants of sound location selectivity in bat inferior colliculus: a combined dichotic and free-field stimulation study. *J Neurophysiol,* 54(4):757-

81.

Fuzessery ZM, Razak KA, Williams AJ (2011) Multiple mechanisms shape selectivity for FM sweep rate and direction in the pallid bat inferior colliculus and auditory cortex. *J Comp Physiol A,* 197:615–623.

Gabriele ML, Brunso-Bechtold JK (2000) Plasticity in the development of afferent patterns in the inferior colliculus of the rat after unilateral cochlear ablation. *J Neurosci,* 20(18):6939-49

Gabriele ML, Brunso-Bechtold JK, Henkel CK (2000) Development of afferent patterns in the inferior colliculus of the rat: Projection from the dorsal nucleus of the lateral lemniscus. *J Comp Neurol,* 416:368–82.

Gaese BH, and Ostwald J (2001) Anesthesia changes frequency tuning of neurons in the rat primary auditory cortex. *J Neurophysiol,* 86: 1062-66

Gale SD, Perkel DJ (2010) A basal ganglia pathway drives selective auditory responses in songbird dopaminergic neurons via disinhibition. *J Neurosci,* 30:1027–1037.

Gale SD, Person AL, Perkel DJ (2008) A novel basal ganglia pathway forms a loop linking a vocal learning circuit with its dopaminergic input. *J Comp Neurol,* 508:824–839.

Geal-Dor M, Freeman S, Li G, Sohmer H (1993) Development of hearing in neonatal rats: air and bone conducted ABR thresholds. *Hear Res,* 69(1): 236-42

Gentner TQ (2004) Neural systems for individual song recognition in adult birds. *Annals of the New York Academy of Sciences,* 1016:282–302.

Gentner TQ, and Margoliash D (2003) Neuronal populations and single cells representing learned auditory objects. *Nature,* 424: 669-674

Gill P, Woolley SM, Fremouw T, and Theunissen FE (2008) What's that sound? Auditory area CLM encodes stimulus surprise, not intensity or intensity changes. *J Neurophysiol,* 99: 2809-2820

Gill P, Zhang J, Woolley SM, Fremouw T, and Theunissen FE (2006). Sound representation methods for spectro-temporal receptive field estimation. *J Comput Neurosci,* 21: 5-20

Girman SV, Sauve Y, and Lund RD (1999) Receptive field properties of single neurons in rat primary visual cortex. *J Neurophysiol,* 82: 301-311

Glass I, Wollberg Z (1983) Auditory Cortex Responses to Sequences of Normal and Reversed Squirrel Monkey Vocalizations. *Brain Behav Evol,* 22:13–21.

Gleich O, Manley GA (2000) The Hearing Organ of Birds and Crocodilia. In: *Comparative Hearing: Birds and Reptiles, Springer Handbook of Auditory Research*. New York, NY: Springer New York. 70–138

Gobes SMH, Bolhuis JJ (2007) Birdsong Memory: A Neural Dissociation between Song Recognition and Production. *Curr Biol,* 17:789–793.

Goldstein MH, Kiang NYS, and Brown RM (1959) Responses of the Auditory Cortex to Repetitive Acoustic Stimuli. *Journal of the Acoustical Society of America,* 31: 356-64

Grace JA, Amin N, Singh NC, Theunissen FE (2003) Selectivity for Conspecific Song in the Zebra Finch Auditory Forebrain. *J Neurophysiol,* 89:472–87.

Grana, GD, Billimoria, CP, Sen K (2009) Analyzing variability in neural responses to complex natural sounds in the awake songbird. *J Neurophysiol*, 101(6):3147-57.

Hahnloser RH, Kotowicz A (2010) Auditory representations and memory in birdsong learning. *Curr Opin Neurobiol,* 20:332–339.

Hahnloser RHR, Kozhevnikov AA, Fee MS (2002) An ultra-sparse code underliesthe generation of neural sequences in a songbird. *Nature,* 419:65–70.

Hahnloser RHR, Wang CZH, Nager A, Naie K (2008) Spikes and bursts in two types of thalamic projection neurons differentially shape sleep patterns and auditory responses in a songbird. *J Neurosci,* 28:5040–5052.

Hall JW, Grose JH (1991) Notched-Noise Measures of Frequency Selectivity in Adults and Children Using Fixed-Masker-Level and Fixed-Signal-Level Presentation. *J Speech Hear Res,* 34:651–60.

Han YK, Köver H, Insanally MN, Semerdjian JH, Bao S (2007) Early experience impairs perceptual discrimination. *Nat Neurosci,* 10:1191–1197.

Hara K, and Harris RA (2002) The anesthetic mechanism of urethane: the effects on neurotransmitter-gated ion channels. *Anesth Analg,* 94: 313-318

Hasselmo, ME, Linster, C, Patil, M, Ma, D, and Cekic, M (1997) Noradrenergic suppression of synaptic transmission may influence cortical signal-to-noise ratio. *J Neurophysiol*, 77(6):3326-39.

Hensch TK (2005) Critical period plasticity in local cortical circuits. *Nat Rev Neurosci,* 6(11): 877-88

Hill DN, Mehta SB, and Kleinfeld D (2011) Quality metrics to accompany spike sorting of extracellular signals. *J Neurosci,* 31(24):8699-705

Hosino T, Okanoya K (2000) Lesion of a higher-order song nucleus disrupts phrase level complexity in Bengalese finches. *NeuroReport* ,11:2091.

Hubel DH, and Wiesel TN (1962) Receptive fields, binocular interaction and functional architecture in the cat's visual cortex. *J Physiol,* 160: 106-54.

Huetz C, Philibert B, and Edeline JM (2009) A spike-timing code for discriminating conspecific vocalizations in the thalamocortical system of anesthetized and awake guinea pigs. *J Neurosci,* 29: 334-350

Immelmann K (1969) Song development in the zebra finch and other estrildid finches. *Bird vocalizations, 61.*

Insanally MN, Köver H, Kim H, Bao S (2009) Feature-dependent sensitive periods in the development of complex sound representation. *J Neurosci,* 29:5456–62.

Iverson, P, Kuhl, PK, Akahane-Yamada R, Diesch E, Tohkura Y, Ketterman A, and Siebert C (2003) A perceptual interference account of acquisition difficulties for non-native phonemes. *Cognition,* 87(1):B47-B57

Janata P, Margoliash D (1999) Gradual emergence of song selectivity in sensorimotor structures of the male zebra finch song system. *J Neurosci,* 19:5108–5118.

Jarvis, ED (2004) Learned Birdsong and the Neurobiology of Human Language. *Annals of the New York Academy of Sciences,* 1016:749–777.

Jarvis ED et al. (2005) Opinion: Avian brains and a new understanding of vertebrate brain evolution. *Nat Rev Neurosci,* 6:151–159.

Jeanne JM, Thompson JV, Sharpee TO, Gentner TQ (2011) Emergence of learned categorical representations within an auditory forebrain circuit. *J Neurosci,* 31:2595–2606.

Jensen JK, Neff DL (1993) Development of basic auditory discrimination in preschool children. *Psychological Science,* 4(2): 104-7.

Joshua M, Elias S, Levine O, and Bergman H (2007) Quantifying the isolation quality of extracellularly recorded action potentials. *J Neurosci Methods,* 163: 267-282

Kandler K, Gillespie DC (2005) Developmental refinement of inhibitory sound-localization circuits. *Trends in Neurosciences* ,28:290–296.

Kao MH, Doupe AJ, Brainard MS (2005) Contributions of an avian basal ganglia–forebrain circuit to real-time modulation of song. *Nature,* 433:638–43.

Karten, HJ (1968) The ascending auditory pathway in the pigeon (*Columba livia*) II. Telencephalic projections of the nucleus ovoidalis thalami. *Brain Res,* 11(1): 134-53

Keller GB, and Hahnloser RH (2008) Neural processing of auditory feedback during vocal practice in a songbird. *Nature,* 457: 187-90

Kelley DB (1980) Auditory and vocal nuclei in the frog brain concentrate sex hormones. *Science,* 207(4430): 553.

Kelley DB, Nottebohm F (1979) Projections of a telencephalic auditory nucleus–field L–in the

canary. *J Comp Neurol,* 183(3): 455-469.

Keuroghlian AS, Knudsen EI (2007) Adaptive auditory plasticity in developing and adult animals. *Progress in Neurobiology,* 82:109–121.

Kim G, Kandler K (2003) Elimination and strengthening of glycinergic/GABAergic connections during tonotopic map formation. *Nat Neurosci,* 6:282–290.

Klug A, Bauer EE, Hanson JT, Hurley L, Meitzen J, Pollak GD (2002) Response selectivity for species-specific calls in the inferior colliculus of mexican free-tailed bats is generated by inhibition. *J Neurophysiol,* 88:1941–1954.

Knudsen DP, Gentner TQ (2010) Mechanisms of song perception in oscine birds. *Brain and Language,* 115:59–68.

Knudsen EI, and Konishi M (1978) A neural map of auditory space in the owl. *Science,* 200: 795-97

Knudsen EI, Konishi M (1979) Mechanisms of sound localization in the barn owl (Tyto alba). *J Comp Physiol A,* 133:13–21.

Konishi M (1965) The Role of Auditory Feedback in the Control of Vocalization in the White-Crowned Sparrow. *Zeitschrift für Tierpsychologie,* 22:770–783.

Konishi M (1970) Comparative neurophysiological studies of hearing and vocalizations in songbirds. *J Comp Physiol A,* 66:257–72.

Konishi M (1985) Birdsong: from behavior to neuron. *Ann Rev Neurosci,* 8(1): 125-70

Konishi M (1989) Birdsong for neurobiologists. *Neuron,* 3: 541-549

Kotak VC, Sanes DH (2000) Long-lasting inhibitory synaptic depression is age- and calcium-dependent. *J Neurosci,* 20:5820–26.

Kozhevnikov AA, Fee MS (2007) Singing-related activity of identified HVC neurons in the zebra finch. *J Neurophysiol,* 97:4271–83.

Krützfeldt NOE, Logerot P, Kubke MF, Wild JM (2010) Connections of the auditory brainstem in a Songbird, Taeniopygia guttata. I. Projections of nucleus angularis and nucleus laminaris to the auditory torus. *J Comp Neurol,* 518:2109–34.

Kuffler SW (1953) Discharge patterns and functional organization of mammalian retina. *J Neurophysiol,* 16: 37-68

Kuhl, PK (1994) Learning and representation in speech and language. *Curr Opin Neurobiol,* 4:812-22

Kuhl, PK (2010) Brain mechanisms in early language acquisition. *Neuron,* 67(5): 713-727.

Leao RN, Berntson A, Forsythe ID (2004) Reduced low-voltage activated K+ conductances and enhanced central excitability in a congenitally deaf (dn/dn) mouse. *J Physiol,* 559(1): 25-33

LeBeau FE, Malmierca MS, and Rees A (2001) Iontophoresis in vivo demonstrates a key role for GABA(A) and glycinergic inhibition in shaping frequency response areas in the inferior colliculus of guinea pig. *J Neurosci,* 21: 7303-7312

LeBlanc, MM, Goode, CT, MacDougall-Shackleton, EA, Maney, DL (2007) Estradiol modulates brainstem catecholaminergic cell groups and projections to the auditory forebrain in a female songbird. *Brain Research,* 1171:93-103.

Lei H, Mooney R (2010) Manipulation of a central auditory representation shapes learned vocal output. *Neuron,* 65:122–134.

Leong D, Puil E, and Schwarz D (2004) Ketamine blocks non-N-methyl-D-aspartate receptor channels attenuating glutamatergic transmission in the auditory cortex. *Acta Otolaryngol,* 124: 454-458

Leppelsack JH (1974) The effect of acoustic parameters on single unit responses in higher stations of the auditory pathway of birds. *Symposium Mechanoreception,* 243-9.

Lewi, J, Butera, R, and Paninski, P (2009) Sequential optimal design of neurophysiology experiments. *Neural Computation*, 23:619-87.

Lewicki, MS (1996) Intracellular characterization of song-specific neurons in the zebra finch auditory forebrain. *J Neurosci* 16: 5855-63

Lewicki MS, Arthur BJ (1996) Hierarchical organization of auditory temporal context sensitivity. *J Neurosci* 16:6987–98.

Logerot P, Krützfeldt NOE, Wild JM, Kubke MF (2011) Subdivisions of the auditory midbrain (n. mesencephalicus lateralis, pars dorsalis) in zebra finches using calcium-binding protein immunocytochemistry. Perkel D, ed. *PLoS one* 6:e20686.

London SE, Clayton DF (2008) Functional identification of sensory mechanisms required for developmental song learning. *Nat Neurosci,* 11:579–86.

Long MA, Fee MS (2008) Using temperature to analyse temporal dynamics in the songbird motor pathway. *Nature,* 456:189–94.

Lynch, KS, and Ball, GF (2008) Noradrenergic deficits alter processing of communication signals in female songbirds. *Brain, Behavior and Evolution,* 72:207-14.

Macdonald RL, Rogers CJ, and Twyman RE (1989) Barbiturate regulation of kinetic-properties of the GABAa receptor channel of mouse spinal neurons in culture. *J Physiol-London* 417: 483-500,

Maney, DL, Cho, E, and Goode, CT (2006) Estrogen-dependent selectivity of genomic responses to birdsong. *European Journal of Neuroscience*, 23(6):1523-9.

Margoliash D (1983) Acoustic parameters underlying the responses of song-specific neurons in the white-crowned sparrow. *J Neurosci,* 3: 1039-1057

Margoliash D (1986) Preference for autogenous song by auditory neurons in a song system nucleus of the white-crowned sparrow. *J Neurosci,* 6:1643–1661.

Margoliash D, and Fortune ES (1992) Temporal and harmonic combination-sensitive neurons in the zebra finch's HVc. *J Neurosci,* 12: 4309-4326

Marler P (1970) Birdsong and speech development: Could there be parallels? There may be basic rules governing vocal learning to which many species conform, including man. *American Scientist,* 669-73

Martin Wild J, Karten HJ, Frost BJ (1993) Connections of the auditory forebrain in the pigeon (columba livia). *J Comp Neurol,* 337:32–62.

Maul KK, Voss HU, Parra LC, Salgado-Commissariat D, Ballon D, Tchernichovski O, and Helekar SA (2010) The development of stimulus-specific auditory responses requires song exposure in male but not female zebra finches. *Dev Neurobiol,* 70(1): 28-40.

Maxon AB, Hochberg I (1982) Development of psychoacoustic behavior: sensitivity and discrimination. *Ear and Hearing,* 3:301.

McCasland JS (1987) Neuronal control of bird song production. *J Neurosci,* 7:23–39.

Meliza CD, Chi Z, Margoliash D (2010) Representations of conspecific song by starling secondary forebrain auditory neurons: toward a hierarchical framework. *J Neurophysiol,* 103(3): 1195-1208.

Meliza CD, Margoliash D (2012) Emergence of selectivity and tolerance in the avian auditory cortex. *J Neurosci,* 32(43): 15158-68.

Mello, CV (2002) Mapping vocal communication pathways in birds with inducible gene expression. *J Comp Physiol A*, 188(11-12):943-959.

Mello C, Nottebohm F, Clayton D (1995) Repeated exposure to one song leads to a rapid and persistent decline in an immediate early gene's response to that song in zebra finch telencephalon. *J Neurosci,* 15:6919–6925

Mello, CV, Pinaud, R, & Ribeiro, S (1998) Noradrenergic system of the zebra finch brain: immunocytochemical study of dopamine-Beta-hydroxylase. *J Comp Neurol*, 400(2):207-228.

Mello CV, Vates GE, Okuhata S, Nottebohm F (1998) Descending auditory pathways in the

adult male zebra finch (Taeniopygia guttata). *J Comp Neurol,* 395:137–160.

Moore DR (1990) Auditory brainstem of the ferret: bilateral cochlear lesions in infancy do not affect the number of neurons projecting from the cochlear nucleus to the inferior colliculus. *Developmental Brain Research,* 54(1): 125-30.

Moore DR, Cowan JA, Riley A (2011) Development of auditory processing in 6-to 11-yr-old children. *Ear and Hearing,* 32(3):269-85.

Moore DR, Kowalchuk NE (1988) An anomaly in the auditory brain stem projections of hypopigmented ferrets. *Hear Res,* 35(2):275-8.

Moore JK, Fred H Linthicum J (2009) The human auditory system: A timeline of development. *International journal of audiology,* 46(9):460-78.

Moore RC, Lee T, Theunissen FE (2013) Noise-invariant Neurons in the Avian Auditory Cortex: Hearing the Song in Noise Kording KP, ed. *PLoS Comput Biol,* 9:e1002942.

Müller CM, Leppelsack HJ (1985) Feature extraction and tonotopic organization in the avian auditory forebrain. *Exp Brain Res,* 59:587–599.

Nakamoto KT, Jones SJ, and Palmer AR. Descending projections from auditory cortex modulate sensitivity in the midbrain to cues for spatial position. *J Neurophysiol,* 99: 2347-2356, 2008.

Nagel KI, Doupe AJ (2008) Organizing principles of spectro-temporal encoding in the avian primary auditory area field L. *Neuron* ,58:938–955.

Naie K, Hahnloser RHR (2011) Regulation of learned vocal behavior by an auditory-motor cortical nucleus in juvenile zebra finches. *J Neurophysiol,* jn-01035.

Narayan R, Grana G, and Sen K (2006). Distinct time scales in cortical discrimination of natural sounds in songbirds. *J Neurophysiol* 96: 252-258

Nelken I, Rotman Y, and Bar Yosef O (1999) Responses of auditory-cortex neurons to structural features of natural sounds. *Nature,* 397: 154-157

Nick, TA, and Konishi, M (2001) Dynamic control of auditory activity during sleep: correlation between song response and EEG. *Proc Nat Acad Sci USA,* 98(24):14012-6.

Nicoll RA, Eccles JC, Oshima T, and Rubia F (1975) Prolongation of hippocampal inhibitory postsynaptic potentials by barbiturates. *Nature,* 258: 625-627

Nishikawa K, and MacIver MB (2000) Membrane and synaptic actions of halothane on rat hippocampal pyramidal neurons and inhibitory interneurons. *J Neurosci,* 20: 5915-5923

Nottebohm F (1970) Ontogeny of bird song. *Science,* 167: 950-956

Nottebohm F, Arnold AP (1976) Sexual dimorphism in vocal control areas of the songbird brain.

Science, 194:211–213.

Nottebohm F, Kelley, DB, Paton JA (1982) Connections of vocal control nuclei in the canary telencephalon. *J Comp Neurol,* 207(4): 344-357.

Okanoya K, and Dooling RJ (1987) Hearing in passerine and psittacine birds: a comparative study of absolute and masked auditory thresholds. *J Comp Psychol,* 101: 7-15

Oleskevich S, Walmsley B (2002) Synaptic transmission in the auditory brainstem of normal and congenitally deaf mice. *J Physiol*, 540(2): 447-55.

Ondracek JM, Hahnloser RHR (2014) Advances in Understanding the Auditory Brain of Songbirds. In: I*nsights from Comparative Hearing Research*, 347–388 Springer Handbook of Auditory Research. New York, NY: Springer New York.

Oswald A, Reyes AD (2008) Maturation of intrinsic and synaptic properties of layer 2/3 pyramidal neurons in mouse auditory cortex. *J Neurophysiol*, 99(6):2998-3008.

Otazu GH, Tai LH, Yang Y, Zador, AM (2009) Engaging in an auditory task suppresses responses in auditory cortex. *Nat Neurosci*, 12(5):646-54.

Paninski L (2004) Maximum likelihood estimation of cascade point-process neural encoding models. *Network,* 15: 243-262

Paninski L, Pillow J, and Lewi J (2007) Statistical models for neural encoding, decoding, and optimal stimulus design. *Prog Brain Res*, 165: 493-507

Paton JA, Kelley DB, Sejnowski TJ, Yodlowski ML (1982) Mapping the auditory central nervous system ofXenopus laevis with 2-deoxyglucose autoradiography. *Brain Research*, 249:15–22.

Pena JL, Konishi M (2001) Auditory spatial receptive fields created by multiplication. *Science*, 292:249–252.

Pinaud R, Mello CV (2007) GABA immunoreactivity in auditory and song control brain areas of zebra finches. *Journal of Chemical Neuroanatomy*, 34:1–21.

Pittson S, Himmel AM, and MacIver MB (2004) Multiple synaptic and membrane sites of anesthetic action in the CA1 region of rat hippocampal slices. *BMC Neurosci*, 5: 52

Pollak GD, Bodenhamer RD (1981) Specialized characteristics of single units in inferior colliculus of mustache bat: frequency representation, tuning, and discharge patterns. *J Neurophysiol*, 46(3): 605-20.

Quiroga RQ, Nadasdy Z, and Ben-Shaul Y (2004) Unsupervised spike detection and sorting with wavelets and superparamagnetic clustering. *Neural Comput*, 16(8):1661-87.

Poon PWF, Chen X (1992) Postnatal exposure to tones alters the tuning characteristics of

inferior collicular neurons in the rat. *Brain Research,* 585:391–394.

Razak KA, Richardson MD, Fuzessery ZM (2008) Experience is required for the maintenance and refinement of FM sweep selectivity in the developing auditory cortex. *Proc Natl Acad Sci USA,* 105:4465–4470.

Read HL, Winer JA, and Schreiner CE (2001) Modular organization of intrinsic connections associated with spectral tuning in cat auditory cortex. *Proc Natl Acad Sci USA,* 98: 8042-8047

Riebel, K, Smallegange, IM, Terpstra, NJ, and Bolhuis, JJ (2002) Sexual equality in zebra finch song preference: evidence for a dissociation between song recognition and production learning. *Proceedings of the Royal Society of London, Biological Science*s, 269(1492):729-33.

Rieke F, Bodnar DA, and Bialek W (1995) Naturalistic stimuli increase the rate and efficiency of information transmission by primary auditory afferents. *Proc Biol Sci,* 262: 259-265

Rose, M (1914) Über die cytoarchitektonische Gliederung des Vorderhirns der Vögel. *J Psychol Neurol,* 21: 278-352

Rust NC, Mante V, Simoncelli EP, and Movshon JA (2006) How MT cells analyze the motion of visual patterns. *Nat Neurosci,* 9: 1421-1431

Rutkowski RG, Shackleton TM, Schnupp JW, Wallace MN, and Palmer AR (2002) Spectrotemporal receptive field properties of single units in the primary, dorsocaudal and ventrorostral auditory cortex of the guinea pig. *Audiol Neurootol,* 7: 214-227

Sanes, DH (2003) Development of synaptic function and integration in central auditory. *J Neurosci,* 13(6): 2627-37

Sanes DH, Bao S (2009) Tuning up the developing auditory CNS. *Curr Opin Neurobiol,* 19:188-99

Sanes DH, Constantine-Paton M (1983) Altered activity patterns during development reduce neural tuning. *Science*, 221:1183–85.

Sanes DH, Constantine-Paton M (1985) The development of stimulus following in the cochlear nerve and inferior colliculus of the mouse. *Developmental Brain Research* 22:255–267.

Sanes DH, Woolley SMN (2011) A behavioral framework to guide research on central auditory development and plasticity. *Neuron,* 72:912–929.

Sanes JR, and Jessell T (2013) Experience and the refinement of synaptic connections. In: *Principles of Neural Science,* 5th ed, Kandel E,et al. eds, : pp1259-83. McGraw-Hill Medical

Sceniak MP, and MacIver MB (2006) Cellular actions of urethane on rat visual cortical neurons in vitro. *J Neurophysiol,* 95: 3865-3874

Scharff C, Nottebohm F (1991) A comparative study of the behavioral deficits following lesions of various parts of the zebra finch song system: implications for vocal learning. *J Neurosci,* 11:2896–2913.

Schmidt MF, Konishi M (1998) Gating of auditory responses in the vocal control system of awake songbirds. *Nat Neurosci,* 1:513–518.

Schneider DM, Woolley SMN (2010) Discrimination of communication vocalizations by single neurons and groups of neurons in the auditory midbrain. *J Neurophysiol,* 103:3248–3265.

Schneider DM, Woolley SMN (2011) Extra-classical tuning predicts stimulus-dependent receptive fields in auditory neurons. *J Neurosci,* 31:11867–11878.

Schneider DM, Woolley SMN (2013) Sparse and background-invariant coding of vocalizations in auditory scenes. *Neuron,* 79:141–152.

Schnupp JW, Mrsic-Flogel TD, and King AJ (2001) Linear processing of spatial cues in primary auditory cortex. *Nature,* 414: 200-204

Scholfield CN (1980) Potentiation of inhibition by general anaesthetics in neurones of the olfactory cortex in vitro. *Pflugers Arch,* 383: 249-255

Schreiner CE, Urbas JV (1986) Representation of amplitude modulation in the auditory cortex of the cat. I. The anterior auditory field (AAF). *Hear Res,* 21:227–241.

Schreiner CE, Urbas JV (1988) Representation of amplitude modulation in the auditory cortex of the cat. II. Comparison between cortical fields. *Hear Res,* 32:49-64

Schumacher JW, Schneider DM, Woolley SMN (2011) Anesthetic state modulates excitability but not spectral tuning or neural discrimination in single auditory midbrain neurons. *J Neurophysiol,* 106:500–514.

Seidl AH, Grothe B (2005) Development of sound localization mechanisms in the mongolian gerbil is shaped by early acoustic experience. *J Neurophysiol,* 94(2): 1028-36

Sen K, Theunissen FE, Doupe AJ (2001) Feature analysis of natural sounds in the songbird auditory forebrain. *J Neurophysiol,* 86:1445–58.

Shaevitz SS, Theunissen FE (2007) Functional connectivity between auditory areas field L and CLM and song system nucleus HVC in anesthetized zebra finches. *J Neurophysiol,* 98(5): 2747-64

Shahidullah S, Hepper PG (1994) Frequency discrimination by the fetus. *Early Human Development,* 36:13–26.

Smeets, WJ, and Gonzalez, A (2002) Catecholamine systems in the brain of vertebrates: new perspectives through a comparative approach. *Brain Research Reviews*, 33(2-3): 308-79.

Smith VA, Yu J, Smulders TV, Hartemink AJ, Jarvis ED (2006) Computational Inference of Neural Information Flow Networks. *PLoS Comput Bio,*. 2:e161.

Sockman, KW, and Salvante, KG (2008) The integration of song environment by catecholaminergic systems innervating the auditory telencephalon of adult female European starling. *Developmental Neurobiology*, 68(5):656-68.

Speechley WJ, Hogsden JL (2007) Continuous white noise exposure during and after auditory critical period differentially alters bidirectional thalamocortical plasticity in rat auditory cortex in vivo. *European Journal of Neuroscience*, 26(9): 2576-84.

Spitz, R (1945) Hospitalism: an inquiry into the genesis of psychiatric conditions in early childhood. *The Psychoanalytic Study of the Child*, 1: 53.

Spetner NB, Olsho LW (1990) Auditory Frequency Resolution in Human Infancy. *Child Development*, 61:632–652.

Stripling R, Volman SF, Clayton DF (1997) Response modulation in the zebra finch neostriatum: relationship to nuclear gene regulation. *J Neurosci*, 17:3883–3893.

Sun YJ, Wu GK, Liu B-H, Li P, Zhou M, Xiao Z, Tao HW, Zhang LI (2010) Fine-tuning of pre-balanced excitation and inhibition during auditory cortical development. *Nature*, 465:927–931.

Šuta D, Kvašňák E, Popelář J, Syka J (2003) Representation of Species-Specific Vocalizations in the Inferior Colliculus of the Guinea Pig. *J Neurophysiol*, 90:3794–3808.

Sutter ML, and Schreiner CE (1991) Physiology and topography of neurons with multipeaked tuning curves in cat primary auditory cortex. *J Neurophysiol*, 65: 1207-1226

Takahashi TT, Keller CH (1992) Commissural connections mediate inhibition for the computation of interaural level difference in the barn owl. *J Comp Physiol A* 170:161–169.

Ter-Mikaelian M, Sanes DH, and Semple MN (2007) Transformation of temporal properties between auditory midbrain and cortex in the awake Mongolian gerbil. *J Neurosci*, 27: 6091-6102.

Theunissen, FE, Amin, N, Shaevitz SA, Woolley, SMN, Fremouw, T, and Hauber, ME (2008) Song selectivity and the songbird brain. In: *Neuroscience of Birdsong*, Cambridge University Press. Zeigler and Marler, eds.;157-73.

Theunissen FE, Amin N, Shaevitz SS, Woolley SMN, Fremouw T, Hauber ME (2004) Song selectivity in the song system and in the auditory forebrain. *Annals of the New York Academy of Sciences*, 1016:222–45.

Theunissen, FE, Sen, K, and Doupe, AJ (2000) Spectral-temporal receptive fields of nonlinear auditory neurons obtained using natural sounds. *J Neurosci*, 20(6):2315-31.

Theunissen FE, and Shaevitz SS (2006). Auditory processing of vocal sounds in birds. *Curr Opin Neurobiol*, 16: 400-7

Thompson JF, and Gentner TQ (2010) Song recognition learning and stimulus-specific weakening of neural responses in the avian auditory forebrain. *J Neurophysiol*, 103(4): 1785-97.

Tritsch NX, Bergles DE (2010) Developmental regulation of spontaneous activity in the mammalian cochlea. *J Neurosci*, 30:1539–1550.

Truccolo W, Eden UT, Fellows MR, Donoghue JP, and Brown EN (2005). A point process framework for relating neural spiking activity to spiking history, neural ensemble, and extrinsic covariate effects. *J Neurophysiol*, 93: 1074-89

Uziel A, Romand R, Marot M (2009) Development of Cochlear Potentials in Rats. *International Journal of Audiology*, 20(2): 89-100.

van Rossum MC (2001) A novel spike distance. *Neural Comput*, 13: 751-763.

Vates GE, Broome BM, Mello CV (1996) Auditory pathways of caudal telencephalon and their relation to the song system of adult male zebra finches (Taenopygia guttata). *J Comp Neurol*, 366(4): 613-42.

Vates GE, Nottebohm F (1995) Feedback circuitry within a song-learning pathway. *Proc Nat Acad Sci USA*, 92:5139–43.

Vates GE, Vicario DS, Nottebohm F (1997) Reafferent thalamo- "cortical" loops in the song system of oscine songbirds. *J Comp Neurol*, 380:275–90.

Vinje WE, and Gallant JL (2000) Sparse coding and decorrelation in primary visual cortex during natural vision. *Science*, 287: 1273-1276.

Vyas, A, Harding, C, McGowan, J, Snare, R, and Bogdan, D (2008) Noradrenergic neurotoxin, N-(2-chloroethyl)-N-ethyl-2-bromobenzylamine hydrochloride (DSP-4), treatment eliminates estrogenic effects on song responsiveness in female zebra finches (*Taeniopygia guttata*). *Behavioral Neuroscience*, 122(5):1148-57.

Wang L, Narayan R, Grana G, Shamir M, and Sen K (2007) Cortical discrimination of complex natural stimuli: can single neurons match behavior? *J Neurosci*, 27: 582-589

Wang X (2000) On cortical coding of vocal communication sounds in primates. *Proc Nat Acad Sci USA*, 97:11843–11849.

Wang X, Lu T, Bendor D, and Bartlett E (2008) Neural coding of temporal information in auditory thalamus and cortex. *Neuroscience,* 157: 484-94

Wang X, Lu T, Snider RK, and Liang L (2005) Sustained firing in auditory cortex evoked by preferred stimuli. *Nature,* 435: 341-346

Waterhouse BD, Moises, HC, and Woodward, DJ (1998) Phasic activation of the locus coeruleus enhances responses of primary sensory cortical neurons to peripheral receptive field stimulation. *Brain Research,* 790(1-2):33-44

Waterman, SA, and Harding, CF (2008) Neurotoxic effects of DSP-4 on the central noradrenergic system in male zebra finches. *Behavioral Brain Research,* 188(2):271-80

Wehr M, Zador AM (2003) Balanced inhibition underlies tuning and sharpens spike timing in auditory cortex. *Nature,* 426:442–446

Wehr M, and Zador AM (2005) Synaptic mechanisms of forward suppression in rat auditory cortex. *Neuron,* 47: 437-445

Weliky M, Bosking WH, and Fitzpatrick D (1996) A systematic map of direction preference in primary visual cortex. *Nature,* 379: 725-728

Wild JM (1993) Descending projections of the songbird nucleus robustus archistriatalis. *J Comp Neurol,* 338(2): 225-41.

Wild JM (1994) Visual and somatosensory inputs to the avian song system via nucleus uvaeformis (Uva) and a comparison with the projections of a similar thalamic nucleus in a nonsongbird, *Columbia livia*. *J Comp Neurol,* 349:512–535.

Wild JM, Krützfeldt NOE, Kubke MF (2010) Connections of the auditory brainstem in a songbird, Taeniopygia guttata. III. Projections of the superior olive and lateral lemniscal nuclei. *J Comp Neurol,* 518:2149–2167.

Williams SM, Nast A, Coleman MJ (2012) Characterization of synaptically connected nuclei in a potential sensorimotor feedback pathway in the zebra finch song system. Soares D, ed. *PLoS one,* 7:e32178.

Winkowski DE, Knudsen EI (2006) Top-down gain control of the auditory space map by gaze control circuitry in the barn owl. *Nature,* 439:336–339.

Winkowski, DE, and Knudsen, EI (2007) Top-down control of multimodal sensitivity in the barn owl optic tectum. *J Neurosci,* 27(48):13279-91

Woolley SC, & Doupe AJ (2008) Social context-induced song variation affects female behavior and gene expression. *PLoS Biol,* 6(3):525-37

Woolley SMN, Casseday JH (2004) Response properties of single neurons in the zebra finch

auditory midbrain: response patterns, frequency coding, intensity coding, and spike latencies. *J Neurophysiol,* 91:136–51.

Woolley SM, and Casseday JH (2005). Processing of modulated sounds in the zebra finch auditory midbrain: responses to noise, frequency sweeps, and sinusoidal amplitude modulations. *J Neurophysiol*, 94: 1143-57

Woolley SM, Fremouw TE, Hsu A, and Theunissen FE. (2005) Tuning for spectro-temporal modulations as a mechanism for auditory discrimination of natural sounds. *Nat Neurosci,* 8: 1371-79

Woolley SMN, Gill PR, Fremouw T, Theunissen FE (2009) Functional groups in the avian auditory system. *J Neurosci,* 29:2780–93

Woolley SMN, Gill PR, Theunissen FE (2006) Stimulus-dependent auditory tuning results in synchronous population coding of vocalizations in the songbird midbrain. *J Neurosci,* 26:2499–2512

Woolley SMN, Hauber ME, Theunissen FE (2010) Developmental experience alters information coding in auditory midbrain and forebrain neurons. *Dev Neurobiol,* 70:235–52.

Woolley SMN, Portfors CV (2013) Conserved mechanisms of vocalization coding in mammalian and songbird auditory midbrain. *Hear Res,* 305:45–56.

Xie R, Gittelman JX, and Pollak GD (2007) Rethinking tuning: in vivo whole-cell recordings of the inferior colliculus in awake bats. *J Neurosci,* 27: 9469-9481

Yan W, Suga N (1998) Corticofugal modulation of the midbrain frequency map in the bat auditory system. *Nat Neurosci,* 1:54–8.

Yates GK, Manley GA, Köppl C (2000) Rate-intensity functions in the emu auditory nerve. *J Acoust Soc Am,* 107:2143–54.

Zann, RA (1996) The Zebra Finch. Oxford University Press.

Zaretsky MD, Konishi M (1976) Tonotopic organization in the avian telencephalon. *Brain Research,* 111:167–71.

Zeng S, Zhang X, Peng W, Zuo M (2004) Immunohistochemistry and neural connectivity of the Ov shell in the songbird and their evolutionary implications. *J Comp Neuro,* 470:192–209.

Zhang LI, Bao S, Merzenich MM (2001) Persistent and specific influences of early acoustic environments on primary auditory cortex. *Nat Neurosci,* 4:1123–1130.

Zhou X, Merzenich MM (2008) Enduring effects of early structured noise exposure on temporal modulation in the primary auditory cortex. *Proc Nat Acad Sci.* 105:4423–28.

Zurita P, Villa AE, de Ribaupierre Y, de Ribaupierre F, and Rouiller EM (1994) Changes of single unit activity in the cat's auditory thalamus and cortex associated to different anesthetic conditions. *Neurosci Res* 19: 303-316

Appendix: Protocol for construction and implantation of chronic single channel Microdrive

[These notes are modified from the original protocol developed by Keller and Hahnloser (2008). The protocol has been adapted for the purposes of the experiments described in Chapter 5, is designed to help future Woolley lab members continue this work.]

Tools and materials:

1) #55 forceps (OK if bent up)
2) #55 forceps (fine points for wire stripping)
3) #5 forceps.
4) 90 degree wire cutters
5) EREM blue handled wire cutters
6) feather blade scalpel
7) Elastic string
8) 0.001" platinum iridium coated wire
9) 0.005" silver wire, 0.002" coated
10) Hard man non-sag epoxy
11) Silver bearing solder
12) Cerro matrix low temperature solder
13) Faulhaber minimotors (part number: 0206 A 001 B 021 47:1 Y2825)
14) Polymide tubing (A-M Systems: 0.0045" ID, 0.0005" Wall; Microlumen 145-1.5)
15) Minutien pins (use fine pins for surgery, large pins for glue application)
16) 14-channel banana to omnetics breakout box (custom made)

Getting started, tips and tricks:

1) Using non-sag epoxy:

    a. The main trick with the non-sag epoxy is to use equal parts of each, but only prepare a small amount at a time. One packet should last for at least 1 entire Microdrive assembly, but could easily cover 2 or 3 assemblies. Once open, the package can be used for a long time as long as the two components don't mix.

    b. At the start of a day, place a small amount of each component on a piece of paper. When a dab of epoxy is required, use a tooth pick to acquire a small dot of each component, and mix it together on an isolated part of the paper. Repeat whenever necessary. If you cannot accurately apply the epoxy with the toothpick, sharpen it with a scalpel, or use a large insect pin.

    c. Dry time should be appox. 10 minutes. Longer dry times indicate that even amounts of each component were not used. Try putting a small dot of pink component onto the slowly drying mixture to speed up the process. If that doesn't

help, add a little clear component. If that doesn't work, don't overload with epoxy, just let it dry overnight. You can test the solidity of the epoxy with a can of compressed air. Wet epoxy will ripple with the air pressure.

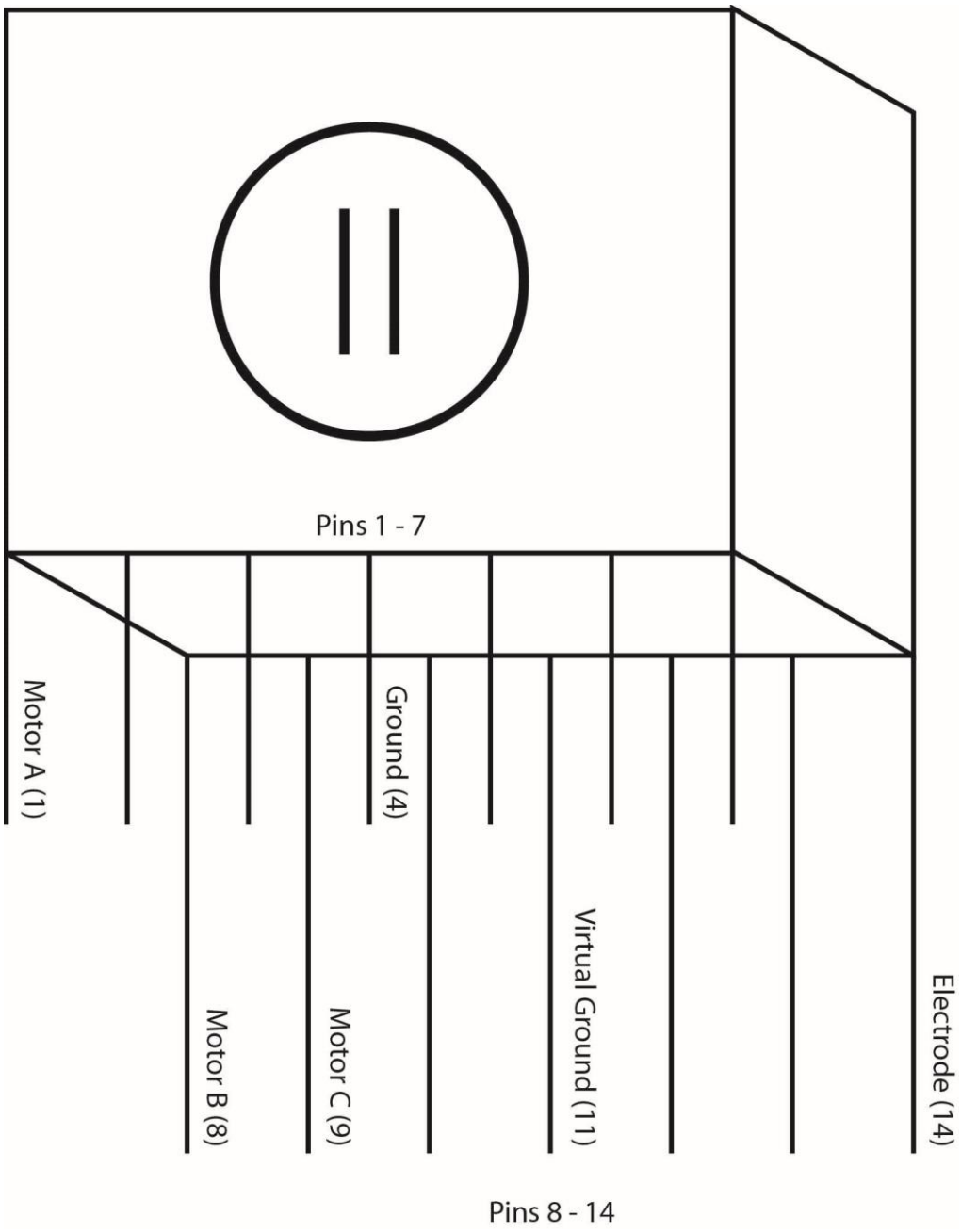

Figure A.1: Wiring schematic for the omnetics connector.

2) Testing the motor:

a. The major concern is to not supply too much voltage or current. There are limits listed on the Faulhaber spec page. Keep in mind the limits for the motor exceed the limits for the gear box in terms of RPMs. The max RPM for the motor should be about 20,000, but the default is 120,000, and the max that you should ever drive is approximately 224.

b. Before turning on the power supply, make sure that the motion controller box (analog dials) are turned all the way counter clockwise. The default setting for the motion manager software is to use the analog box as a control source (sor 1).

c. Turn on the power source, making sure the voltage is set to 7.0 V (+/- 0.5 V). The current should be set to 0.2 A.

d. Open motion manager software and type in the following start-up protocol (";" *indicates comments, do not enter into motion manager*):

    i. sor 0 ;source command for computer control

    ii. lpc 200 ;limit peak current to 200mA

    iii. ov 1000 ;max output voltage set to 1000mV

    iv. sp 224 ;max speed 224 positions per second, approx. 600 um per minute.

    v. ho 0 ;home the motor, set current position to 0

    vi. Drive the motor. There are a variety of ways to test the motor, depending on the goal at hand. If you just want to make sure the motor isn't going to overheat, try a simple velocity command:

        1. v112 ;move approximately 300um per minute, should advance the shuttle if the wiring is correct.

        2. v -112 ;retract motor 300um per minute

        3. If wiring to the breakout box isn't driving motor in correct direction, simply swap two wires.
        4.

e. To test positioning, utilize the la (absolute position goal) and lr (relative position goal) commands.

    i. ho 0 ;home the motor

    ii. lr 99256 ;advance the motor exactly 1 mm at a velocity of sp

    iii. la 0 ;return home (ideally equivalent to lr -99256)

iv. The motor does not have a sensor, so if it gets stuck then it will keep counting and move to an inaccurate location.

f. Use the above settings for testing the motor at various stages of assembly (before mounting on the body, after mounting on the body, especially after connecting to omnetics, etc.). At the above settings the motor should drive smoothly up and down the axis, and should not overheat (observable by simply touching the motor. Make sure to wire up so that the forward commands move the shuttle forward! Try to keep wiring consistant across microdrives and teathers. This will make life easier

g. The motor may start to get hot with the above settings. This is bad, but not necessarily the end of the world. To prevent over-heating, try using a smaller amount of current (lpc 150). This may fail to drive the motor, but if not, then you're good to go.

Part 1: Assembling the motor/chassis interface

1) Attach omnetics connector (Fig. A.1, A.2).

   a. Obtain a plastic body component (remove plastic tip component if necessary with small screwdriver).

   b. Using two small dots of non-sag epoxy, glue a 14-pin male omnetics connector to the flat side of the body. Input face of omnetics should be flush with motor mounting face. (Dry time, approx.10 minutes).

   c. Now the assembly can be mounted onto the female adapter, which receives power from the silver breakout box.

   d. Cut the top row of omnetics soldering pins to approx. 1.5 to 2mm. Bottom row should be even with the tip end of the body (need to be trimmed). Use 90 degree forceps to cut the pins.

2) Mount the motor to the body:

   a. Screw a shuttle onto the motor axis. The shuttle should be fairly loose on the threads of the axis from top to bottom. Wire up the motor directly to the motion controller and test to make sure it doesn't overheat (see motor testing instructions above). Also check to see that the shuttle can be driven up and down the motor

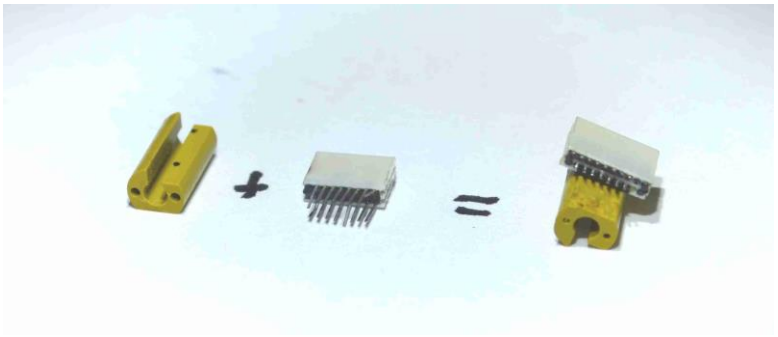

Figure A.2: Glue 14-pin omnetics connector to the body of the microdrive.

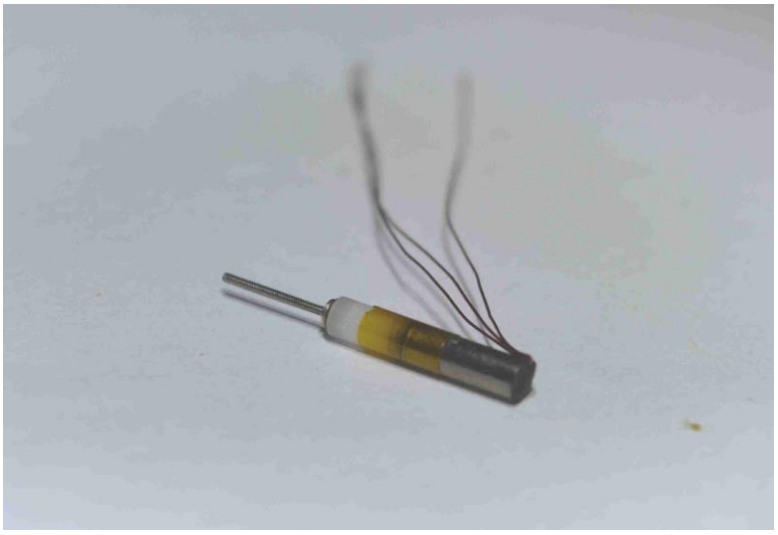

Figure A.3: Encase the motor and gearbox with 4mm polymide tubing.

axis without getting stuck! Use a can of compressed air if plastic flakes are left in the threads of the motor axis. Drive the shuttle up and down until motion is completely smooth. **Very important to make sure the shuttle doesn't stick before mounting the motor!** If you are having severe sticking problems, obtain the proper threading tool from a machine shop and clean out the shuttle threads.

b. Cut 4mm of MicroLumen polymide tubing (diam. 1.89mm, see components list) to encase the junction of the motor and gear box. The motor and gear box can be very easily separated if not secured (Fig. A.3).

c. Remove the shuttle from the motor axis, and insert axis into the polymide tubing. Slide the tubing to the junction of the motor and gear box (Fig. A.3).

d. Attach the tip and secure with two screws.

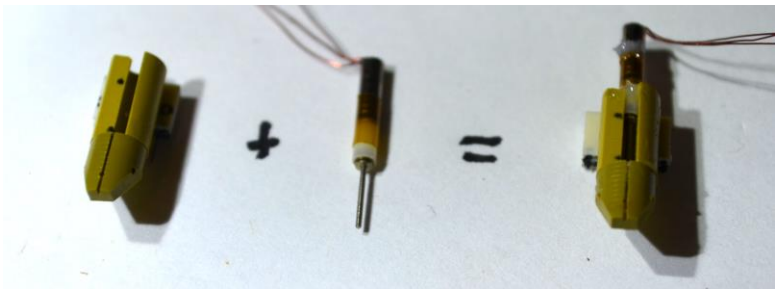

Fig. A.4: Glue motor in place at the top of the body. Use the tip to gauge how far the motor axis rests within the shuttle guide slot.

e. Insert the motor axis into the shuttle such that the axis protrudes approx. 0.5mm. Insert the motor/shuttle assembly into the body assembly so that 0.5mm of axis are in the whole of the tip, and the polymide tubing should be just touching the body assembly.

f. Glue the motor in place by placing a small dab of epoxy at the junction of the gearbox, body, and polymide tubing at the start of the shuttle guide slit (see Figure 1a). Be sure not to get any glue on the moving parts (be conservative). Dry time approx. 10 minutes (Fig. A.4).

g. Test the motor! Shuttle should continue to drive smoothly. If it gets stuck, not all hope is lost. Remove the tip, and push the motor through the polymide tubing such that the shuttle protrudes from the body. Try to loosen up this way and reassemble.

h. Solder the motor cables to pins 1, 8 and 9 on the omnetics (see omnetics wiring scheme in appendix). Test for appropriate wiring and that positive v-commands advance the motor (Fig. A.5).

i. Glue the motor wires in place. First, make sure the wires are bundled from the motor to the omnetics and are flat against the assembly. Put non-sag glue on along the omnetics/body junction, coating the wires (dry time 10 min). Then another dab at the origin of the wires at the motor (dry time 10 min). Then one last dab where the motor and body make a 90 degree angle (dry time 10min; Fig. A.4).

3) Insert the lateral positioner screw and a fixation bar (anything that fits into the 0.5mm hole in the side of the tip should be fine. Recommend tungsten wire if available). Glue the fixation bar in place at each of the two holes (Fig. A.6).

Figure A.5: Solder motor wires to pins 1, 8, and 9. Glue the wires into place along the junction of the body and omnetics connector. Insert a fixation bar (black pin) through the tip).

Part 2: wiring up ground and electrode wires to the omnetics connector

1) Attach the electrode wire:

    a. Cut 3 cm of 0.005" mm diameter coated silver wire (see list of components above) and uncoat approx. 3mm on one end.

    b. Insert the uncoated end of the silver wire into the whole in the shuttle from below. The uncoated end should protrude from the top of the shuttle, and then wrap down into the groove of the shuttle. Glue the protruding uncoated end to the shuttle near the top hole (Fig. A.6). **Be sure not to glue the shuttle to the axis or the body! Don't get too much glue in the shuttle because we need to solder the electrode there!**

    c. Lead the loose end of the wire around the body relatively tightly, cut it to the appropriate length to solder it to pin 14 (Fig. A.6).

    d. Test the motor! Make sure the shuttle drives up and down unrestricted by the electrode wire. Also measure the extent of the motor axis from top to bottom. Should be longer than 300,000 position units. After testing, drive the shuttle to the motor extent of the assembly.

    e. Use a short piece of elastic string to tie the silver wire leading from the shuttle to the Omnetics connector, to the fixation bar (see photo above). I like to do two loops around the electrode wire (Fig. A.6). **Shuttle should be at motor end while connecting the elastic thread. Tension should still exist even when the shuttle is driven to the other end. If there is too much slack in the elastic , you can get microphonic noise. If it is too loose, you can make another loop (or two) around the fixation bar.**

Figure A.6: Connect the electrode wire to the shuttle, glue it to the top of the shuttle, solder it to pin 14, and attach elastic string to the fixation bar and wire to add tension.

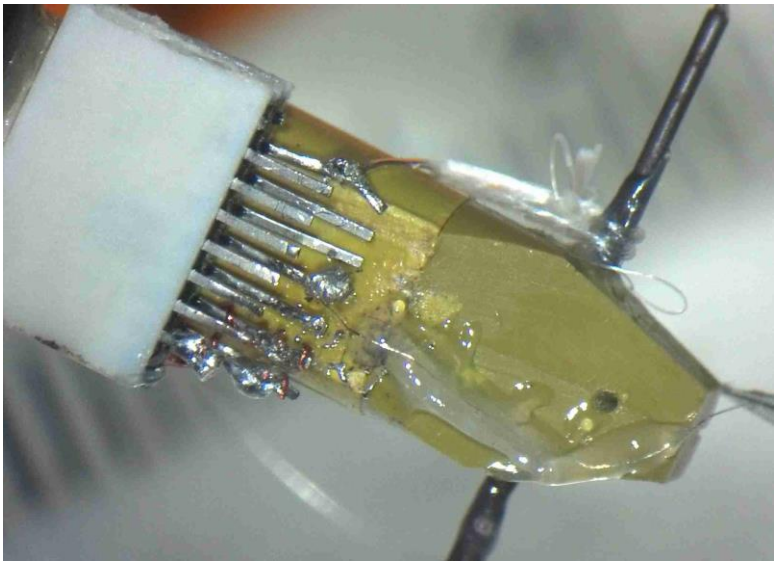

Figure A.7: Solder the reference wire to pin 11and glue in place.

2) Attach the virtual ground (reference electrode):

   a. Cut a 3 cm piece of 0.001 inch diameter coated platinum-iridium wire. Apply a thin coat of solder to virtual ground pin (pin 11) before soldering wire. Uncoat and solder one end to the virtual ground pin with a little more solder. This takes a few tries usually because the silver bearing solder doesn't adhere well to the platinum iridium (Fig. A.7).

   b. Lead the wire in a tight angled path to the tip of the assembly, gluing it in three separate spaces (1. near the body/tip junction; 2. lateral to screw; 3. At the center

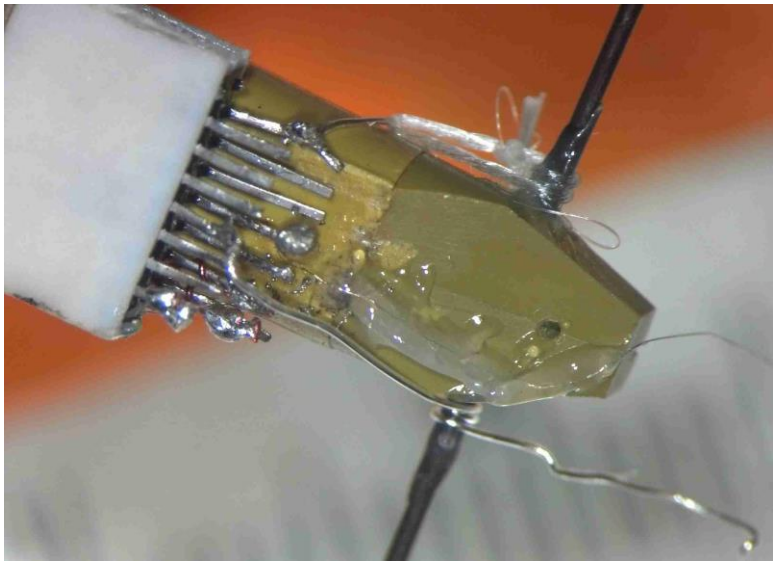

Figure A.8: Attach the ground wire to pin 4, wrap it around the fixation bar, and glue it in place.

of the tip). Use normally closed forceps to keep the wire tight during gluing. Once the wire is glued in place, encase the whole wire in glue for the extent of the chassis tip (Fig. A.7).

c. At the tip, bend and cut it such that the tip of the wire is parallel to the electrode guide channel and extends 0.5 to 1 mm from the tip. Uncoat the wire on the first 200 um (use cutting forceps, this can be very difficult and annoying). Think like a zen master here.

3) Attach the actual ground (Fig. A.8):

Cut a 6 cm piece of 0.005" diameter coated silver wire and uncoat the wire everywhere except for the first 15mm. Uncoat another 3 mm from the still coated end and solder it to the ground pin (pin 4). Lead the wire to the end of the fixation bar on the opposite side of the silver wire leading to the shuttle and wrap it once around, then glue it in place.

4) Make sure shuttle is as close as possible to the motor end of the axis, but keep in mind that it can get stuck if it is too far up the axis.

5) Prepare the electrode and guide tube:

a. Cut ~6.5 mm of polyimide tubing (.004" inner diameter). The guide tube should span the entire length of the electrode guide channel and protrude at the tip by about 500 – 1000 microns.

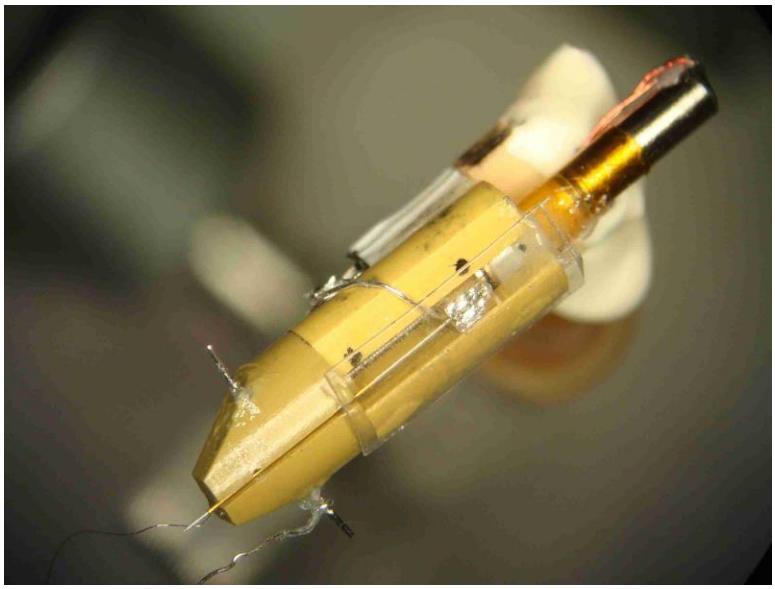

Figure A.9: Cut electrode to desired length, insert into polymide guide tube, solder to shuttle, and fix guidetube to tip with dab of epoxy. Finally, attach a clear plastic cover to prevent the bird from breaking the electrode.

b. Cut the desired electrode to length using the 90 degree cutters of #5 forceps (~12.5 mm – measure to adjust this value for every experiment. Ideally the tip of the electrode should be flush with the tip of the guide tube when the shuttle is fully retracted. This prevents damage to the electrode tip during the rest of assembly and implantation), then uncoat 1mm of the wire by crushing the glass coating with forceps. This takes practice, so start out by using the back end of the extra long electrodes (i.e. cut off some excess electrode, then attempt to cut it to a specific length and trim the glass for 1mm). If you mess up during the actual electrode cut, that electrode becomes useless.

c. Carefully slip the guide tube over the back end of the electrode and place it such that it covers the tip.

d. Place the electrode/guide tube in the electrode guide channel such that the back end rests on the shuttle. Make sure the electrode lies flat in the electrode guide channel, glue the electrode in place on the shuttle and solder the uncoated end of the electrode to the silver wire using Cerro matrix (turn the soldering iron all the way down). Fix the guide tube with a small dab of non-sag epoxy in a place at the end of the electrode guide channel closer to the shuttle (fixed at the top of channel, but still bendable with lateral positioning screw; Fig. A.9).

e. Protect the guide tube from exposure to dental cement:

    i. Take a small ball of wax, chip off a piece, and melt it near the fixation point with soldering iron (don't fill in the entire guide channel with wax, only top 25% above positioning screw).

ii. When implanting, cover rest of guide channel and positioning screw with wax/oil mixture.

6) Cut and bend a piece (~ 4 x 2mm) clear plastic (overhead transparency, or folder tab) to shape and glue it to the body to cover the electrode. The bird can reach this area with its foot (Fig. A.9).

7) For implantation, the electrode should extend 200um from the tip of the guide tube, unless you're going to search for neurons during implant, in which case extend maximally (Fig. A.9).

Part 3: implantation procedure. The following assumes basic knowledge of general surgery and anesthesia protocols. Expect the entire procedure to last 2 – 6 hours depending on proficiency, not including animal recovery time.

1) Start with normal procedures:

   a. Prepare the animal by fasting for 60 minutes.

   b. Induce anesthesia with 0.3cc equithesin, and boosters as needed (30 min apart).

   c. Remove feathers from scalp, then place in stereotax. Numb the scalp with lidocain, topically and subcutaneously, then make a circular incision and expose the bone.

   d. Remove first layer of skull to expose y sinus, then using a pipette in the stereotax, mark the desired coordinates for craniotomy.

2) Proceed with implantation:

   a. Craniotomy procedure differs for juveniles and adults:

      i. Juveniles: should only have thin layer over forebrain, just cut a small hole (.5mm diam) over region of interest. Cut multiple pairs of holes (1 – 2 mm apart) around the craniotomy to insert insect pins. The hole pairs should be over 1mm away from craniotomy so that the implant is surrounded by pins, not covering them.

      ii. Adults: remove the top layer of skull in a 2mm x 2mm square (at least) around craniotomy area. Then remove spicules and small hole in second layer for craniotomy. Insect pins are not needed as anchors, but you should make small holes across the 1st layer of skull to allow dental cement to seep into the bone.

b. Place the microdrive in the sterotax adapter and align the electrode tip to the medial edge of the craniotomy. The lateral positioner screw should be facing the midline, so that turning it will move the electrode laterally.

c. Retract microdrive after aligning it to appropriate ml/ap coordinates.

d. Make a small craniotomy posterior to the y sinus for inserting the ground electrode.

e. Use a syringe to fill the electrode guide tube with mineral oil. Holding a drop of oil to the tip of the guide tube should fill it.

f. Poke a hole in the dura with a syringe.

g. Advance microdrive until the tip of the guide tube is 50 – 200 microns in the brain. Make sure both the guide tube and virtual ground have penetrated the brain.

h. Fill the space between the microdrive and brain, surrounding guide tube, with wax (60% paraffin wax and 40% mineral oil) to ensure that the electrode and guide tube are not cemented in place.

i. Fix the microdrive to the skull with a few drops of dental acrylic, and allow it to dry.

j. Trim the ground electrode back so that only 1cm or so sits beneath the skull. Insert the ground.

k. Cover the entire area of the exposed skull, including the ground wire, with dental cement.

l. When the cement is dry, try to drive the electrode 200um very slowly. Hopefully everything is working at this point.

3) Troubleshooting during recordings:

a. *Large movement artifacts and no neural signal.* Combined with an increase of noise RMS, this is a good indication of a broken electrode or loose connection. Test by passing a small current in a superficial region with the pulse generator. If there is a broken connection somewhere, try soldering again (add a small amount of resin flux to cerro matrix, that has helped in the past). If the connections are good and clean then the electrode might be busted. This happens commonly on implant. You CAN replace the electrode if you are super careful. JWS has removed the electrode, then put a new one face first through the guide tube. This fixed a problem 2/3 times.

b. *Periodic signal loss or noise at certain bird positions.* This may indicate a bad teather/headstage or poor grounding. Grounding sometimes deteriorates over time, so if the problem progresses over time this is probably that. Don't expect to record forever. If you have multiple teathers, try swapping for a new one.

c. *Decent neural signal but huge movement artifacts.* This is most likely due to a break in the reference wire if you're in a differential amplification setup. See if you can resolder the connection of the reference wire at the omnetics. If it's intact, it's possible that the wire is broken within the dental cement, in which case you will be hard pressed to get a clean recording when the bird moves.

d. *Sound (singing or playback) corrupts the electrode signal.* Microphonic noise can be reduced by adding tension to the electrode wire. It is also possible to ground the speaker using Faraday shielding.

e. *Everything seems fine with the construction, but I'm getting electrical interference and movement artifacts.* Oddly, a humidifier sometimes fixes this. Place a humidifier next to the recording chamber. You can also encase the entire implant in copper foil and ground it to pin 4. This is often unnecessary, but sometimes fixes a lot of noise problems.